U.S. - JAPAN COORDINATED PROGRAM

FOR

MASONRY BUILDING RESEARCH

REPORT NO. 8.2-1

PB93-214674

RELIABILITY OF CONCRETE MASONRY WALL STRUCTURES

by

GARY C. HART
GEORGE TIBERIUS ZORAPAPEL

DECEMBER 1991

supported by:

NATIONAL SCIENCE FOUNDATION

GRANT NO. BCS-8722863

UCLA

Department of Civil Engineering

This report presents the results of a research project which was part of the U.S. Coordinated Program for Masonry Building Research. The program constitutes the United States part of the United States - Japan Coordinated Masonry Research Program conducted under the auspices of the Panel on Wind and Seismic Effects of the U.S.-Japan Natural Resources Development Program (UJNR).

This material is based on work supported by the National Science Foundation under the direction of Program Director, Dr. S.C. Liu.

Any opinions, findings, and conclusions or recommendations expressed in this publication are those of the authors and do not necessarily reflect the views of the National Science Foundation and/or the United States Government.

RELIABILITY OF CONCRETE MASONRY WALL STRUCTURES

by

Gary C. Hart
George Tiberius Zorapapel
Department of Civil Engineering
University of California, Los Angeles

December 1991

ACKNOWLEDGEMENTS

This TCCMAR report represents the Ph.D. Dissertation of Dr. Zorapapel under the Ph.D. chairmanship of Dr. Hart. We wholeheartedly thank Professor Dan M. Frangopol from the University of Colordo in Boulder for his valuable comments and suggestions after reading several drafts of this dissertation. We also wish to thank members of Dr. Zorapapel's committee Dr. Moshe F. Rubinstein, Dr. Samuel Aroni, Dr. George Apostolakis and Dr. Mladen Vucetic. Special gratitude is due to Dr. Niaz Ahmed Sajjad for numerous discussions and suggestions.

TABLE OF CONTENTS

CHAPTER 1

INTRODUCTION

1.1 MOTIVATION OF THE RESEARCH

1.1.1 General

It is not economically acceptable to design and build structures that will resist earthquake ground motion excitations while maintaining elastic behavior. The currently accepted earthquake design criterion for life safety applied to buildings requires that the building not collapse if subjected to an earthquake ground motion of maximum expected level. Consequently, the calculation of inelastic response is of critical importance in evaluating the ability of a building to withstand a major earthquake. Two types of performance are possible in a concrete masonry wall: either the wall can undergo large deformations while partially maintaining its strength (ductile behavior) or the wall can suddenly lose its strength (brittle behavior) and potentially collapse.

The use of concrete masonry walls as an earthquake lateral force resisting system for high rise structures requires the system be ductile. If concrete masonry is confined, it can sustain large strain levels and suitable ductility. It is only recently that studies have been performed to evaluate practical and efficient ways to confine concrete masonry. These studies concluded that the stress-strain

relationship for concrete masonry confined with different types of confinement schemes is different from the stress-strain relationship of reinforced concrete.

The natural framework to describe the performance of building structures to earthquake excitation is structural reliability theory. Historically, this discipline started with the estimation of the probability of failure of a single structural component based on a knowledge of the probabilities distributions of the involved random variables. In the 1970's a breakthrough was made in structural reliability theory by introducing the concept of a safety index that only requires the knowledge of the first and second moments of the random variables. It then followed that the use of "First Order Second Moment" approach further advanced the use of safety calibration for the development of design criteria at the element level.

Soon it became obvious that the multi-component behavior had a severe impact on the probability of failure of the structure. The problem of predicting the system reliability has been formulated starting from the reliability of its components. The system reliability theory developed, in the last fifteen years, methods for estimating the probability of failure for structures such as frames and trusses subjected to static loads. Structural walls are elements with more complex behavior than the elements that constitute a truss or frame and the reliability analysis of such walls has seldom been attempted even at the component level.

1.1.2 Basic Problems Related to Reliability Analysis of Structural Systems Subjected to Earthquake Ground Motions

The major difficulty in estimating the probability of failure of any element or structure subjected to earthquake shaking is created by the extremely large uncertainty associated with the load. It is recognized that it is not possible to accurately assess either the distribution or the moments of the random variables associated with the ground motion excitation at a site. Even if the activity in some potential earthquake sources may be described probabilistically with a relatively good confidence, the uncertainty associated with the local soil amplification is very large.

In the current structural design practice, this shortcoming is overcome by providing structures with critical components that do not fail in a brittle manner but, rather, continue to deform inelastically. Meanwhile, the acceleration response of the system in the inelastic domain decreases and the displacement response increases. The yielding components continue to resist their yield level load while going through deformations that are further imposed on the structure. An individual wall fails when its ultimate deformation or ultimate limit state is reached. After a certain number of walls reach their ultimate limit state, collapse of the structure is likely to occur. The amount of deformation that the structure can sustain from the first yield limit state to the ultimate system limit state quantifies the available ductility of the structure. Our objective, therefore is to make sure that the

subject structure has the available ductility necessary to undergo the deformations required. Levels of *component* ductility are now required in current building codes and no conscious effort is made to produce acceptable levels of *structural system* ductility.

It is proposed that the structural reliability of walls be separated into three steps:

(1) Determine the statistical variability of the *component* ductility.

(2) Determine the statistical variability of the *structural system* ductility starting from the statistics of the component ductility.

(3) Perform a reliability analysis at the *structural level* introducing earthquake load uncertainty. The limit state equations will be written in terms of ductility demand and ductility capacity.

There are several advantages of this approach:

(1) The first two steps are purely structural problems where the earthquake load is not involved. Thus, the results will have a reasonable degree of confidence.

(2) At the structural level, the effects of redundancy can be emphasized separately from the system ductility. Then, the beneficial effects of redundancy and ductility can be combined to the advantage of the structural system. At the same time, tridimensional effects like the variation of the axial force due to spatial ground motion excitation can be accounted for.

(3) The uncertainty in response spectrum ordinates associated with local amplification is higher for elastic systems than for the inelastic systems. When the ductility demand increases, the uncertainty decreases. In this finding lies the potential for a more confident safety calibration of the seismic risk of structures.

(4) Reliability theory in general deals with low probabilities that are associated with two major difficulties: lack of practical meaning and inaccuracy of results when using Monte Carlo simulation. The proposed approach shifts the domain of interest to higher probabilities that are easier to handle and understand.

1.1.3 Objective and Importance of this Research

The goal of this research is limited to the first two steps of the general approach outlined in the previous section that are the determination of the statistical variability of the wall ductility and the structural system ductility. The results will be presented in a format that is specific to structural reliability analysis and uses the safety index of ductile behavior.

The object of the study are structures consisting of flexural structural walls, i.e. structural walls where the possibility of a shear mode of failure is precluded.

The importance of this research for structural engineering stems from the need to find efficient solutions for lateral force resisting systems of new structures

as well as a confident estimation of the strength reserve incorporated in existing structures.

1.2 STATE OF THE ART REVIEW IN STRUCTURAL SYSTEM RELIABILITY

1.2.1 System Reliability

According to the classical theory of system reliability, a structure is considered at a fixed point in time, and the state of the structure is assumed to depend only on the present state of its elements. Each element is assumed to be either in a functioning state or in a failed state. A binary state indicator variable a_i is defined as equal to 1 when the *i*-th element is functioning and 0 when it has failed. A state indicator variable a_s, called the "structure function" is defined as a function of $a_1,...,a_n$ (Barlow and Proschan, 1975; Madsen, Krenk, and Lind, 1986). A "cut set" is defined as a set of elements that produce the failure of the system. A minimal cut set is defined as a cut set that does not contain any other cut set. Similarly, a "path set" is defined as a set of elements that can assure the survival of the system. A minimal path set is defined as a path set that contains no other path set (Contini and Poucet, 1988). The structure function can be expressed as a function of minimal cut sets and minimal path sets. This format allows for a systematic estimation of the probability of failure of the system. Different expressions for lower and upper bounds of this probability as a function of the

probability of failure of the components have been proposed by Cornell (1967), Vanmarcke (1971), and Ditlevsen (1979).

A theoretical system that has captured the attention of many researchers was defined by Daniels (1945). The system consists of a bundle of fibers with independently, identically distributed component strengths, a constant modulus of elasticity and perfect equal load-sharing among the unbroken fibers. The behavior of fibers is ideally brittle. Daniels found a recursive scheme for the determination of the probability distribution of system strength and derived the Gaussian distribution as a limiting distribution of system strength for an infinite number of components.

Rackwitz and Golwitzer (1988) studied small size Daniels systems with stochastic dependence between the different components and arbitrary force-deformation curve. They introduced a more complex definition of component ductility as a function of the ratio between the inelastic and elastic energy. According to this definition, they place the components in different ductility categories ranging from ideal brittle to ideal ductile. Calculating the reliability index of systems with increasing number of elements shows that the ideal brittleness corresponds to the least increase in reliability. Ideal ductility provides the largest increase in reliability index with the increasing number of elements.

1.2.2 Redundancy

One of the most ambiguous concepts in the theory of structural reliability is redundancy. For the ordinary structural engineer redundancy is analogous with static indeterminacy and its efficacy can be measured by the number of degrees of static indeterminacy. It has been stated (Corotis et al., 1988), arguably, that redundancy is a quality that represents the "availability of ordinarily not required capacity". In fact, the additional static indeterminacy may amount, in most cases, to additional capacity, hence reliability, of the system. However, for certain types of loadings (termal, differential settlement) redundancy is harmful to the system reliability (Yao, 1988). In seismic design, the practice to provide "seismic gaps" between sub-structures of different dynamic characteristics is a typical example of avoiding detrimental redundancy.

If redundancy is an intrinsic characteristic of the structural system, the *effects of redundancy* are different according to the type of loading. These effects are considered beneficial if there is an increase in system reliability with respect to the component reliability.

Attempts have been made to quantify the efficacy of redundancy using a *Redundancy Factor*. Frangopol and Nakib (1991) present a series of such redundancy measures, grouped in two categories: deterministic and probabilistic.

The emphasis is placed on estimating the capability of the structural system to carry load after one or more of its members have failed. An example of deterministic definition for the Redundancy Factor is

$$R = \frac{Q_{intact}}{(Q_{intact} - Q_{damaged})}$$

where

Q_{intact} = ultimate strength of the undamaged system

$Q_{damaged}$ = ultimate strength of the system after one or more members have failed

The probabilistic measures of redundancy effects acknowledge the uncertainty in loads and strengths. The proposed definitions for redundancy factors are:

$$R_1 = \frac{\beta_C}{\beta_{WM}}$$

$$R_2 = \beta_C - \beta_{WM}$$

$$R_3 = \frac{(\beta_C - \beta_{WM})}{\beta_C}$$

where

β_C = safety index of the intact system with respect to collapse

β_{WM} = safety index of the weakest member

More general definitions can be obtained by replacing the safety index of the weakest member with the safety index of the intact system with respect to *any* first member failure, β_{AM}. Another alternative is offered by replacing the safety indices with the corresponding probabilities of failure.

An important distinction made by Frangopol et al. (1991) is between the design-oriented measures of redundancy effects and evaluation-oriented measures. The object of latter measures of redundancy effects are the existing, damaged structures. To account for the given damage state, β_{WM} or β_{AM} is replaced by the safety index of the damaged system, β_D.

De, Karamchandani, and Cornell (1989) define the Redundancy Factor as the conditional probability of system failure given the first failure of any member. They also define a Complexity Factor as a ratio between the probability that any first member failure occurs and the probability of failure of the weakest member. The Complexity factor measures the adverse system effect on the first failure event due to the presence of more than one failable member.

Rackwitz and Golwitzer (1988) showed that Daniels systems provide the most efficient redundancy, i.e. the highest increase in system reliability with increasing number of elements. However, if the correlation between components is high and/or the coefficient of variation of the load exceeds the one of strength significantly, the gain in reliability when increasing the number of elements becomes insignificant. Apparently surprising, an increased resistance variability in a brittle system may produce increased system reliability. In fact that happens

because the authors imposed a constant element safety index; in order for the standard deviation to increase, the average element strength has to decrease and the system reliability consequently decreases.

Cornell (1988 b) defines the "probabilistic redundancy" as the effect of the stochastic variations of resistance of different parallel elements about a common mean that does not permit the structure to collapse when the first member fails. The "balanced systems" defined as systems with elements having a common mean load-to-capacity ratio (De, Karamchandani, and Cornell, 1989) possess a high "probabilistic redundancy". The Daniels systems are the least "probabilistically redundant" because of the load-sharing property. The probabilistic redundancy concept will be given a special attention in this research because it is an appropriate model for parallel systems consisting of semi-ductile elements subjected to earthquake excitations.

1.3 ORIGINAL CONTRIBUTION

1.3.1 General

This research is divided into four parts. The First Part, treated in Chapter 2, studies the sensitivity of the lateral force-deformation behavior of a reinforced concrete masonry flexural wall to the variations in material characteristics and magnitude of the axial force. The Second Part (Chapter 4), provides a new statement of the wall reliability problem independent of the strong motion excitation, and solves the problem for the wall studied in the First Part. Finally, the Third Part (Chapter 5) expands on the findings of the previous chapter to provide a new insight into the reliability of structural systems composed of reinforced concrete masonry walls, based on conclusions regarding the system ductility and redundancy effects. Chapter 3 and Appendix E identify and solve a new problem of the reliability theory: the safety index in a multistate space.

1.3.2 Sensitivity Analysis of a Concrete Masonry Wall with Minimum Vertical Reinforcement

Monte-Carlo numerical simulations are performed on a concrete masonry wall with minimum vertical reinforcement and confinement of the vertical steel using "Confinement Combs" (Hart et al., 1987). The force-deformation relationships for

walls subjected to static lateral loading and an axial force applied at the top are computed. The material characteristics of the concrete and reinforcing steel, the height of the plastic hinge measured from the base of the wall, and the level of the axial force are considered as "input" random variables. A model for the stress-strain curve of concrete masonry confined with the "Confinement Comb" was used to simulate the behavior in the plastic range (Sajjad, 1990).

The wall behavior depends on the material properties of the concrete masonry and reinforcing steel as "input" parameters and is characterized by the following "output" parameters: yield moment and ultimate moment of the wall at its base, yield curvature, and displacement, ultimate moment, curvature and displacement, as well as curvature and displacement ductilities.

The study of the dependence of the output parameters to the input parameters consists of two steps:

(1) We establish the most likely values for the mean and coefficients of variation of each input variable with the exception of the axial load. Then we perform a Monte Carlo simulation for this "central case" and determine the mean values and the coefficients of variation of each of the output variables.

(2) We study the sensitivity of the mean and coefficient of variation of each output variable to variations in the means and coefficients of variation of the input variables.

The most important conclusions are:

(1) The input parameters that introduce the highest uncertainty in the output parameters are the axial load on the wall and, for the ultimate displacement and displacement ductility, the height of the plastic hinge.

(2) As expected, higher concrete masonry maximum compressive stress and maximum usable strain produce higher ductility, and higher steel yield stress produces lower ductility displacement. The insensitivity of curvature ductility to the increase in steel yield stress was less than expected.

(3) When axial load is large, the output parameters are more sensitive to increases of the mean value of the concrete masonry maximum compressive stress. When the axial load is small, the output variables are more sensitive to increases in the mean value of steel yield stress. This occurs because low axial load implies a ductile limit state of yielding of the steel while a large axial load produces a brittle limit state characterized by concrete masonry crushing, thus governed by the compressive strength of concrete.

(4) The output variables are insensitive to the variables of the model for the concrete masonry stress strain curve other than maximum usable strain.

(5) The ultimate curvature is independent of the axial load.

(6) Several coefficients of variations of the output parameters have a narrow range of variation. The curvature ductility has an almost constant coefficient of variation: 20%. The approximative values of the coefficients of variation of yield curvature and yield displacement are both 10% whereas for ultimate curvature the coefficient of variation is 20%. The values for the coefficient of variation for ultimate displacement and ductility displacement are strongly dependent on the axial load, decreasing from a high of 26%-29% for 5% of the maximum axial load to a low of 13%-17% for 40% of the maximum axial load.

(7) For axial loads that do not produce brittle failure, the histograms for curvature ductility exhibit a symmetric shape, suggesting the possibility of fitting to a normal model, while the displacement ductility appears to be lognormally distributed.

1.3.3 Safety Index in a Multistate Space

When the ultimate limit state is conditioned by the previous occurrence of one or more other limit states, the safety index can not be found using the classical First Order Second Moment solution (Hasofer-Lind). Instead of one limit state surface in the space of normalized random variables, each condition introduces a new surface characterizing that particular limit state. Each

"conditional surface" splits the ultimate limit state surface into two regions: one region where the respective condition is fulfilled and other where it is not fulfilled. If the design point (the closest point from the conditional surface to the origin) is found in an undesirable region of the ultimate surface, a "false solution" could be achieved. The "true solution" is to be found on the n-dimensional curve resulting from the intersection of the ultimate and conditional surfaces. The problem then becomes to find the point on the intersection curve that is closest to the origin of the space of normalized coordinates.

In some engineering problems, the ultimate limit state can not be described by an equation. Instead, the failure can be obtained through a certain sequence of conditional limit states. An example is the reinforced concrete masonry column subjected to bending and compression. Since the brittle failure has to be avoided, the yielding of the tension steel has to occur before the crushing of the concrete masonry. The first conditional surface is represented by the equation f_y-f_s=0, while the second is ϵ_{mu}-ϵ_c=0. Here f_s is the stress demand in the tension steel, f_y is the yield stress in the tension steel, ϵ_{mu} is the maximum usable strain in the concrete masonry and ϵ_c is the strain demand in the concrete masonry. If the distance to the second surface is smaller than the distance to the first surface and the design point is in the region where $f_s > f_y$, then this is a "false solution" because there is no concern associated with a ductile failure. The "true solution" is likely to be found on the intersection of the two surfaces.

When the design point must be searched for on a curve rather than a surface (like it is in the Hasofer-Lind problem), the iterative algorithms used to find the design point cannot be used. This research identifies the problem of the failure conditioned by the previous occurrence of several limit states and presents a new iterative algorithm that uses Lagrange Multipliers to obtain the Design Point and the Safety Index.

1.3.4 Reliability Analysis of a Single Flexural Wall

The theoretical framework introduced in the previous section allows for a restatement of the reliability of a flexural wall subjected to strong ground motion excitations. Since an estimate of the first and second moments for the parameters of future ground motion at a certain site has an extremely large uncertainty, an ultimate state equation that contains the load will be unrealistic. Therefore, a reasonable way to approach the reliability of wall systems is to provide the wall with a ductile behavior and then require limits on available ductility. From this prospective, the reliability of the wall is viewed as the conditional probability that ductility demand will be less than ductility capacity, given that the wall will behave ductile. This concept leads to a two step approach:

Step (1) Determine the probability of ductile behavior and define the associated safety index.

Step (2) Determine the probability that the ductility demand will be less than the ductility capacity.

The limit state equation linking the ductility demand to the ductility capacity should be written at the structural system level. The present approach permits this desideratum by splitting the *First Step* into two tasks:

Task (1) Estimating the probabilistic distribution of the ductility capacity and the associated safety index for individual walls;

Task (2) Estimating the probabilistic distribution of the available ductility and the associated safety index for the structural system.

The *Second Step* of the problem is beyond the scope of this research. However, in conceiving the format for the safety index to be produced within the first step one has to bear in mind the need for compatibility to the second step product. A comprehensive representation of the probabilistic information regarding the available ductility should be correlated to a similar index describing the seismic activity of a site or region.

Under conditions of large uncertainty in the level of lateral loading, it is fair to state that a flexural wall must behave in a ductile manner to withstand a major earthquake. This research shows that for several walls of different shapes in plan (rectangular, T-shape, L-shape), the ultimate displacement capacity at the top of the wall remains smaller than the displacement demand derived from a typical design response spectrum for Downtown Los Angeles. This finding proves the validity of the proposed approach. This research defines a "Ductility Index" as the

safety index of the ductile behavior. The ductility index presents several advantages.

(1) Unlike the classical safety index, tributary to an extremely uncertain load, the ductility index can be estimated with reasonable accuracy.

(2) The ductility index can be used to calibrate the design prescriptions for flexural walls.

(3) Since the ductility index is a comprehensive representation of the probabilistic information regarding the available ductility, chances are that it may be directly correlated with a similar index describing the seismic activity of a site or region. That may lead to a long overdue breakthrough in the seismic analysis, where the established force concept constitutes a major obstacle to a better understanding of the real behavior.

The Ductility Index is defined as

$$\beta_{\mu} = \frac{\overline{\mu} - 1}{\sigma_{\mu}}$$

where

$\overline{\mu}$ = the expected value of ductility

σ_{μ} = the standard deviation of ductility

The ductility μ can be either the curvature ductility or the displacement ductility. A ductility index based on displacement ductility was preferred to an index based on curvature ductility because:

(1) For small values of axial force, the Curvature Ductility Index results in unrealistically high values due to the lack of invariance of the Ductility Index to different mappings of the limit state surfaces.

(2) The Curvature Ductility Index is more sensitive than the Displacement Ductility Index to variations in the statistical parameters of the input variables.

(3) The Displacement Ductility Index can be directly used at the structural system level for: the estimation of the system ductility, the possibility of constraining different walls in a building to undergo the same displacement at a floor level, and the possibility that we can obtain a format for the ductility capacity that can be equated with a similar format for the earthquake ductility demand.

Besides the Ductility Index, this research defines and studies a more easily understood measure of the brittleness of a reinforced concrete masonry wall. This measure is the frequency of brittle behavior and it is defined as the number of realizations that result in brittle behavior divided by the total number of realizations in a Monte Carlo simulation. An alternate Safety Index can be defined as the Inverse Standardized Gaussian Function of the Frequency of Brittle Behavior. This index, although more easy to understand, has several shortcomings if compared to the Ductility Index:

(1) It requires the unrealistical assumption that the frequency of brittle behavior is normally distributed.

(2) It underestimates the Safety Index, especially for coefficients of variation of the axial load that exceed 10%.

(3) It requires thousands of realizations of Monte Carlo simulations when the mean axial force is smaller than 25% of the maximum.

The case-study wall mentioned in Section 1.3.2 is used to investigate both the Ductility Index and the Frequency of the Brittle Behavior for different values of the parameter statistics of the mechanical characteristics of steel and concrete, as well as the axial load.

1.3.5 Reliability of Concrete Masonry Flexural Wall Structures

The study of the ductility capacity and ductility index is expanded to the structural systems composed of several (two to eight) flexural walls connected in the horizontal plane with rigid diaphragms. The effects of redundancy created by the presence of more walls working in parallel is studied. The complementary roles of ductility and redundancy in shaping a global quality of the system - robustness - is explored in this part of the research.

When the structure is subjected to a set of static lateral forces applied at the story levels where one wall reaches its yield load, a redistribution of forces among the remaining elements results. In a seismic base excitation, the successive yielding and/or failure of walls leads to a decrease in the level of total force input

in the structure. Hence, a masonry multiple wall seismic resisting system is not characterized by a redistribution of load like a Daniels System. Because of the significant increase in the fundamental natural period of vibration, the structural response is governed by displacement rather than acceleration. If we treat this problem using an equivalent static approach, the structure is subjected to imposed displacements rather than inertial forces. Under a monotonic increasing displacement imposed equally to all of the participating walls, the walls will reach consecutively their ultimate capacity limit state until the structure reaches its ultimate system limit state. Thus, the structural system studied in this research fits the definition of a *balanced system* when the axial load corresponding to each wall has the same mean value and coefficient of variation. The variation of axial load among the walls is mainly due to the randomness in live load distribution across the floor. In the case when cross-walls are present, the simultaneous excitation on the direction perpendicular to the walls under study may induce compression in some walls and tension in the others. This structural system is *unbalanced*.

In this research, the ultimate displacement for a structural system is considered to occur when all but the last wall have reached their individual wall ultimate limit state. The yield displacement of the structure is defined consistently with the yield displacement of a bilinear model, based on a "stylized" load-deflection curve for the structure. We define the System Ductility as the ratio between the displacement of the structural system at the ultimate limit state and the displacement of the structural system at the yield limit state.

For the balanced systems, the redundancy can be understood as Cornell's *probabilistic redundancy*, i.e. the effect of the stochastic variations of resistance of different parallel elements about a common mean that does not permit the structure to reach its ultimate limit state when the first member fails. The basic difference between the safety index in this research as compared to the classic safety index precludes the utilization of any of the probabilistic redundancy indices existing in the literature as discussed in Section 1.2.2. We define the Redundancy Ratio as the ratio between the displacement at the top of the building corresponding to the ultimate system limit state and the displacement corresponding to the first reaching of the ultimate limit state in a component wall. Since the Redundancy Ratio is a random variable, its mean and coefficient of variation characterize the *probabilistic redundancy* of the system.

Besides the parameters that govern the ultimate capacity of one wall (as described in Section 1.3.2) there are additional factors that have an influence on the system ductility and redundancy: the size of the system (the number of walls), the covariance matrix corresponding to each material parameter distributed among walls and the distribution and correlation of axial load among walls. To study this influence, Monte Carlo simulations have been performed on samples of structures consisting of two to eight walls. Each statistical sample contains 750 structures. Because of the necessity of controlling the correlation of input variables, the generation of random values requires a special attention. An original method to minimize the sample bias and instability is presented.

For the balanced systems, the System Ductility and the Redundancy Ratio appear to have a contradictory character as it results from the two main conclusions:

(1) The mean redundancy ratio increases with the number of walls at a much higher rate than the mean system ductility increases.

(2) Unlike the coefficient of variation of system ductility that decreases when the number of walls increases, the coefficient of variation of redundancy ratio is independent of the number of walls.

According to its definition, the mean value of the redundancy ratio mirrors the scatter in the system ductility and, apparently, it should exhibit similar features to the coefficient of variation of the system ductility. The observation of this research that the mean redundancy ratio increases when the coefficient of variation of the system ductility decreases is explained by the rapport between scatter and uncertainty and constitutes one of the most interesting findings of this research.

When the uncertainty in system ductility increases because the uncertainty in material properties or axial loads increases, the redundancy ratio increases. However, an increase in the number of walls without changing the statistics of the material properties or axial load does not increase the uncertainty. The increase in the number of walls is similar to increasing the size of a statistical sample. This produces a more confident estimate associated with a smaller sampling variance. This decrease in uncertainty is revealed by the decrease in the coefficient of variation of system ductility. At the same time, the ratio of the two extremes of the sample increases. This increase is not a consequence of an increase in

uncertainty; in a larger sample the expected maximum is greater and the expected minimum is smaller according to the properties of the ordered statistics. This explains why the scatter in system ductility reflected by the redundancy ratio increases, while the overall uncertainty in the system decreases. Hence, both system ductility and redundancy ratio, although apparently contradictory, provide their beneficial effects to the system behavior. We call *robustness* the system quality that combines the beneficial effects of the system ductility and redundancy to the advantage of the balanced system.

Similarly to the Ductility Index, we define the System Ductility Index (SDI) as a function of the statistics of the System Ductility:

$$SDI = \frac{\overline{SD} - 1}{\sigma_{SD}}$$

where:

$\overline{SD}$ = the mean value of the System Ductility

σ_{SD} = the standard deviation of the System Ductility

Besides the quantification of safety with respect to ductile behavior, the System Ductility Index fulfills the conditions for measuring the system robustness. The results of the Monte Carlo simulations show that:

(1) The System Ductility Index increases with the mean value of the System Ductility and this is the beneficial effect provided by the System Ductility.

(2) The System Ductility Index increases when the scatter of the System Ductility decreases; this decrease in uncertainty is attributed to the increase in the number of walls, and consequently to an increase in redundancy.

Several important conclusions result from the Monte Carlo simulations:

(1) The increase in axial load produces a decrease in the mean values of the system ductility, redundancy ratio, and system ductility index. The coefficient of variation of system ductility increases while the coefficient of variation of redundancy ratio decreases when the axial load is increasing.

(2) The increase in correlation of material properties among the walls of the structure produces a slight increase in the coefficient of variation of the system ductility. There is practically no effect on the mean system ductility, while the mean and coefficient of variation of redundancy ratio increase with the correlation only for the 40% axial load case. However, the system ductility index decreases markedly when the correlation increases.

(3) The mean value of the ratio between the displacement corresponding to structural failure and the average displacement corresponding to any failure of a wall can measure the additional capacity of the structure to withstand imposed displacements. Using a sufficient

number of walls, this additional capacity varies from 8% to 19% as a function of the axial load.

This research accords a special attention to unbalanced systems created by the presence of T-shaped walls and the consideration of simultaneous earthquake excitation in two horizontal directions. Both the mean value and coefficient of variation of the system ductility resulted in large values. However, the system ductility index is smaller than the system ductility index corresponding to the value of the system ductility index for the weakest of the two balanced subsystems contained in the unbalanced system, and may reach dangerously low values. This finding has to be construed as an indicator that flanged walls may not be a good system to use in high seismic zones. Further research is needed in this area of flanged wall performance.

The results of this research can be used to provide a probabilistic back-up for the Capacity Reduction Factors for concrete masonry codes. For example, Hart and Sajjad (1989) recommended for masonry design an upper limit for the design axial load of 65% of the balanced axial load of the wall. According to this research, the corresponding safety index of one wall with respect to ductile behavior (Ductility Index) is 1.2. However, considering the *robustness* of the structural system composed of reinforced masonry walls, the corresponding System Ductility Index results 1.75 for two-wall systems and 4 for eight-wall systems. The lower-bound value is the same as the safety index recommended for seismic loads by Ellingwood et al. (1980). Consequently, the value of the Capacity Reduction Factor recommended by Hart and Sajjad is conservative.

CHAPTER 2

SENSITIVITY ANALYSIS OF A CONCRETE MASONRY WALL WITH MINIMUM VERTICAL REINFORCEMENT

2.1 GENERAL

The first step in the investigation of the seismic performance of concrete masonry walls is the study of the lateral force-deformation behavior of a single wall. The performance of the wall is characterized in this chapter by the relationship between the walls' overturning moment and (1) the curvature of the wall at its base, and (2) the horizontal displacement at the top of the wall.

A wall exhibits ductile behavior if the vertical steel yields before crushing of the masonry. If the axial force acting on the section is sufficiently large, or the section is over-reinforced, then the vertical steel will not yield prior to the crushing of the masonry. The ductility of a wall increases when the concrete masonry is confined. Hart et al. (1987,1988) presented experimentally verified analytical models that demonstrated the "ductile" performance of concrete masonry confined with a "confinement comb" and several other masonry confinement schemes. Sajjad (1990) developed an experimentally verified constitutive relationship for concrete masonry confined with a "confinement comb" and this research will use

the Sajjad constitutive relationship. A modified version of the IMFLEX Program (Hart, Sajjad, and Basharkah, 1990) has been used in this chapter to compute force-deformation relationships.

In this chapter, Monte-Carlo numerical simulations are performed on a concrete masonry wall that is one part of the lateral force resisting system of the structure showed in Figure 2.1.1 and discussed in Appendix B. The wall is located on Line 2. The wall under consideration is 90 foot tall, 8 inches thick and is reinforced vertically with #4 bars located at 32 inches on center. The horizontal shear steel is assumed to be sufficient to prevent shear failure. The vertical steel is confined using the confinement comb. All cells in the wall are grouted.

The behavior of the wall depends on the material properties of the concrete masonry and reinforcing steel. These properties as well as the level of the vertical (axial) force on the wall are considered as "input" random variables. The "input" variables are:

(1) f'_m = concrete masonry maximum compressive stress.

(2) f_y = steel yield stress.

(3) A, C = shape variables in Sajjad model (Sajjad, 1990) for the confined concrete masonry stress-strain curve.

(4) ϵ_{mu} = the maximum usable strain in the concrete masonry; this strain corresponds to a stress equal to 50% of the maximum compressive stress.

(5) ϵ_{su} = the ultimate steel strain.

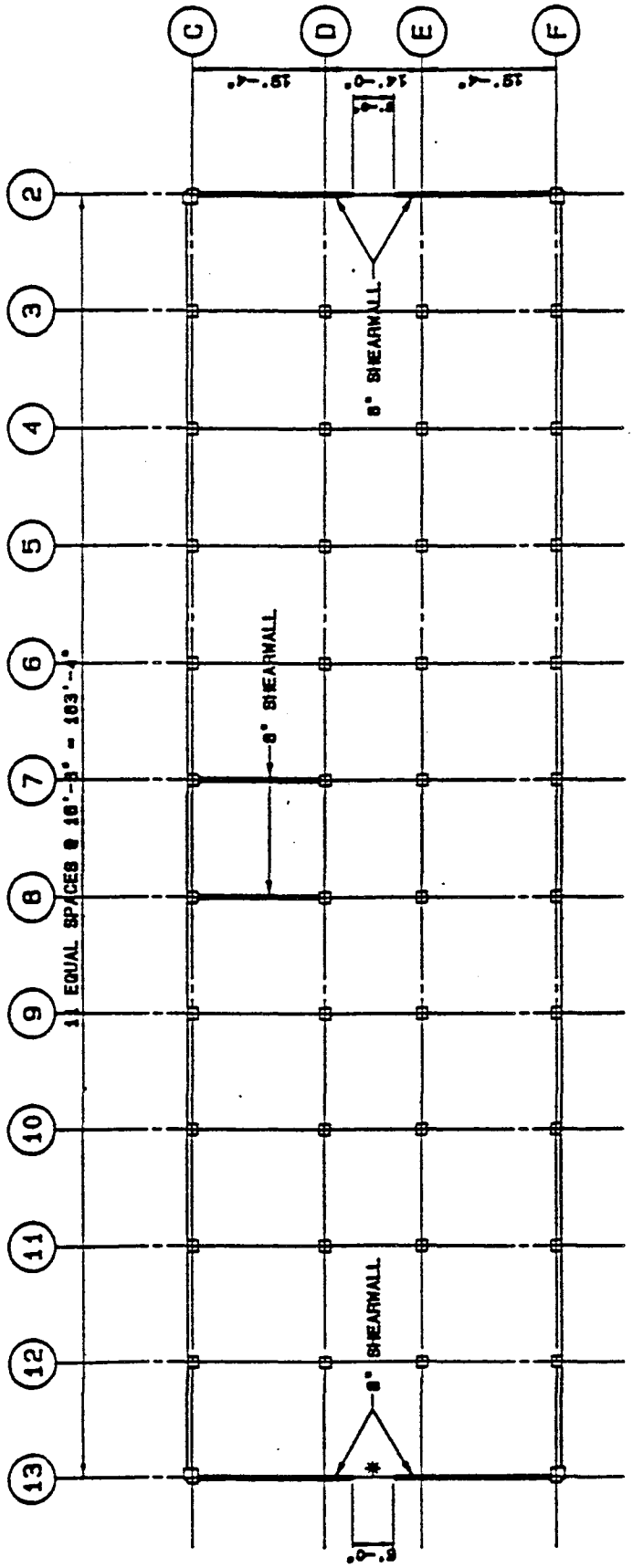

FIGURE 2.1.1 PLAN LAYOUT OF A CONCRETE MASONRY BUILDING

(5) H_p = height of the plastic hinge measured from the base of the wall.

(6) P = axial load on the top of the wall.

The wall behavior is characterized by the following "output" variables:

(1) M_y = yield moment of the wall at its base.

(2) ϕ_y = yield curvature of the wall at its base.

(3) d_y = displacement at the top of the wall when the vertical steel first yields.

(4) M_u = ultimate moment of the wall when the masonry strain is equal to its maximum usable strain.

(5) ϕ_u = curvature at the base of the wall in the plastic hinge region of the wall.

(6) d_u = displacement at the top of the wall when the masonry strain is equal to its maximum usable strain.

(7) μ_ϕ = curvature ductility (ϕ_u/ϕ_y).

(8) μ_d = displacement ductility (d_u/d_y).

The research described in this chapter studies the relationship between the output variables and the input variables. The study is performed using the following two steps:

Step 1 We determine the most likely or *expected* values for the mean and coefficients of variation of each input variable with the exception of the axial load. The axial load, P, is considered

deterministic in this chapter in order to obtain a clearer picture of the wall behavior. Then we perform a Monte Carlo simulation study for this "central case" to determine the mean and coefficient of variation of each of the output variables. We also plot a frequency histogram for each output variable.

Step 2 We study the sensitivity of the mean and coefficient of variation of each of the output variables to the means and coefficients of variation of the input variables.

2.2 THE CENTRAL CASE

2.2.1 General

Table 2.2.1 gives the values used in this research for the mean and coefficient of variation (C.O.V.) of each of the input random variables. The random variables are considered to be uncorrelated, based on the test results presented in Appendix A. Figure 2.2.1 shows a plot of the confined stress-strain curve used in this research. The equations for this curve are:

$$f_m = f'_m[-A\epsilon^2_m + (\frac{1}{\epsilon_u} + A\epsilon_u)\epsilon_m] \qquad (2.2.1)$$

$$f_m = f'_m[C + (1-C)e^{-B(\epsilon_m - \epsilon_u)}] \qquad (2.2.2)$$

where

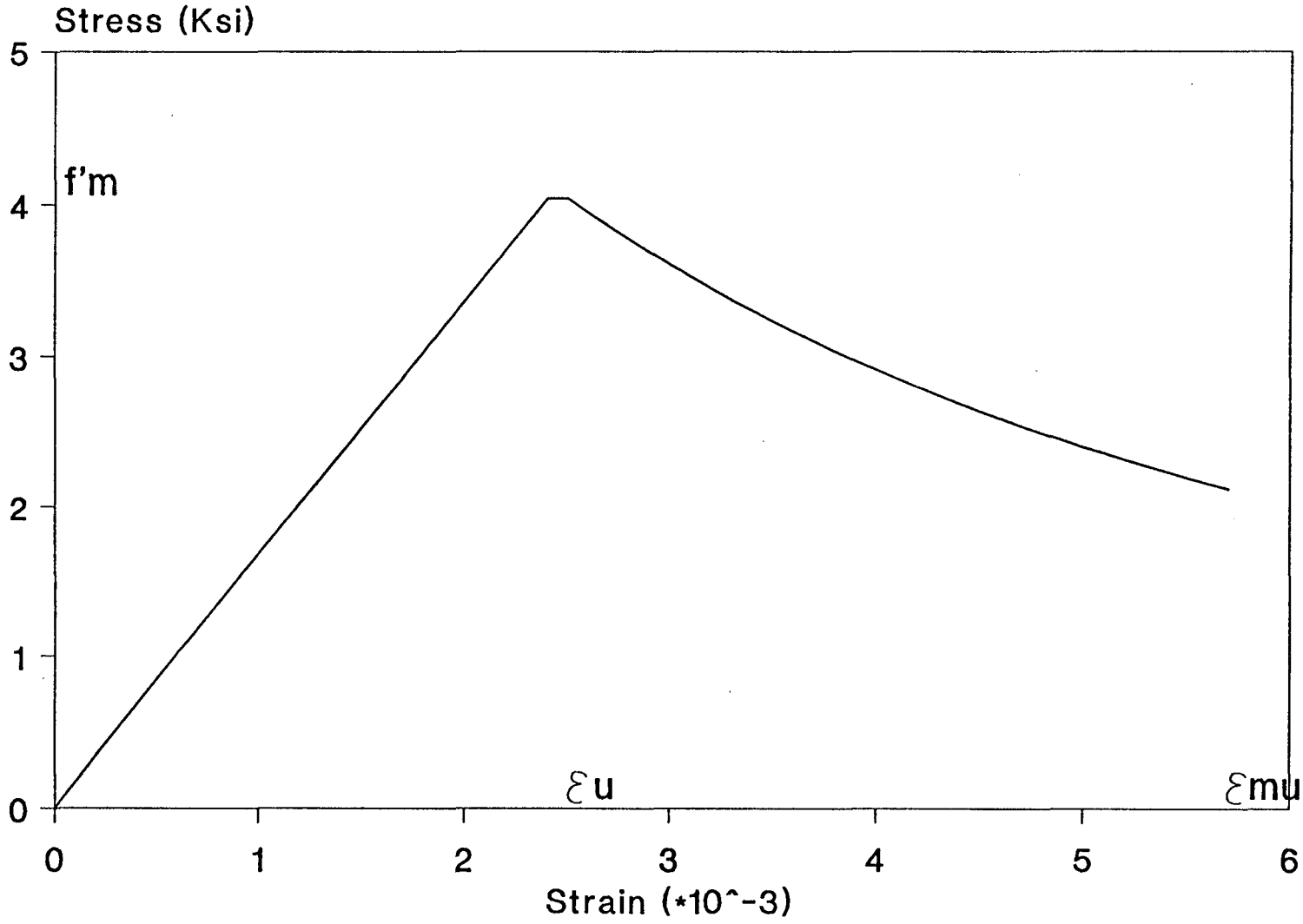

FIGURE 2.2.1 STRESS-STRAIN CURVE FOR CONFINED MASONRY

ϵ_m = masonry strain

ϵ_u = strain corresponding to maximum compressive stress

f_m = masonry stress

A,B,C = coefficients that are function of f'm and the confinement characteristics

Equation (2.2.1) corresponds to the rising branch ($0 < \epsilon_m < \epsilon_u$) and equation (2.2.2) corresponds to the falling branch (see Figure 2.2.1).

TABLE 2.2.1
Description of Input Random Variables

Variable	Probability Density Function	Mean	C.O.V.	Source
C	Normal	0.226	30%	Sajjad, 1990
ϵ_{mu}	Normal	0.0057	15%	Appendix B
f'_m	Normal	4.1 Ksi	10%	Appendix B
f_y	Normal	66.8 Ksi	8.26%	Mirza, Mc.Gregor,1979
ϵ_{su}	Normal	0.11	5%	Assumed
H_p	Normal	140 in	25%	Assumed

The mean values for f'_m and ϵ_{mu} were derived from the results of the tests performed at the University of Colorado (Sajjad, 1990) and the details are presented in Appendix B. The shape variable A is considered to be deterministically dependent on f'_m according to the formula (Sajjad, 1990):

$$A = \frac{4.8x10^6}{f'_m} \qquad (2.2.3)$$

The axial load P is considered to be deterministic. The six values of P considered in this research ranged from 0 to 40 percent of $A_g f'_m$, where A_g is the gross cross-sectional area of a horizontal section of the wall. The load $A_g f'_m$ is hereafter referred to as the maximum axial load. The dead load of the wall is approximatively 2% of the maximum axial load. The balanced axial load is approximately 40% to 50% of the maximum axial load.

A Monte Carlo simulation study was performed for 750 realizations of the vector formed by the input basic random variables in Table 2.2.1 for each value of P. For large axial forces and certain combinations of input variables values a brittle failure of the wall occurs. A brittle failure is defined in the next section. For the purposes of calculating the statistics, these cases were eliminated when calculating the statistics for the yield variables (M_y, ϕ_y, and d_y). When calculating the ductility variables (μ_ϕ and μ_d) in this chapter, a value of 1 was assigned in case of brittle behavior.

The margin of error for a sample size of 750 is 1% for the mean values and 5% for the coefficients of variation.

2.2.2. Variation of Statistics of the Output Variables with Axial Load.

This research considers the following three distinct limit states for the wall:

Limit State 1: The steel attains its ultimate strain in tension before the masonry crushes in compression. This limit state exists when the strain in the steel is equal to its rupture strain. This is defined to be a ductile limit state and the steel yields prior to the wall reaching this limit state.

Limit State 2: The steel attains its yield strain in tension before the masonry crushes in compression. The strain in the steel is less than its rupture strain. This limit state exists when the masonry compression strain is equal to its maximum usable strain. This is a ductile limit state.

Limit State 3: The masonry crushes in compression before the steel attains its yield strain in tension. This limit state exists when the masonry compression strain is equal to its maximum usable strain. This is a brittle limit state.

The variation of the output variables can be better understood if the limit state is known for a particular level of axial force. The Monte Carlo simulation indicates that:

(1) For the zero axial load case only Limit State 1 occurs. This situation of such a small axial load seldom exists; however, it can be visualized for the case of flanged walls subjected to horizontal forces in two orthogonal directions (see Section 5.3.2) or as being representative of a beam.

(2) For the 2.5% axial load case, the Limit State 1 occurs in 37% of the realizations and Limit State 2 occurs in the remaining realizations. This is important because no brittle failures occurred.

(3) For the 5%, 10% and 20% axial load cases only the second limit state occurs. Again this is important because it means that no brittle failures occurred.

(4) For the 40% axial load case, Limit State 2 occurs in 92% of the realizations while Limit State 3 (i.e. brittle behavior) occurs in the remaining 8% of the cases.

The results of the six sets of Monte Carlo simulation are presented in Table 2.2.2 and Figures 2.2.3 through 2.2.8. The variation of mean values of the yield and ultimate moments with the axial load is presented in Figure 2.2.3. As expected, the mean values of yield and ultimate moments increase in magnitude with increasing axial load. The mean ultimate moment is greater than the mean yield moment up to 20% of the maximum axial load. The ultimate moment reduces to a value smaller than the yield moment and its rate of increase becomes almost flat for an axial load greater than 20% of the maximum load.

The decrease of the value of the ultimate moment below the value of the yield moment occurs only at large strains. When the axial force is small, the centroid of the compressive force in the masonry moves closer to the extreme compression fiber when the deformation of the wall increases. For a large axial force, the compression stress at the extreme fiber of the masonry starts

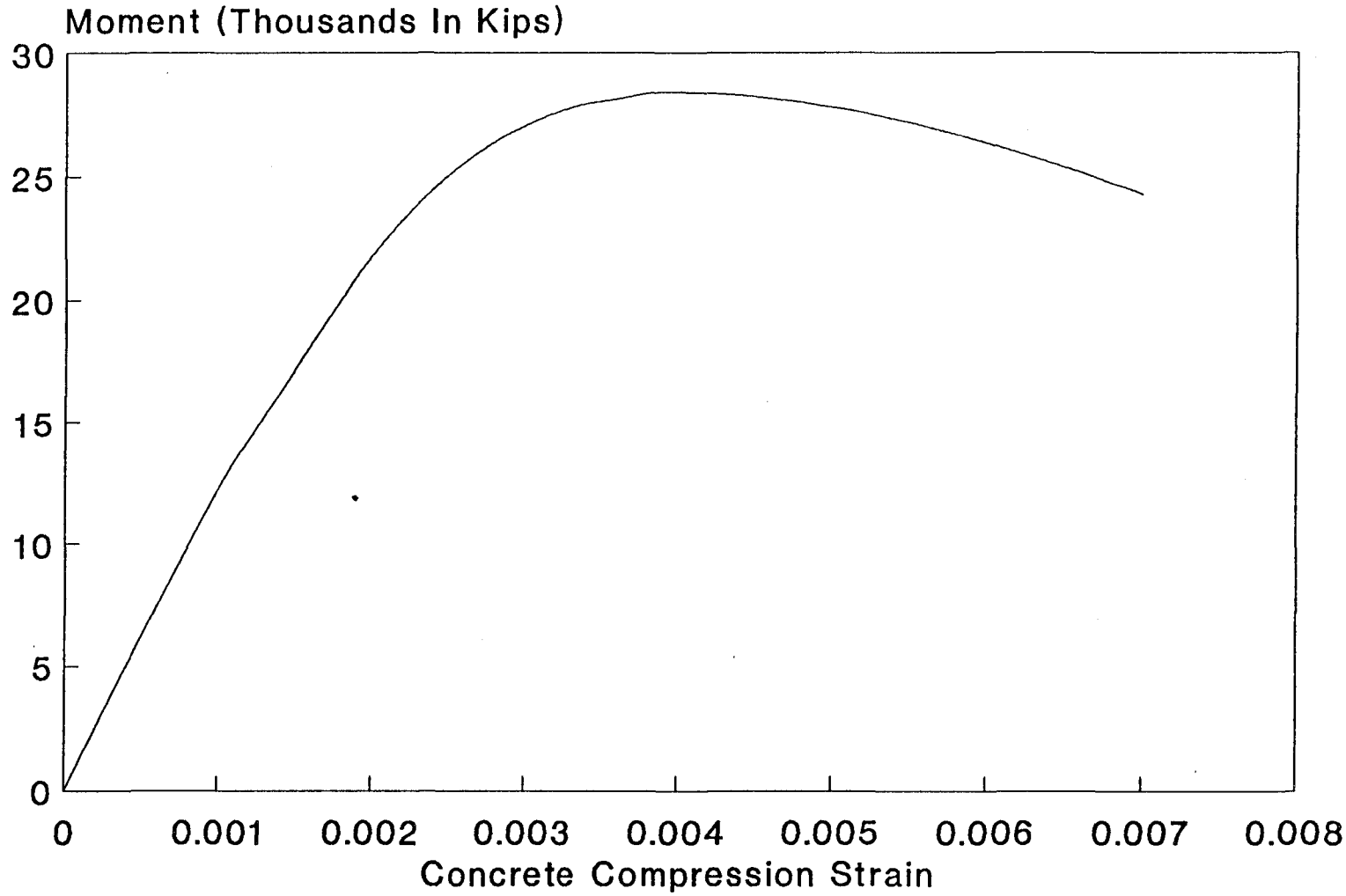

FIGURE 2.2.2 MOMENT-STRAIN RELATIONSHIP FOR LARGE AXIAL LOAD

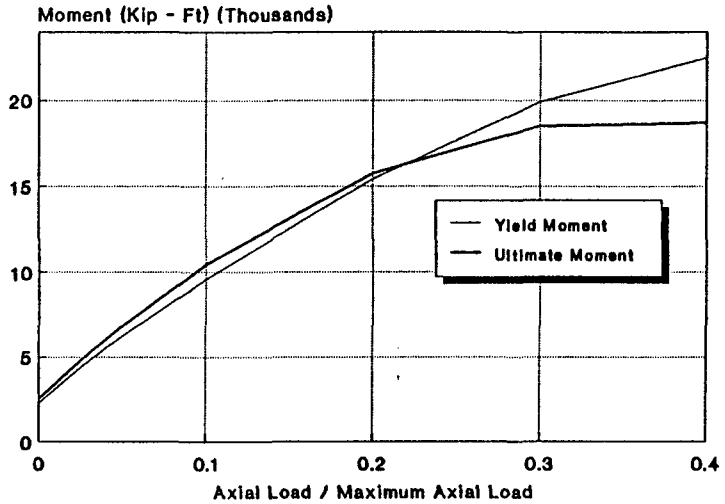

FIGURE 2.2.3 MEAN MOMENT

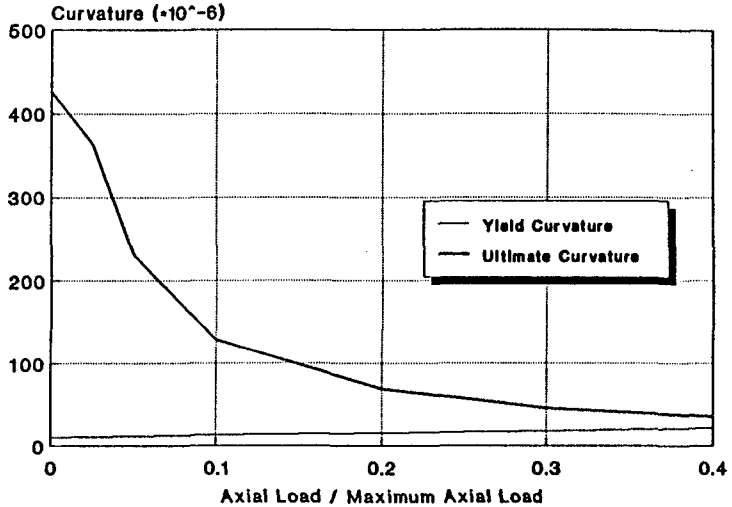

FIGURE 2.2.4 MEAN CURVATURE

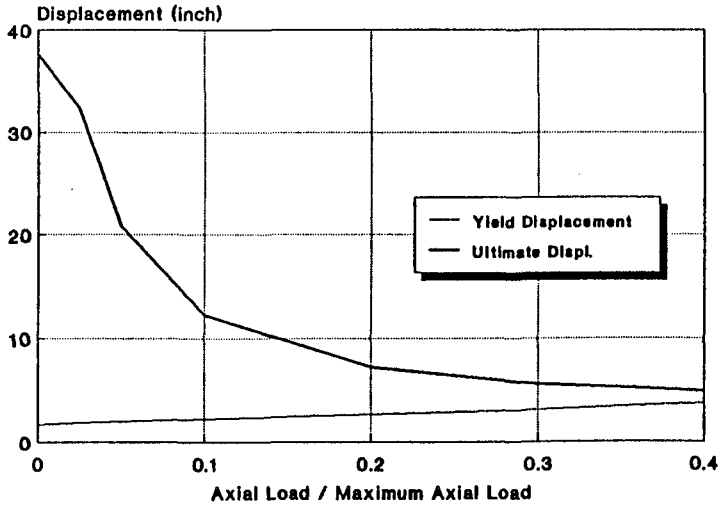

FIGURE 2.2.5 MEAN DISPLACEMENT

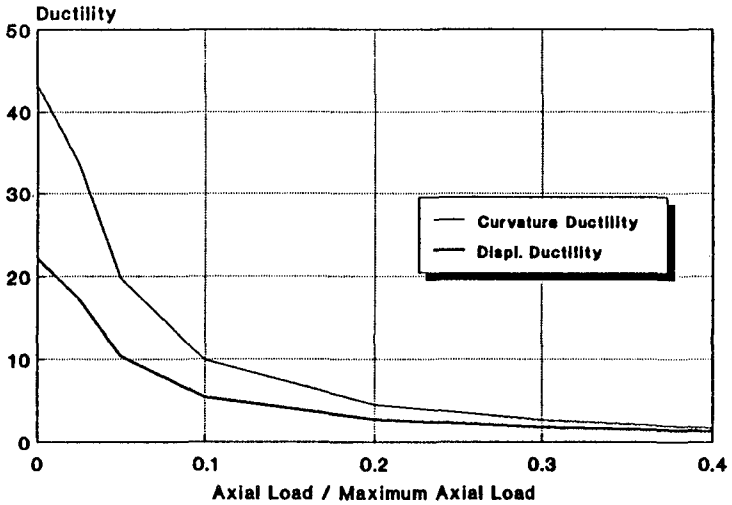

FIGURE 2.2.6 MEAN DUCTILITY

decreasing rapidly after reaching compression strains greater than 0.004 to 0.005. As a consequence, the centroid of the compressive force in masonry starts moving in the opposite direction (i.e. away from the extreme compressive fiber and back toward the center of the wall) in order to compensate for the decrease in the stress at this strain. This movement reduces the lever arm between the compression and the tension forces, producing the decrease of the ultimate moment. As shown in Figure 2.2.2, this phenomenon does not usually occur when the maximum usable strain is considered at the typical design code value of 0.003.

Table 2.2.2
Mean Values of Output Variables Characterizing Wall Response - Central Case

P / Pmax (%)	M_y Ft-K	ϕy ($*10^{-6}$)	d_y Inch	M_u Ft-K	ϕ_u ($*10^{-6}$)	d_u Inch	μ_ϕ	μ_d
0	2,308	9.9	1.7	2,574	426	37.7	43.3	22.2
2.5	4,354	10.9	1.9	4,780	364	32.3	33.6	17.3
5	6,215	11.7	2.0	6,824	230	20.8	19.8	10.4
10	9,606	13.1	2.3	10,439	129	12.3	10.0	5.5
20	15,426	15.5	2.7	15,754	69	7.3	4.5	2.7
30	19,924	18.0	3.1	18,508	46	5.6	2.6	1.8
40	22,470	21.5	3.7	18,708	36	4.9	1.7	1.3

The variation of mean values of the yield and ultimate curvatures with the axial load is presented in Figure 2.2.4. Figure 2.2.5 shows the variation of the mean yield and mean ultimate displacements. The mean values of the yield curvature and yield displacement are much less sensitive to the magnitude of the

axial load while the corresponding ultimate values decrease dramatically with increasing axial load. Consequently, the mean value of the curvature and displacement ductilities exhibit a decrease with axial load, as shown in Figure 2.2.6. For small values of the axial load, the curvature ductility is almost twice as much as the displacement ductility, but the difference decreases with axial load. As shown in Table 2.2.2, the curvature ductility decreases from a value of 34 (for the 2.5% axial load case) to 1.7 (for the 40% axial load case). For the same range of axial loads, the displacement ductility decreases from 17 to 1.4.

The dependence of the coefficients of variation (C.O.V.) of the output variables on the axial load is shown in Figures 2.2.7 and 2.2.8 and Table 2.2.3. The coefficient of variation of the yield and ultimate moments decrease from 8% (for the zero axial load case) to 2% (between the 10% and 20% axial load cases) and then increases again. This small value for the coefficient of variation (several times smaller than any coefficient of variation of the input variables) occurs because the parameters of the stress-strain curve for concrete masonry that determine the moment capacity of the wall section are correlated with f_y through the force equilibrium equation. This correlation increases when the lever arm between the compression and tension forces decreases (i.e. when the axial force increases). On the other hand, for high axial forces f'_m has a greater influence on the moment capacity than f_y (as it will be shown in Section 2.3.2). Since f'_m possesses a negative correlation with some of the curve parameters, the coefficient of variation of the moment capacity increases again for higher axial loads.

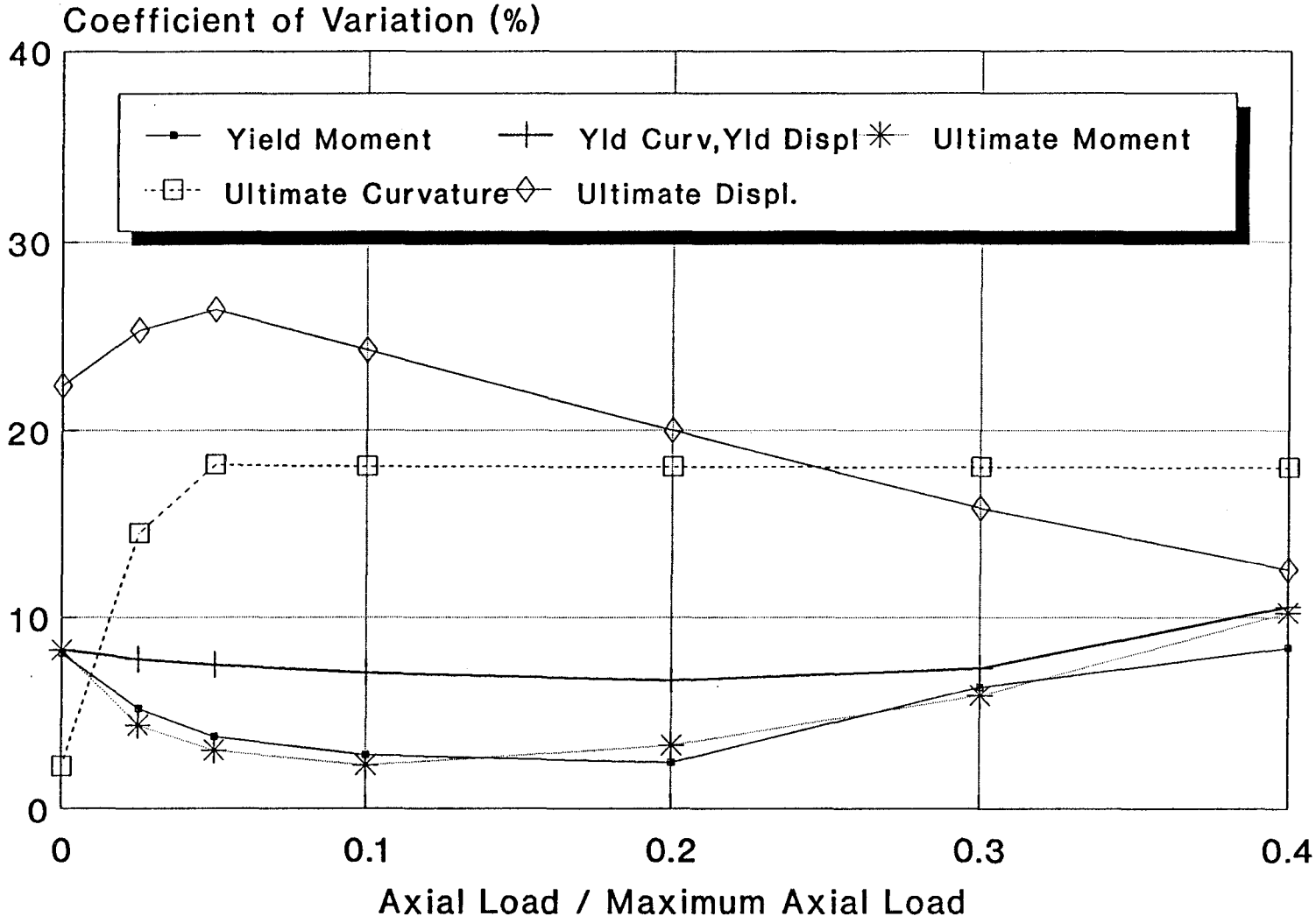

FIGURE 2.2.7 COEFFICIENT OF VARIATION OF OUTPUT PARAMETERS

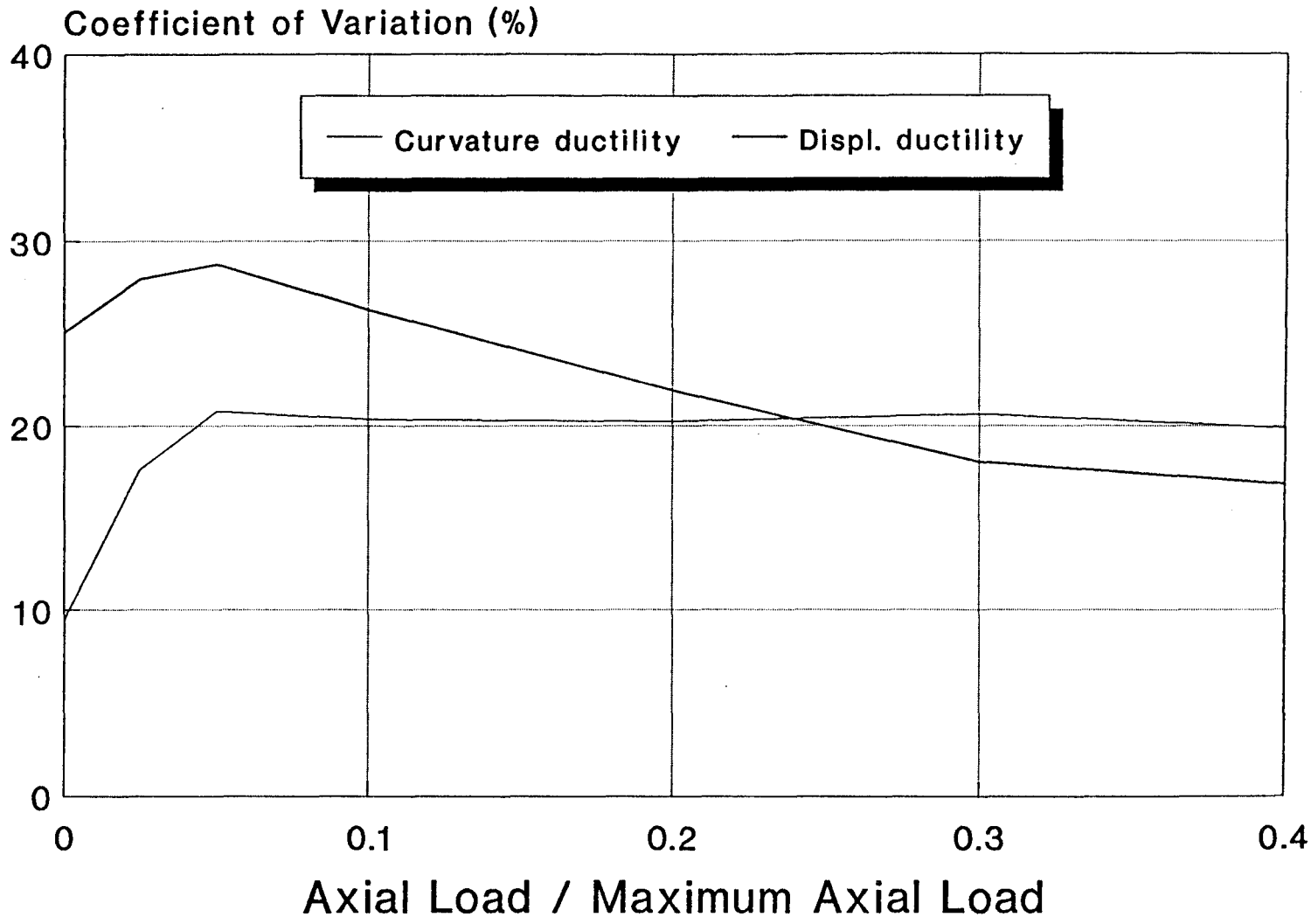

FIGURE 2.2.8 COEFFICIENT OF VARIATION OF OUTPUT PARAMETERS

Table 2.2.3
Coefficients of Variation of Output Variables Characterizing Wall Response - Central Case

P / Pmax (%)	M_y %	ϕ_y %	d_y %	M_u %	ϕ_u %	d_u %	μ_ϕ %	μ_d %
0	8.1	8.3	8.3	8.3	2.2	22.4	9.5	25.1
2.5	5.2	7.8	7.8	4.3	14.5	25.3	17.6	27.9
5	3.8	7.5	7.5	3.0	18.2	26.4	20.8	28.7
10	2.8	7.1	7.1	2.3	18.1	24.3	20.3	26.3
20	2.4	6.7	6.7	3.3	18.1	20.0	20.2	21.9
30	6.3	7.3	7.3	5.9	18.0	15.8	20.6	18.0
40	8.4	10.6	10.6	10.2	18.0	12.5	19.9	16.8

The coefficients of variation of the yield curvature and yield displacement decrease slightly from 8% for the zero axial load case to 7% for the 20% axial load case, then increase to 11%.

The variation of the coefficient of variation of the ultimate curvature and displacement is a function of the limit state. For low axial forces when the Limit State 1 can occur, the coefficient of variation increases with increasing axial load. For axial loads larger than 5% of maximum, the coefficient of variation of the ultimate curvature is almost constant at 18% and the coefficient of variation of the ultimate displacement decreases almost linearly with increasing axial load from 27% to 13%. As a consequence, the coefficient of variation of the curvature ductility is almost constant at 20%, while the coefficient of variation of the displacement ductility decreases from 29% to 17%. This striking difference is due to the high randomness of the plastic hinge height that has a paramount influence on the ultimate displacement but has no influence on the ultimate curvature.

The decrease of the coefficient of variation of the ultimate displacement with the increasing axial force is extremely important for understanding the system redundancy that will be discussed in Section 5.5. The ductility displacement d_u can be expressed as a function of the ultimate curvature ϕ_u, height of the plastic hinge H_p, and wall height H (Park and Pauley, 1975):

$$d_u = \frac{\phi_y H^2}{3} + (\phi_u - \phi_y) H_p (H - \frac{H_p}{2}) \qquad (2.2.4)$$

The product in the second term of the right hand side of Equation (2.2.4) suggests that, supposing approximatively normal distributions for ϕ_y, ϕ_u, and H_p, that the ultimate displacement may be distributed closer to a lognormal probability density function shape than a normal shape. If two random variables X and Y fulfill the relationship

$$Y = \ln X \qquad (2.2.5)$$

and the variable Y is normally distributed, then the variable X is lognormally distributed. The coefficient of variation of X is only a function of the standard deviation of Y:

$$C.O.V._X = \sqrt{e^{\sigma_Y^2} - 1} \qquad (2.2.6)$$

If we accept the analogy between X and d_u on one side and Y and ϕ_u on the other side, then, according to Equation (2.2.6), the coefficient of variation of the displacement ductility decreases when the standard deviation of the ultimate curvature decreases. Since the coefficient of variation of ϕ_u is constant and the mean of ϕ_u decreases when the axial load increases, the decrease of the displacement ductility with increasing axial load can be understood.

2.3 SENSITIVITY OF THE OUTPUT VARIABLES

2.3.1 General

A sensitivity study was performed to study which of the statistics of the input variables has the greatest influence on the statistics of the output variables. The values of the target mean and coefficient of variation of the five random variables in Table 2.2.1 were one at a time increased by 20% to study this sensitivity. The increase was performed each time by increasing one variable, while keeping the other nine statistics for the input variables at the "central" target values. Therefore, a 20% change in the output values indicates a linear variation. The sensitivity study for axial force was performed for three levels of axial force: zero, 20%, and 40% of the maximum load. The percent variation in the mean value and coefficient of variation of each output variable due to each variation in the statistics of the input variables is shown, for each level of axial load, in Tables 2.3.1 through 2.3.6. The percent variation is calculated with respect to the "central" case, emphasizing the sensitivity of each mean value and coefficient of variation of the output variables to the 20% increase in each statistics parameter of the input variables. Figures 2.3.1 through 2.3.8 show the variation of each of these sensitivities as a function of the axial load.

Table 2.3.1
Sensitivity of Mean Values of Output Variables
(Axial Load = 0)

Statistic increased	M_y %	ϕ_y %	d_y %	M_u %	ϕ_u %	d_u %	μ_ϕ %	μ_d %
Mean C								
C.O.V. C								
Mean ϵ_{mu}								
C.O.V. ϵ_{mu}								
Mean f'_m	1	-1	-1		1	1	2	2
C.O.V. f'_m	1					1	-1	
Mean f_y	22	20	20	20	-1	-1	-18	-17
C.O.V. f_y	1					1		1
Mean H_p						18		17
C.O.V. H_p								

Table 2.3.2
Sensitivity of Coefficients of Variation of Output Variables
(Axial Load = 0)

Statistic increased	M_y %	ϕ_y %	d_y %	M_u %	ϕ_u %	d_u %	μ_ϕ %	μ_d %
Mean C								
C.O.V. C								
Mean ϵ_{mu}					-7			
C.O.V. ϵ_{mu}					-10		2	
Mean f'_m	5		1	1	3	1	1	1
C.O.V. f'_m	2	1	1	1	-4	-6		-8
Mean f_y	17	2	2		2	-2	2	-1
C.O.V. f_y	31	21	22	21	-4	-6	22	-3
Mean H_p						-8		-9
C.O.V. H_p						20		17

Table 2.3.3
Sensitivity of Mean Values of Output Variables
(Axial Load = 0.2 $A_g f'_m$)

Statistic increased	M_y %	ϕ_y %	d_y %	M_u %	ϕ_u %	d_u %	μ_ϕ %	μ_d %
Mean C								
C.O.V. C								
Mean ϵ_{mu}				-1	21	18	21	18
C.O.V. ϵ_{mu}								
Mean f'_m	2	-3	-3	6	19	15	22	19
C.O.V. f'_m						1		1
Mean f_y	5	15	15	3	-1	2	-14	-12
C.O.V. f_y						1		1
Mean H_p						12		12
C.O.V. H_p								

Table 2.3.4
Sensitivity of Coefficients of Variation of Output Variables
(Axial Load = 0.2 $A_g f'_m$)

Statistic increased	M_y %	ϕ_y %	d_y %	M_u %	ϕ_u %	d_u %	μ_ϕ %	μ_d %
Mean C								
C.O.V. C								
Mean ϵ_{mu}				-5	-1	5	-1	5
C.O.V. ϵ_{mu}				2	16	9	13	8
Mean f'_m		1	1	12	4	8	5	9
C.O.V. f'_m	2	3	3	17	1	1	2	-1
Mean f_y	5	4	4	1		-6	1	-5
C.O.V. f_y	16	20	20	2	-3		1	-1
Mean H_p						4		1
C.O.V. H_p						11		9

Table 2.3.5
Sensitivity of Mean Values of Output Variables
(Axial Load = 0.4 $A_g f'_m$)

Statistic increased	M_y %	ϕ_y %	d_y %	M_u %	ϕ_u %	d_u %	μ_ϕ %	μ_d %
Mean C				1	1	1	1	7
C.O.V. C								
Mean ϵ_{mu}				-2	21	14	19	19
C.O.V. ϵ_{mu}							1	7
Mean f'_m	10	-9	-9	19	19	8	25	24
C.O.V. f'_m	-1	1	1	-1	1	1		
Mean f_y	2	15	15	2	-1	5	-10	
C.O.V. f_y	-1	1	1			1	-1	
Mean H_p						5		11
C.O.V. H_p								

Table 2.3.6
Sensitivity of Coefficients of Variation of Output Variables
(Axial Load = 0.4 $A_g f'_m$)

Statistic increased	M_y %	ϕ_y %	d_y %	M_u %	ϕ_u %	d_u %	μ_ϕ %	μ_d %
Mean C				1	1	2	1	2
C.O.V. C				1			-1	
Mean ϵ_{mu}				-5	-1	7	7	18
C.O.V. ϵ_{mu}				1	15	13	7	7
Mean f'_m	-45	-27	-27		4	16	8	21
C.O.V. f'_m	17	12	12	19	1	1	9	8
Mean f_y	20	18	18		-1	-1	-4	-9
C.O.V. f_y	-1	10	10		-3		5	4
Mean H_p						9		12
C.O.V. H_p						5		4

2.3.2 Sensitivity of the Yield Moment

The yield moment is most influenced by the masonry maximum compression stress (f'_m) and the steel yielding stress (f_y). The sensitivity of the mean value of yield moment (M_y) to the mean values of f'_m and f_y, as shown in Figure 2.3.1.a, exhibits interesting features.

* The sensitivity to the variation of the mean value of f'_m increases with increasing axial load. There is less than a 2% change for a 20% change in the mean of f'_m for zero and 20% of the maximum load. However,there is a 10% change when the axial load increases to 40% of the maximum load.
* The sensitivity to the variation of the mean value of f_y decreases with increasing axial load. The sensitivity decreases from 22% for zero axial load to 2% when the axial load is 40% of the maximum load.

The sensitivity of the mean value of M_y to the coefficients of variation of these two input variables, as shown in Figure 2.3.1.b, is less than 1% and is not significant from a structural engineering perspective.

The sensitivity of the coefficient of variation of M_y to the mean values of f'_m and f_y, is shown in Figure 2.3.1.c. For zero axial load, a 20% increase in the mean value f'_m produces a 5% increase in the coefficient of variation of M_y while the same 20% increase in f_y produces a 17% increase in the coefficient of variation of M_y. This sensitivity decreases for the 20% of the maximum load but becomes

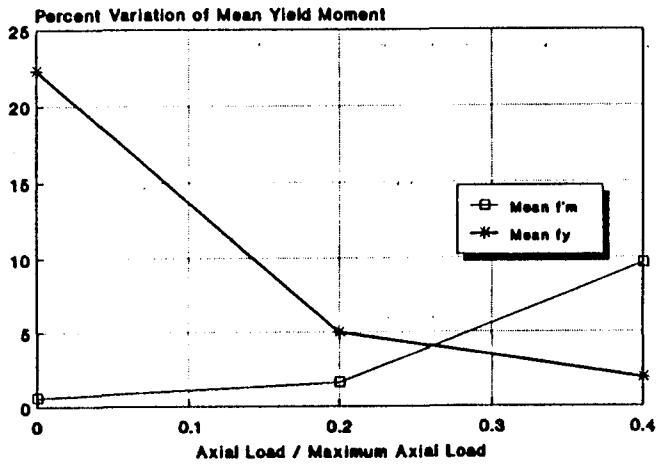

(a) MEAN My TO INCREASE OF MEAN f'm AND fy

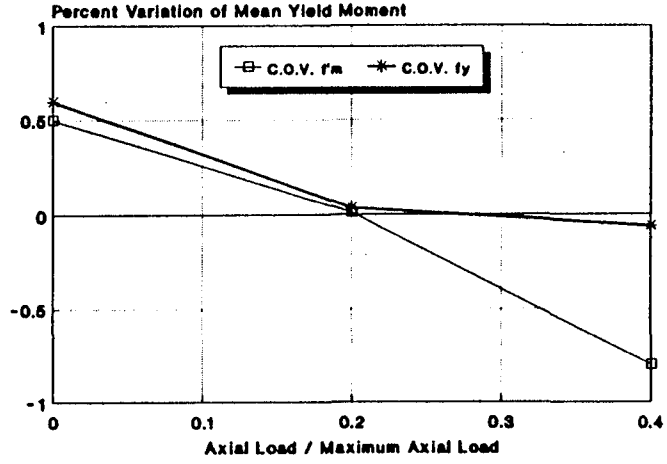

(b) MEAN My TO INCREASE OF C.O.V. OF f'm AND fy

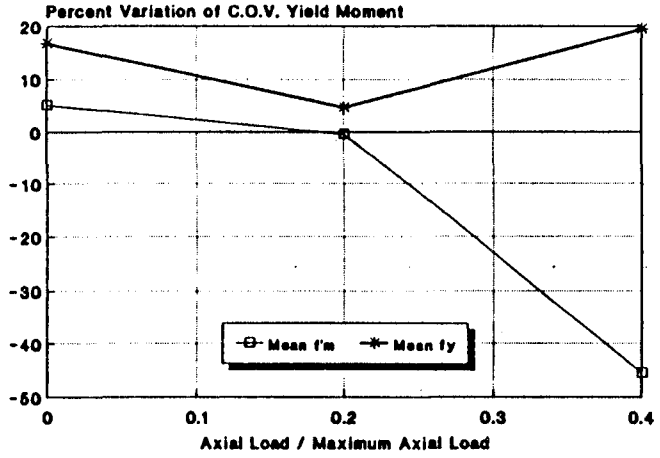

(c) C.O.V. OF My TO INCREASE OF MEAN f'm AND fy

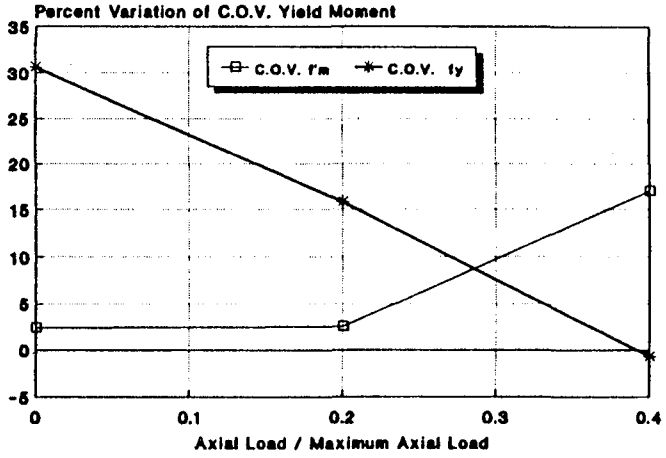

(d) C.O.V. My TO INCREASE OF C.O.V. OF f'm AND fy

FIGURE 2.3.1 PERCENT VARIATION OF YIELD MOMENT FOR A 20% INCREASE IN DIFFERENT STATISTICS OF INPUT VARIABLES

significant for 40% of the maximum load, when the 20% increase in the mean of f'_m produces a 20% increase in the coefficient of variation of M_y and a 20% increase in the mean of f_y produces a 45% decrease in the coefficient of variation of M_y.

The sensitivity of the coefficient of variation of M_y to the coefficients of variation of f'_m and f_y, as shown in Figure 2.3.1.d, exhibits features similar to the sensitivity of the mean of M_y to the mean values of the two input variables.

* The sensitivity to the variation of the coefficient of variation of f'_m increases with increasing axial load. There is low sensitivity for zero and 20% of the maximum load but the sensitivity increases to 17% for an axial load equal to 40% of the maximum load.
* The sensitivity to the variation of the coefficient of variation of f_y decreases almost linearly with increasing axial load from 30% for zero axial load to near zero when the axial force is 40% of the axial load.

In conclusion, M_y exhibits a significant sensitivity to f_y for low axial loads and to f'_m for high axial loads. The only exception to this general trend is the small sensitivity of the coefficient of variation of M_y to the mean value of f_y for large axial loads.

2.3.3 Sensitivity of the Ultimate Moment

The ultimate moment appears to show a significant dependence on f'_m and fy. The sensitivity of the mean value of the ultimate moment (M_u) to the mean values of the four input variables (f'_m, f_y, C and ϵ_{mu}) as shown in Figure 2.3.2.a, exhibits features that are similar to the sensitivity of the mean value of the yield moment (M_y).

* The sensitivity to the variation of the mean value of f'_m increases with increasing axial load. There is practically no sensitivity in the absence of axial load. The sensitivity increases to 19% when the axial load is 40% of the maximum load.
* The sensitivity to the variation of the mean value of f_y decreases with increasing axial load. The sensitivity decreases from 20% for zero axial load to 2% when the axial force is 40% of the axial load.
* The sensitivity to the variation of the mean value of the two variables characterizing the inelastic behavior of concrete masonry (C and ϵ_{mu}) is not significant.

The sensitivity of the mean value of M_u to the coefficients of variation of the four input variables, as shown in Figure 2.3.2.b, is not significant.

The sensitivity of the coefficient of variation of M_u to the mean values of the four variables, as shown in Figure 2.3.2.c, becomes significant only for 20% of the

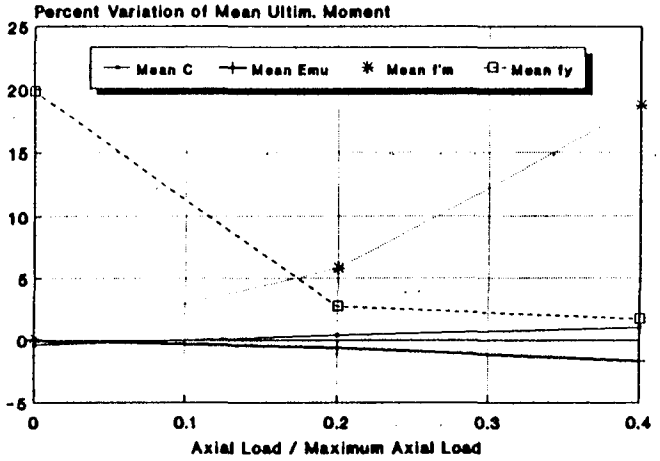

(a) MEAN Mu TO INCREASE OF MEAN C, Emu, f'm, AND fy

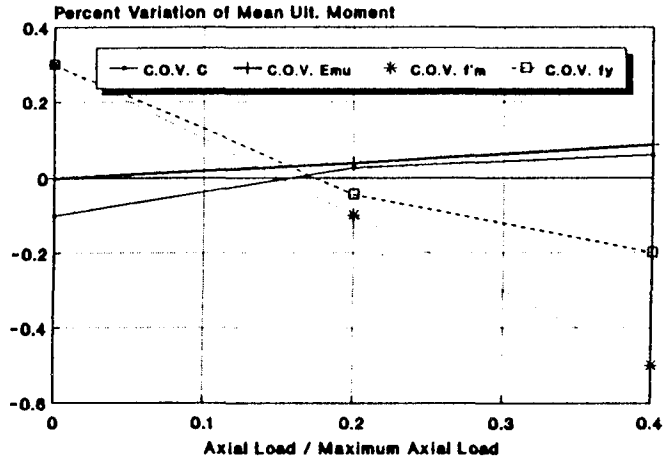

(b) MEAN My TO INCRAESE OF C.O.V. C, Emu, f'm, AND fy

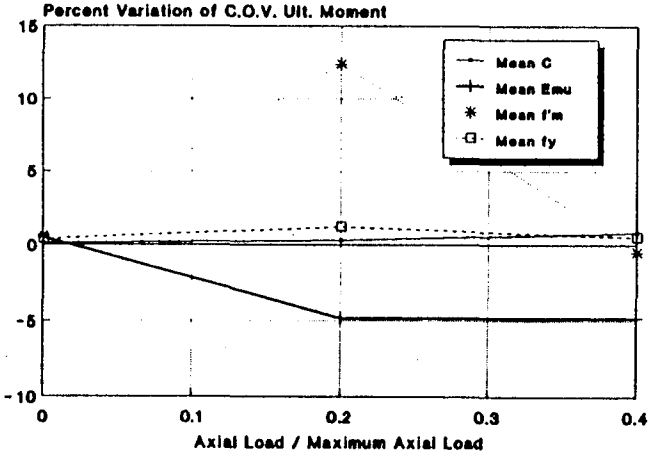

(c) C.O.V. OF Mu TO INCREASE OF MEAN C, Emu, f'm, AND fy

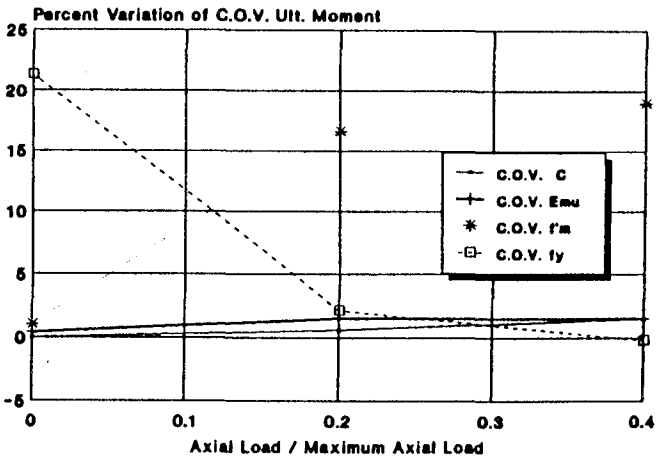

(d) C.O.V. OF Mu TO INCREASE OF C.O.V. C, Emu, f'm, AND fy

FIGURE 2.3.2 PERCENT VARIATION OF ULTIMATE MOMENT (My) FOR A 20% INCREASE IN STATISTICS OF INPUT VARIABLES

maximum load, when the 20% increase in the mean f'_m produces a 12% increase in the coefficient of variation of M_u.

The sensitivity of the coefficient of variation of M_u to the coefficients of variation of the four input variables, as shown in Figure 2.3.2.d, exhibits features similar to the sensitivity of the mean M_u to the mean values of the input variables.

* The sensitivity to the variation of the coefficient of variation of f'_m increases with increasing axial load. There is practically no sensitivity in the absence of axial load. The sensitivity increases to 19% when the axial load is 40% of the maximum load.
* The sensitivity to the variation of the coefficient of variation of f_y decreases with increasing axial load. The sensitivity decreases from 21% for zero axial load to zero when the axial force is 40% of the maximum load.
* The sensitivity to the variation of the coefficient of variation of the two variables characterizing the inelastic behavior of concrete masonry (C and ϵ_{mu}) is not significant.

In conclusion, M_u exhibits significant sensitivity to f_y for low axial loads and to f'_m for high axial loads, while it is insensitive to the variables characterizing the inelastic behavior of concrete masonry.

2.3.4 Sensitivity of the Yield Curvature and Yield Displacement.

The sensitivity of both yield curvature and yield displacement to the variations in the values of the masonry maximum compression stress (f'_m) and steel yielding stress (f_y) exhibits similar features. Consequently, they are presented together in this section.

The sensitivity of the mean values of yield curvature (ϕ_y) and yield displacement (d_y) to the mean values of masonry maximum compression stress (f'_m) and steel yielding stress (f_y), as shown in Figures 2.3.3.a and 2.3.4.a, exhibits the following features.

* The sensitivity to the variation of the mean value of f'_m increases with increasing axial load. There is no sensitivity for zero axial load. The mean value of both ϕ_y and d_y decreases 9% for a 20% increase in the mean f'_m when the axial load is 40% of the maximum load.
* The sensitivity to the variation of the mean value of f_y decreases slightly with increasing axial load from 20% for zero axial load to 15% for 40% of the maximum axial load.

The sensitivity of the mean values of ϕ_y and d_y to the coefficients of variation of the two input variables, as shown in Figures 2.3.3.b and 2.3.4.b, is not significant.

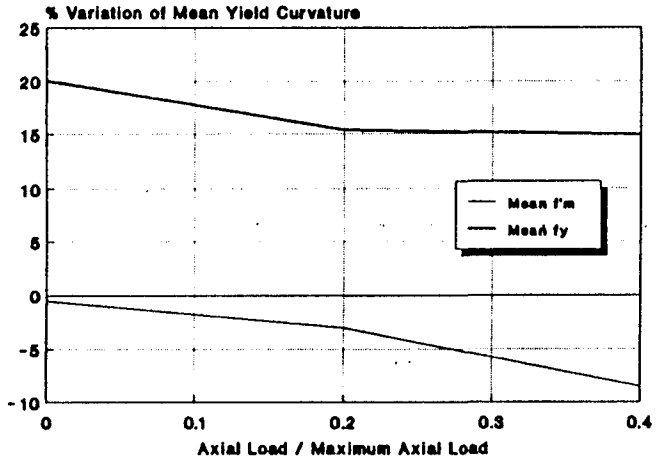

(a) MEAN YIELD CURVATURE TO INCREASE OF MEAN f'm AND fy

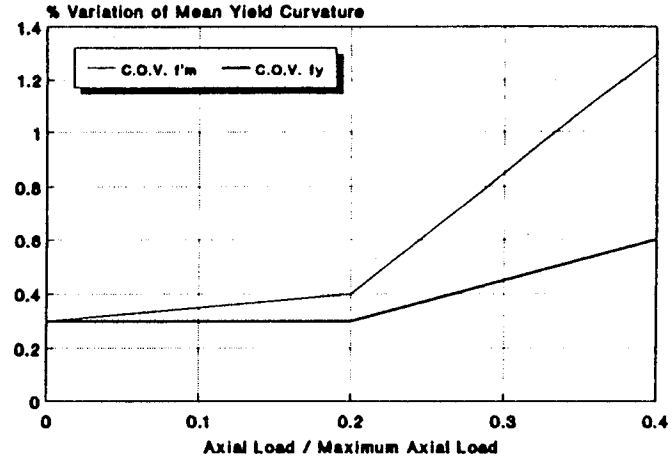

(b) MEAN YIELD CURVATURE TO INCREASE OF C.O.V. OF f'm AND fy

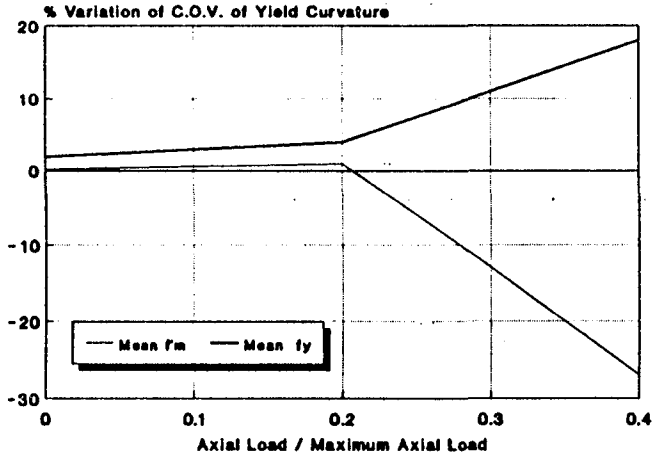

(c) C.O.V. OF YIELD CURVATURE TO INCREASE OF MEAN f'm AND fy

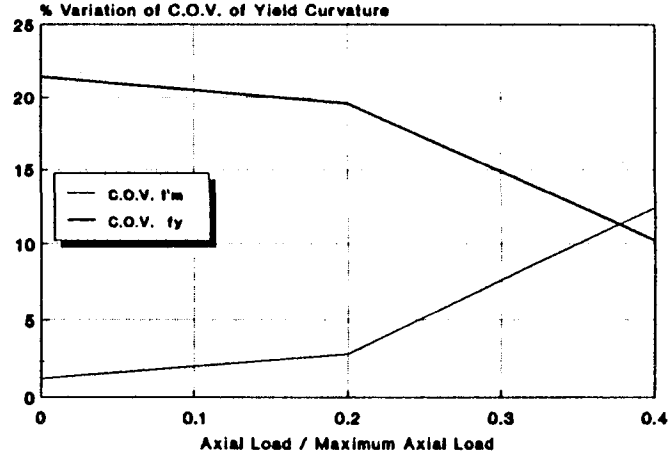

(d) COV OF YIELD CURVATURE TO INCREASE OF COV f'm AND fy

FIGURE 2.3.3 PERCENT VARIATION OF YIELD CURVATURE FOR A 20% INCREASE IN DIFFERENT STATISTICS OF INPUT VARIABLES

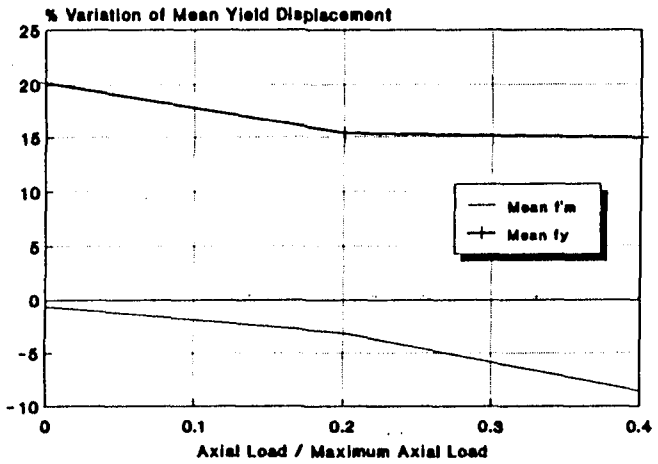

(a) MEAN YIELD DISPLACEMENT TO INCREASE OF MEAN f'm AND fy

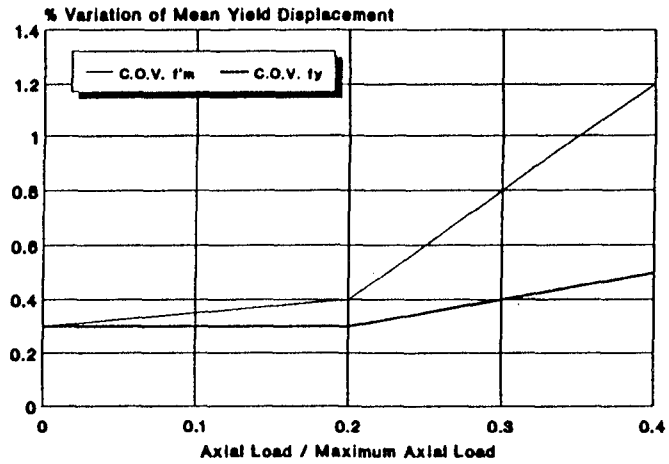

(b) MEAN YIELD DISPLACEMENT TO INCREASE OF C.O.V. f'm AND fy

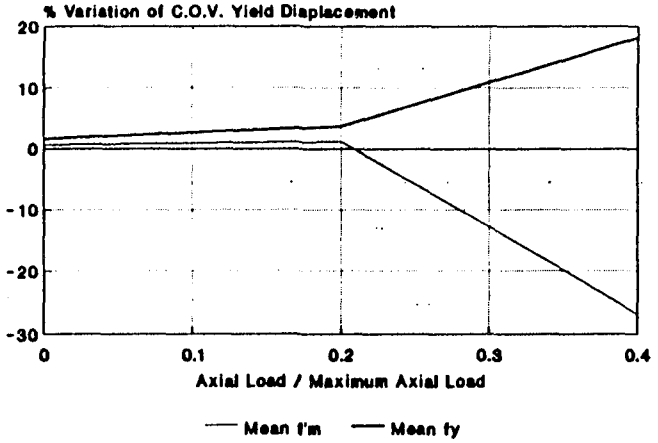

(c)COV OF YIELD DISPLACEMENT TO INCREASE OF MEAN f'm AND fy

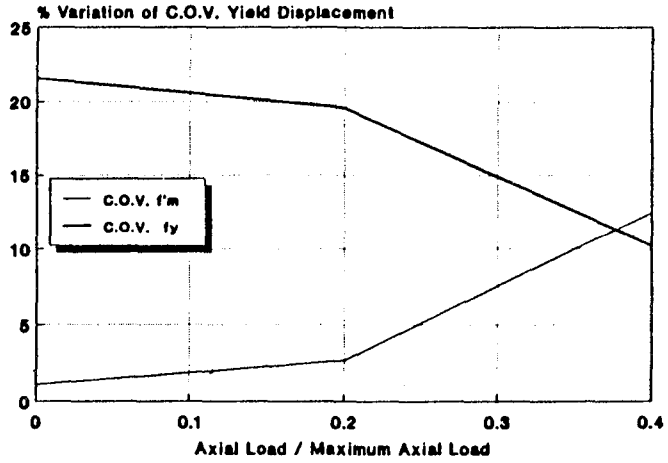

(d) COV OF YIELD DISPLACEMENT TO INCREASE OF COV OF f'm, fy

FIGURE 2.3.4 PERCENT VARIATION OF YIELD DISPLACEMENT FOR A 20% INCREASE IN DIFFERENT STATISTICS OF INPUT VARIABLES

The sensitivity of the coefficients of variation of ϕ_y and d_y to the mean values of f'_m and f_y is shown in Figures 2.3.3.c and 2.3.4.c. This sensitivity becomes significant only for 40% of the maximum load, when the 20% increase in the mean f'_m produces a 27% decrease in the coefficients of variation of ϕ_y and d_y while the 20% increase in the mean value of f_y produces a 18% increase in the coefficients of variation of ϕ_y and d_y.

The sensitivity of the coefficients of variation of ϕ_y and dy to the coefficients of variation of f'_m and f_y, as shown in Figures 2.3.3.d and 2.3.4.d, exhibits features that are similar to the sensitivity of the mean values of ϕ_y and d_y to the mean values of the two input variables.

* The sensitivity to the variation of the coefficient of variation of f'_m decreases with increasing axial load from approximately 20% for an axial load below 20% of the maximum load to 10% for an axial load equal to 40% of the maximum load.
* The sensitivity to the variation of the coefficient of variation of f_y increases with increasing axial load from 1% for zero axial load to 12% when the axial load is 40% of the maximum load.

In conclusion, ϕ_y and d_y are sensitive to f_y especially for low axial loads but are sensitive to f'_m for only high axial loads. The only exception to this general trend is the sensitivity of the coefficient of variation of ϕ_y to the mean value of f_y for large axial loads. The same exception was found previously for the sensitivity of the coefficient of variation of M_y to the mean value of f_y.

2.3.5 Sensitivity of the Ultimate Curvature

When the axial load is zero, the wall reaches its ultimate limit state when the steel strain reaches its rupture value. As a consequence, the mean ultimate curvature (ϕ_u) is not sensitive to changes in statistics of the input variables. For the same reason, the coefficient of variation of ϕ_u is small (approximately 2%) and the slight variations are inconclusive because the margin of error for this sample size is 5%. Consequently, the discussion below concerns only the 20% and 40% axial load cases.

The sensitivity of the mean value of ultimate curvature to the mean values of the four input variables, as shown in Figure 2.3.5.a, is different from the sensitivity of the mean value of the yield curvature (ϕ_y).

* The sensitivity to the variation of the mean value of f'_m is constant with varying axial load: the mean value of ϕ_u increases 18% for a 20% increase in the mean value of f'_m.
* The sensitivity to the variation of the mean value of ϵ_{mu} is constant with varying axial load: the mean value of ϕ_u increases 19% for a 20% increase in the mean value of ϵ_{mu}.
* The sensitivity to the variation of the mean values of C and f_y is not significant.

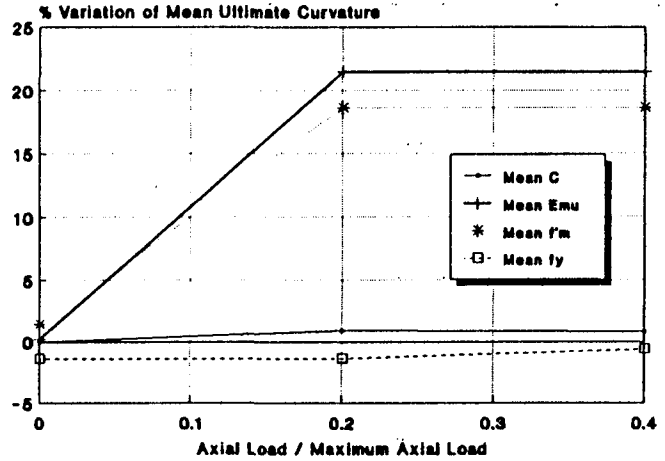

(a)MEAN ULTIMATE CURVATURE TO INCREASE OF MEAN C,Emu,f'm,fy

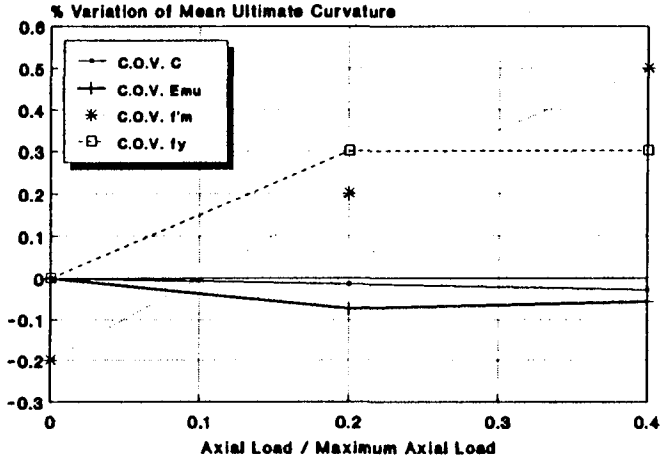

(b) MEAN ULTIMATE CURVATURE TO INCREASE OF COV C,Emu,f'm,fy

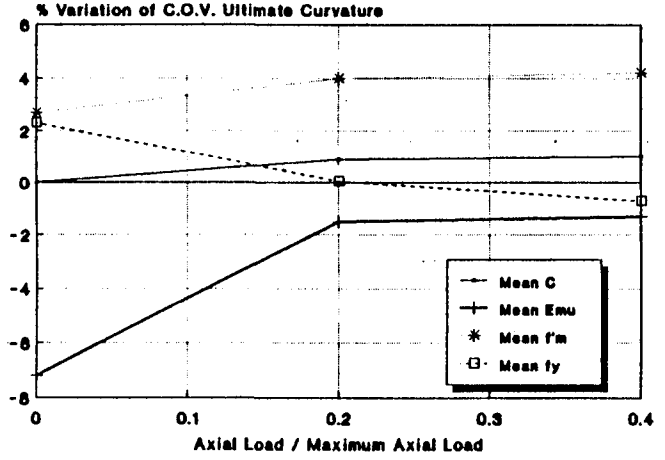

(c)COV OF ULTIMATE CURVATURE TO INCREASE OF MEAN VALUES

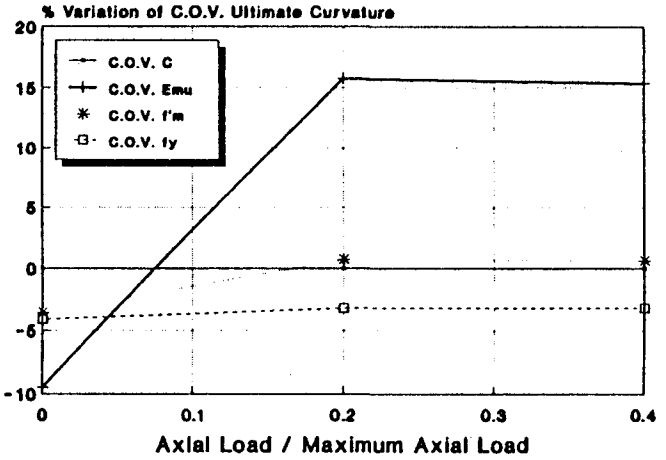

(d)COV OF ULTIMATE CURVATURE TO INCREASE OF COV C,Emu,f'm,fy

FIGURE 2.3.5 PECRENT VARIATION OF ULTIMATE CURVATURE FOR A 20% INCREASE IN DIFFERENT STATISTICS OF INPUT VARIABLES

The sensitivity of the mean value of ϕ_u to the coefficients of variation of the four input variables, as shown in Figure 2.3.5.b, is not significant.

The sensitivity of the coefficient of variation of ϕ_u to the mean values of the four variables is shown in Figure 2.3.5.c. While the 20% increase in the mean value of f'_m produces only 4% increase in the coefficient of variation of ϕ_u, the sensitivity to the other three variable mean values is very small.

The coefficient of variation of ϕ_u is only sensitive to the coefficient of variation of the maximum usable strain. As shown in Figure 2.3.5.d, the coefficient of variation of ϕ_u increases approximately 15% for a 20% increase in the coefficient of variation of ϵ_{mu}.

In conclusion, ϕ_u is sensitive only to ϵ_{mu} and f'_m and is independent of the axial load.

2.3.6 Sensitivity of the Ultimate Displacement

The sensitivity of the mean value of the ultimate displacement (d_u) to the mean values of the five input variables (f'_m, f_y, C, ϵ_{mu}, and H_p), as shown in Figure 2.3.6.a, exhibits the following features.

* For reasons explained in Section 2.3.5, the ultimate displacement for zero axial load is sensitive only to variations in the plastic hinge height.

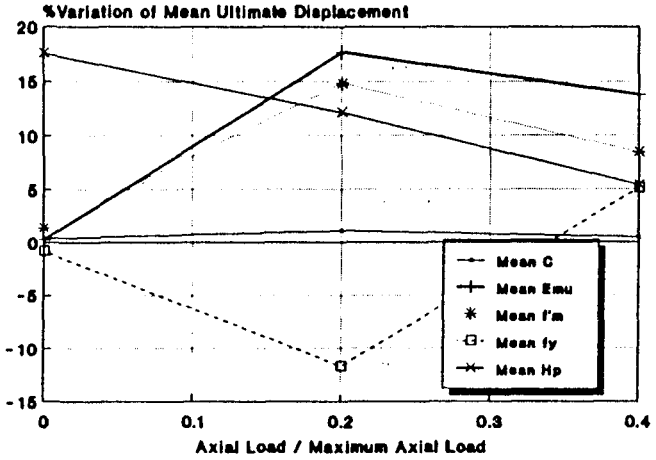

(a) MEAN ULTIMATE DISPLACEMENT TO INCREASE OF MEAN VALUES

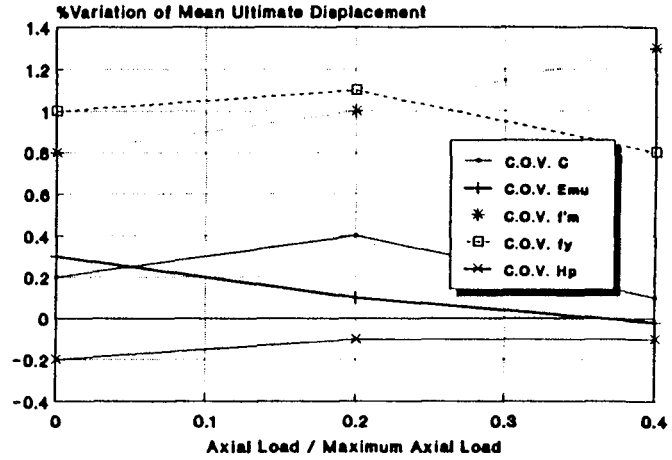

(b) MEAN ULTIMATE DISPLACEMENT TO INCREASE OF C.O.V.

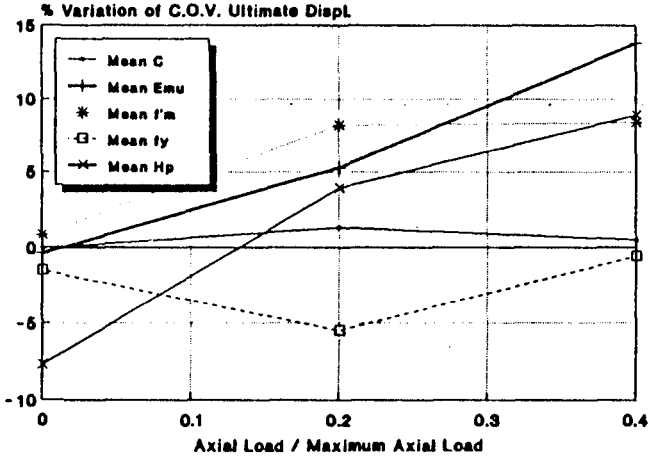

(c) COV OF ULTIMATE DISPLACEMENT TO INCREASE OF MEAN VALUES

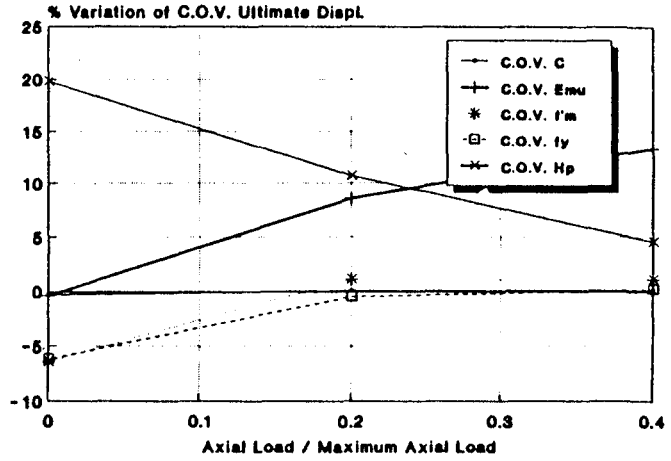

(d) C.O.V. OF ULTIMATE DISPLACEMENT TO INCREASE OF C.O.V.

FIGURE 2.3.6 PERCENT VARIATION OF ULTIMATE DISPLACEMENT FOR A 20% INCREASE IN DIFFERENT STATISTICS OF INPUT VARIABLES

* The sensitivity to the mean value of f'_m decreases from 15% for 20% axial load case to 8% when the axial load is 40% of the maximum axial load.
* The sensitivity to the variation of the mean value of f_y decreases with increasing axial load. The mean value of d_u decreases 12% for a 20% increase of the mean value of f_y for 20% axial case load but increases only 5% when the axial load is 40% of the maximum axial load.
* The sensitivity to the variation of the mean value of ϵ_{mu} decreases from 18% for 20% axial load to 14% when the axial load is 40% of the maximum axial load.
* The sensitivity to the variation of the mean value of H_p decreases from 12% for 20% axial load case to 5% when the axial load is 40% of the maximum axial load.
* The sensitivity to the variation of the mean value of C is not significant.

The sensitivity of the mean value of d_u to the coefficients of variation of the five input variables, as shown in Figure 2.3.6.b, is not significant.

The sensitivity of the coefficient of variation of d_u to the mean values of the five variables is shown in Figure 2.3.6.c.

* The sensitivity to the variation of the mean value of f'_m is small for zero axial load but increases to 8% for the axial loads higher than 20% of the maximum load.

* The sensitivity to the variation of the mean value of ϵ_{mu} increases with increasing axial load from near zero for zero axial load to 14% when the axial load is 40% of the maximum load.
* The sensitivity to the variation of the mean value of H_p is strongly dependent on the axial load. For a 20% increase in the mean H_p, the coefficient of variation of d_u decreases 8% when the axial load is zero but increases 9% when the axial load is 40% of the maximum load.
* The sensitivity to the variation of the mean values of f_y and C is not significant.

The coefficient of variation of d_u, as shown in Figure 2.3.6.d, is sensitive only to the coefficients of variation of the maximum usable strain and length of the plastic hinge.

* The sensitivity to the variation of the coefficient of variation of ϵ_{mu} increases with increasing axial load from zero for zero axial load to 13% when the axial load is 40% of the maximum load.
* The sensitivity to the variation of the coefficient of variation of H_p decreases with increasing axial load from 20% for zero axial load to 5% when the axial load is 40% of the maximum load.

In conclusion, d_u is more sensitive than ϕ_u to the five input variables.

2.3.7 Sensitivity of the Curvature Ductility

The sensitivity of the curvature ductility to the variations in the values of the four input variables exhibits features that are similar to those presented by the sensitivity of the ultimate curvature.

As shown in Figure 2.3.7.a, the mean value of curvature ductility (μ_ϕ) is sensitive only to the mean values of f'_m and ϵ_{mu}.

* The sensitivity to the variation of the mean value of ϵ_{mu} is approximately constant with varying axial load: the mean value of μ_ϕ increases 20% for a 20% increase in the mean ϵ_{mu}.
* The sensitivity to the variation of the mean value of f'_m increases very slightly with the axial load from 22% for the 20% axial load case and 25% for the 40% axial load case.
* The sensitivity to the variation of the mean values of C and f_y is not significant.

The sensitivity of the mean value of μ_ϕ to the coefficients of variation of the four input variables, as shown in Figure 2.3.7.b, is not significant.

The sensitivity of the coefficient of variation of μ_ϕ to the mean values of the four variables is shown in Figure 2.3.7.c.

* A 20% increase in the mean f'_m produces a 1% increase in the coefficient of variation of μ_ϕ for zero axial load and a 8% increase for the 40% axial load case.

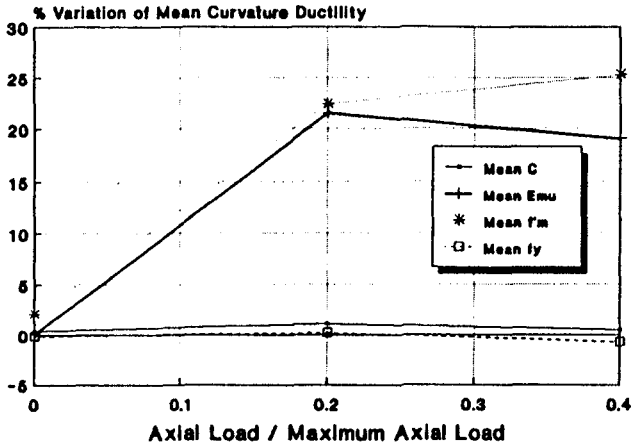

(a) MEAN CURVATURE DUCTILITY TO INCREASE OF MEAN VALUES

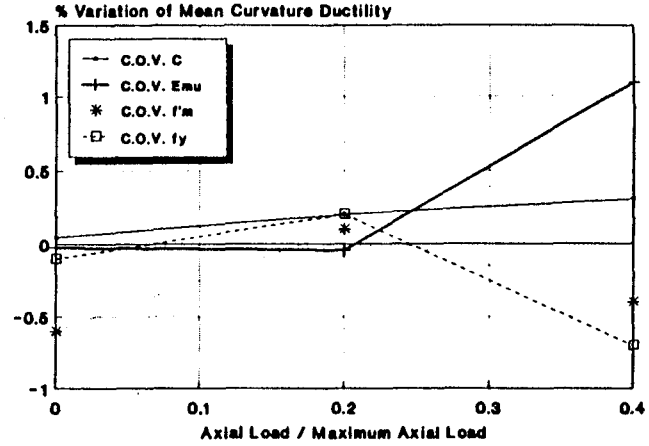

(b) MEAN CURVATURE DUCTILITY TO INCREASE OF C.O.V.

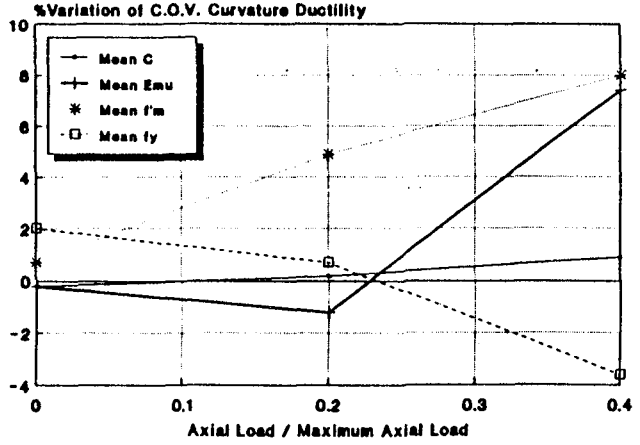

(c) C.O.V. OF CURVATURE DUCTILITY TO INCREASE OF MEAN VALUES

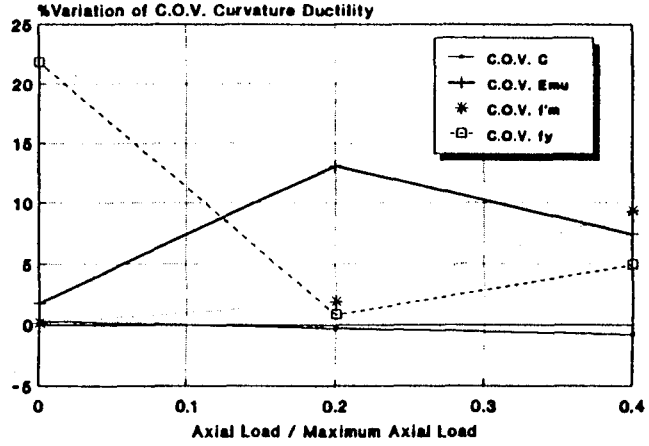

(d) C.O.V. OF CURVATURE DUCTILITY TO INCREASE OF C.O.V.

FIGURE 2.3.7 PERCENT VARIATION OF CURVATURE DUCTILITY FOR A 20% INCREASE IN DIFFERENT STATISTICS OF INPUT VARIABLES

* The sensitivity to the variation of the mean value of ϵ_{mu} becomes significant (7%) only when the axial load is 40% of the maximum load.
* The sensitivity to the variation of the mean values of C and f_y is not significant.

The sensitivity of the coefficient of variation of μ_ϕ to the coefficients of variation of f'_m, f_y, and ϵ_{mu} is strongly dependent on the axial load. As shown in Figure 2.3.7.d, the coefficient of variation increases approximately 22% for a 20% increase in the coefficient of variation of f_y for zero axial load.

As a conclusion, μ_ϕ is more sensitive to ϵ_{mu} and f'_m than it is to f_y.

2.3.8 Sensitivity of the Displacement Ductility

The sensitivity of the displacement ductility to the variations in the values of the five input variables exhibits features that are similar to those presented by the sensitivity of the ultimate displacement.

The sensitivity of the mean value of displacement ductility (μ_d) to the mean values of the five input variables (f'_m,f_y, C, ϵ_{mu}, and H_p), as shown in Figure 2.3.8.a, exhibits the following features.

* The sensitivity to the variation of the mean value of f'_m is small for zero axial load and reaches 18% for higher axial loads.
* The sensitivity to the variation of the mean value of f_y decreases with increasing axial load. The mean value of μ_d decreases 17% for a 20%

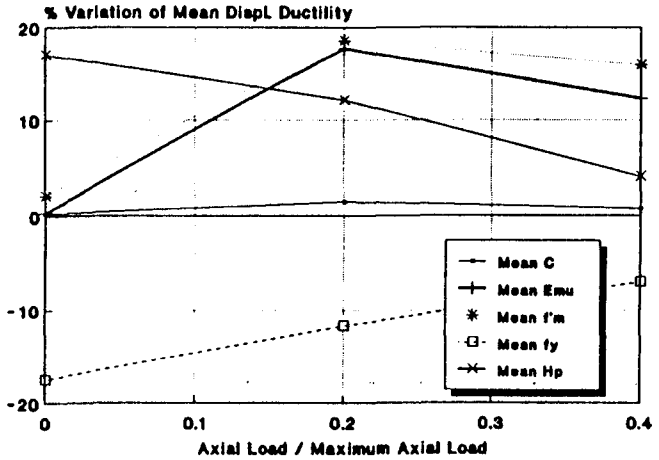

(a)MEAN DISPLACEMENT DUCTILITY TO INCRESE OF MEAN VALUES

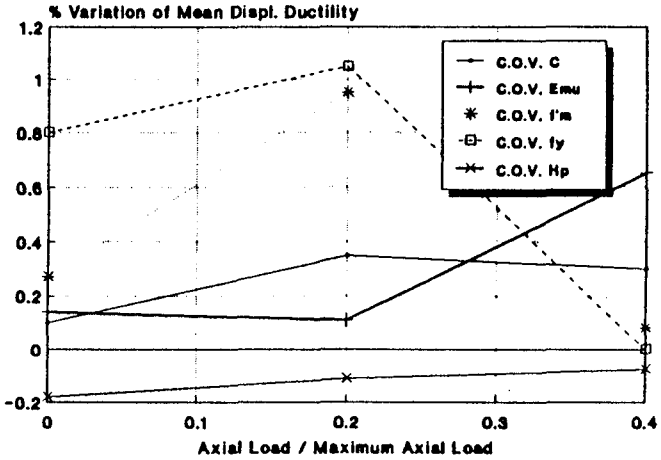

(b) MEAN DISPLACEMENT DUCTILITY TO INCREASE OF C.O.V.

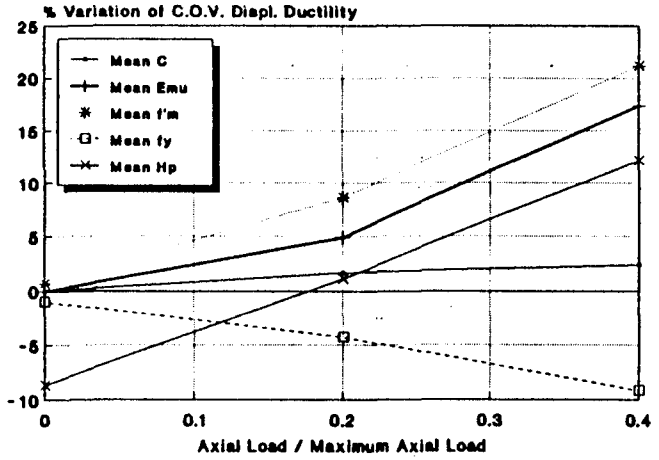

(c)COV OF DISPLACEMENT DUCTILITY TO INCREASE OF MEAN VALUES

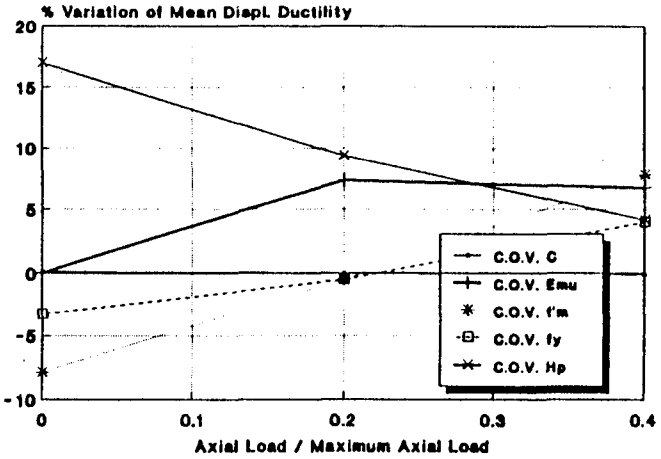

(d) C.O.V. OF DISPLACEMENT DUCTILITY TO INCREASE OF C.O.V.

FIGURE 2.3.8 PERCENT VARIATION OF DUCTILITY DISPLACEMENT FOR A 20% INCREASE IN DIFFERENT STATISTICS OF INPUT VARIABLES

increase of the mean value of f_y for zero axial load but decreases only 7% for the 40% axial load case.

* The sensitivity to the variation of the mean value of ϵ_{mu} is small for zero axial load. For higher axial loads, the sensitivity decreases from 17% for the 20% axial load case to 12% for the 40% axial load case.
* The sensitivity to the variation of the mean value of H_p decreases from 17% for zero axial load to 4% when the axial load is 40% of the maximum axial load.
* The sensitivity to the variation of the mean value of C is not significant.

The sensitivity of the mean value of μ_d to the coefficients of variation of the five input variables, as shown in Figure 2.3.8.b, is not significant.

The sensitivity of the coefficient of variation of μ_d to the mean values of the five input variables is shown in Figure 2.3.8.c.

* The sensitivity to the variation of the mean value of f'_m is small for zero axial load but increases to 21% for the 40% axial load case.
* The sensitivity to the variation of the mean value of f_y is small for zero axial load but reaches a 9% decrease for a 20% increase in the mean value of f_y for the 40% axial load case.
* The sensitivity to the variation of the mean value of ϵ_{mu} increases with increasing axial load from near zero for zero axial load to 18% when the axial load is 40% of the maximum axial load.

* The sensitivity to the variation of the mean value of H_p is strongly dependent on the axial load. For a 20% increase in the mean H_p, the coefficient of variation of μ_d decreases 9% when the axial load is zero but increases 12% when the axial load is 40% of the maximum axial load.

* The sensitivity to the variation of the mean value of C is not significant.

The coefficient of variation of μ_d, as shown in Figure 2.3.8.d, is sensitive only to the coefficients of variation of all the variables but C.

* The sensitivity to the variation of the coefficient of variation of ϵ_{mu} is approximatively 7% when the axial load exceeds 5% of maximum load.

* For a 20% increase in the coefficient of variation of H_p, the coefficient of variation of μ_d increases approximately 17% for zero axial load and increases only 4% when the axial load is 40% of the maximum load.

* The sensitivity to the variation of the coefficient of variation of f'_m is strongly dependent on the axial load. For a 20% increase in the coefficient of variation of H_p, the coefficient of variation of μ_d decreases 8% when the axial load is zero but increases 8% when the axial load is 40% of the maximum load.

* The sensitivity to the variation of the coefficient of variation of f_y is generally small. The different values between 0% and 4% increase for different levels of axial load may be inconclusive because of the large

margin of error for the coefficients of variation (5%) produced by this sample size.

In conclusion, the sensitivity of μ_d is generally lower when the axial load is large.

2.3.9 The range of values for the coefficient of variation of the output variables

After performing a Monte Carlo analysis over a large range of values for each input variable, a good estimate of the possible range of the coefficients of variation of the output variables can be obtained. A very interesting feature is that several coefficients of variations of the output variables (ϕ_y, d_y, ϕ_u, and μ_ϕ) have a narrow range of variation if the zero axial load case is disregarded. The range of values for the coefficients of variation of each output variable when the zero axial load cases are disregarded presented in Table 2.3.7.

Table 2.3.7
Coefficients of Variation of the Output Variables

Output Variable	Coefficient of Variation
M_y	8% - 10%
ϕ_y	7% - 12%
d_y	7% - 12%
M_u	8% - 12%
ϕ_u	18% - 20%
d_u	13% - 27%
μ_ϕ	20% - 22%
μ_d	16% - 29%

The narrow range of variations noted in Table 2.3.7 allows for assigning "off-shelf" values to the coefficients of variation of several output variables, as follows.

* Yield variables (M_y, ϕ_y, and d_y) and ultimate moment (M_u): 10%;

* Ultimate curvature (ϕ_u) and curvature ductility (μ_ϕ): 20%.

For the yield output variables and ultimate moment, minimum uncertainty is obtained when the axial load is 10% to 20% of the maximum axial load. For the ultimate curvature and curvature ductility, minimum uncertainty is found for the zero axial load case. The ultimate displacement and displacement ductility exhibit minimum uncertainty for 40% of the maximum axial load.

2.3.10 Probability density functions for the variables of the wall capacity.

Histograms for curvature and displacement ductility at different levels of axial load are presented in Figures 2.3.9 and 2.3.10. It is worth noting that, in general, the histograms shape does not significantly change with the magnitude of the axial load. There are two exceptions to this observation:

(1) For low axial load the shape of the curvature ductility histogram is governed by the limit states described in section 2.2.1. As shown in Figure 2.3.9, the histogram for zero axial load (where the failure occurs due to rupture of the steel bars) is different from the histogram for the 2.5% axial load case (where the same limit state occurs with a frequency of 37%). In the latter case, the dichotomy in the statistical

WALL WITH MINIMUM VERTICAL REINFORCEMENT	SENSITIVITY STUDY

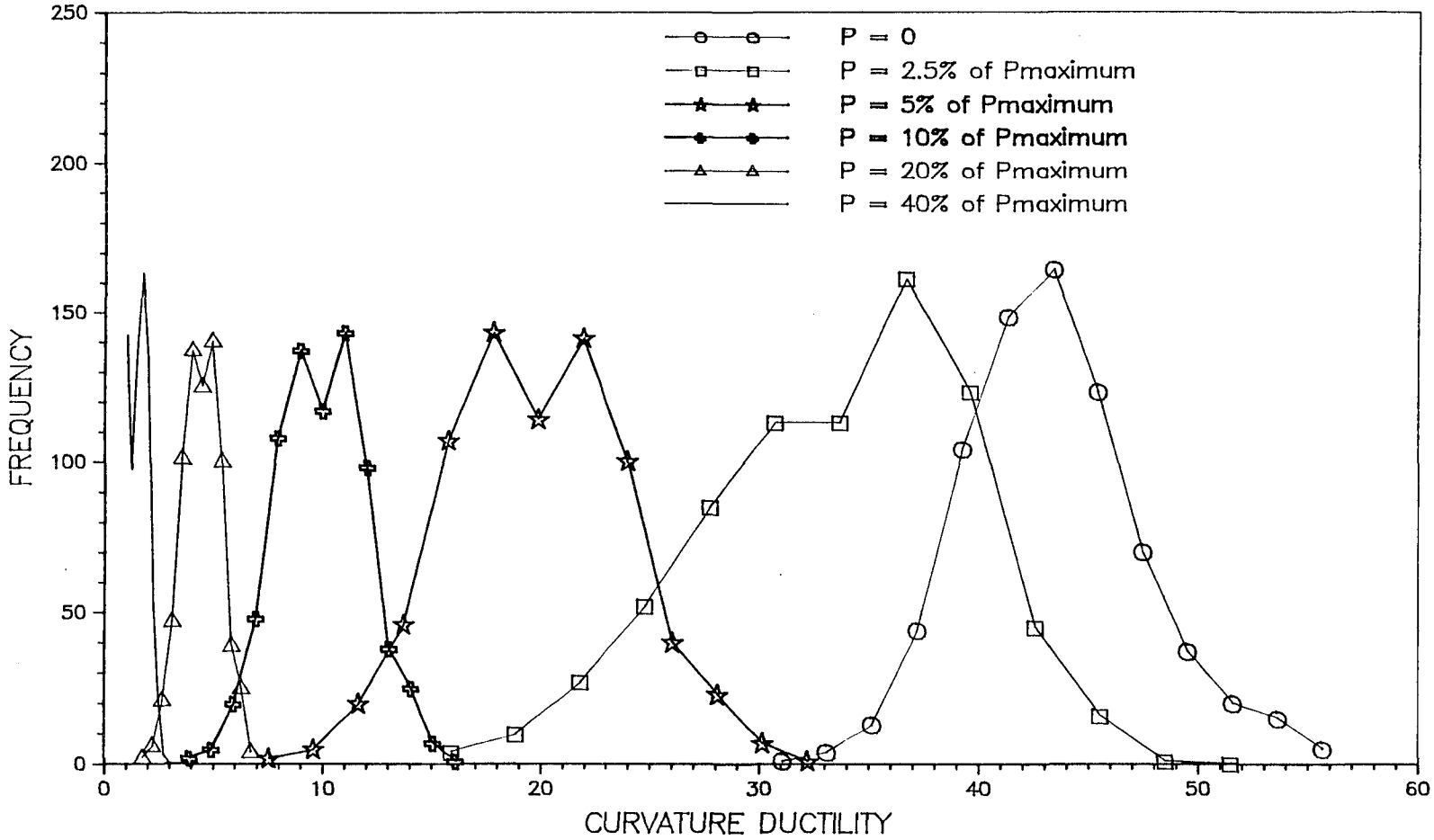

FIGURE 2.39 HISTOGRAMS OF CURVATURE DUCTILITY

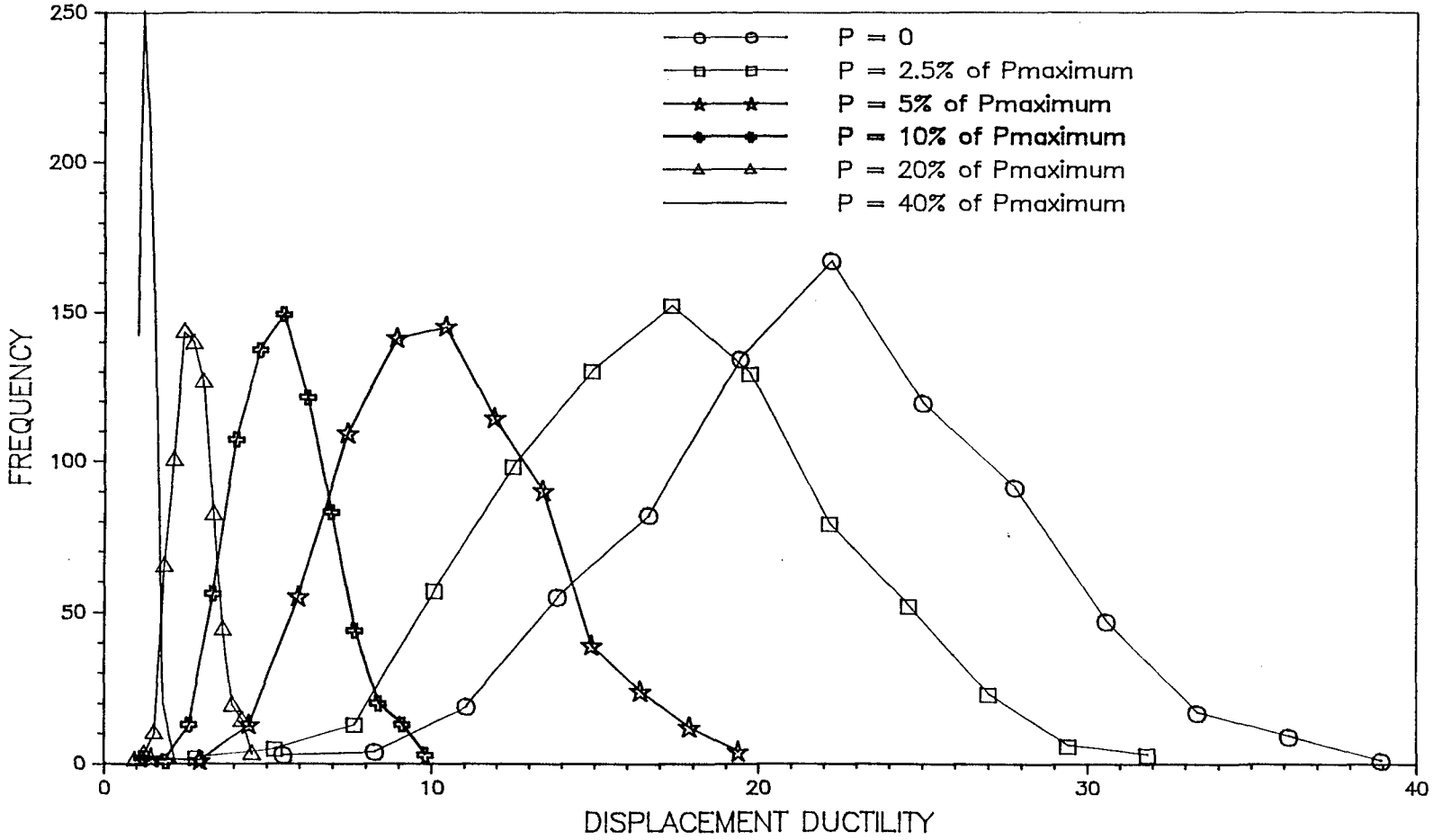

FIGURE 2.3.10 HISTOGRAMS OF DISPLACEMENT DUCTILITY

sample produced by the two different modes of failure is mirrored by the irregular shape of the histogram. It is difficult to explain the bi-modal feature exhibited by the histograms obtained for 5%, 10%, and 20% axial load cases, but at least the feature is consistent for the range of axial load that produces the second limit state only. In the case of displacement ductility, the uncertainty in the plastic hinge length is dominating and the limit states do not have the same discriminatory effect.

(2) For high axial load the histograms distributions are truncated at $\mu = 1$ due to combinations of input variables that result in brittle failure.

For axial loads that do not produce brittle failure the histograms for curvature ductility exhibit a symmetric shape, suggesting the possibility of fitting a normal probability density function model to the data, while the displacement ductility appears to be log-normally distributed. This essential difference is produced by the fact that small values of displacement ductility can be produced even in the absence of the axial load. This is attributed to the random position of the plastic hinge that only comes into play for the displacement ductility. As a consequence, the probability density curves for μ_d are "squeezed" at their left tail and constrained to reduce their spread as their mean value decreases. This condition does not occur for curvature ductility; in absence of this squeeze, μ_ϕ can keep a constant coefficient of variation and the probability density curves can preserve their symmetry.

2.3.11 Conclusions regarding the sensitivity of the wall capacity.

(1) All the output variables characterizing the lateral force resisting capacity are insensitive to the variable C of the Sajjad model for the falling branch of the confined concrete masonry stress-strain curve. However, this conclusion may not be upheld when defining the maximum usable strain at percentages of maximum stress that is lower than 50%. This conclusion is very important because it allows for the characterizing of the randomness of the post-elastic properties of concrete masonry employing only the maximum usable strain.

(2) The input variables that introduce the highest uncertainty in the output variables are the axial load in the wall and, for the ultimate displacement and displacement ductility, the height of the plastic hinge.

(3) For zero axial load, the predominant limit state is the rupture of the steel bars. Consequently, the ultimate output variables are only sensitive to the plastic hinge location and the steel yield stress.

(4) As expected, higher f'_m and ϵ_{mu} produce higher ductility, and higher f_y produces lower ductility displacement. The lack of sensitivity of curvature ductility to the increase in f_y was less than expected.

(5) When the axial load is large, the output variables are more sensitive to increases of the mean value of f'_m. When the axial load is small, the output variables are more sensitive to increases in the mean value of f_y.

This occurs because low axial load implies a ductile limit state of yielding of the steel while a large axial load produces a brittle limit state characterized by concrete masonry crushing, thus governed by the compressive strength of concrete.

(6) The mean values of the output variables are insensitive to the increase of the coefficients of variation of the input variables. This conclusion allows us to use constant coefficients of variation for the material characteristics in our further research.

(7) On the contrary to the previous conclusion, the coefficients of variation of the output variables are sensitive to increases in the mean values of the input variables, especially when the axial load is large. This is attributed to the interdependence between the axial load and some of the input variables. As an example, adding steel has almost the same effect on ultimate capacity as increasing axial load. Consequently, uncertainty varies with steel content (or strength) in a similar way that it varies with axial load. The sensitivity of the coefficients of variation of the output variables to changes in the mean values of the input variables is sometimes higher than the sensitivity to changes in the coefficients of variation of input variables. This is the case for the ductility displacement when the axial load is large.

(8) The ultimate curvature is independent of the axial load.

(9) Several coefficients of variations of the output variables have a narrow range of variation. A remarkable finding is that curvature ductility has an almost constant coefficient of variation: 20%. The approximative value for the yield curvature and yield displacement is 10% whereas for the ultimate curvature it is 20%. The values for ultimate displacement and ductility displacement are strongly dependent on the axial load, decreasing from a high of 26%-29% for 5% of the maximum axial load to a low of 13%-17% for 40% of the maximum axial load.

The above outlined conclusions are valid for deterministic axial loads and the features of the studied wall: a minimum reinforcement ratio and an aspect ratio of approximately 4 to 1.

CHAPTER 3

CONSIDERATIONS IN RELIABILITY ANALYSIS OF MASONRY WALL SYSTEMS

3.1 SECOND MOMENT RELIABILITY INDEX

Estimation of the failure probability even for simple elements is a complex problem because it requires complete knowledge of the probabilistic distributions of all load and resistance parameters. Any decision in selecting a particular distribution must be justified by the accuracy to which the tails (low probability region) of the theoretical distribution follow the real distribution. An oversight in this regard can lead to inaccuracies that can cloud any use of probabilistic methods. A further difficulty is the frequent inability to express the distribution of the load effects in closed form. This naturally leads to the need of using Monte Carlo simulations that are not suitable for estimating low probabilities of failure. In order to avoid this tail sensitivity problem, the so called "second-moment reliability methods" were introduced. The idea behind second-moment reliability theory is that all uncertainties concerning the structural reliability are expressed only in terms of expected values and covariances of the involved load and resistance

parameters, z_i. By equating the load to the resistance function of the given parameters, a limit state equation is obtained:

$$g(z_i) = 0 \qquad (3.1.1)$$

Equation (3.1.1) represents the "failure surface" (or "limit state surface") in the (z_i) space of basic parameters. This leads to a unique division of the space into a "safe set" and a "failure set". The random variable obtained by replacing the parameters z_i in the failure surface is called safety margin or limit state function:

$$M = g(z_i)$$

Cornell (1969) defined a reliability index β_C as the ratio of the expected value of M and the standard deviation of M. Ditlevsen (1973) observed that, according to this definition, β_C depends on the particular choice of failure function. To resolve this ambiguity, Hasofer and Lind (1974) mapped the variables z_i into a set of uncorrelated, standard variables x_i so that the mean value of x_i is 0 and the standard deviation of x_i is 1. They defined the reliability index β_{HL} as the smallest distance from the origin to the failure surface, measured in the (x_i) space. The point on the failure surface that is closest to the origin is called the "design point".

To obtain the design point and the reliability index β_{HL}, the limit state equation is rewritten in terms of the standardized variables x_i:

$$\mathfrak{G}(x_1, x_2, \ldots, x_n) = 0 \qquad (3.1.2)$$

We consider a point in the n-dimensional design space

$$\xi_0 = [x_1^0 x_2^0 ... x_n^0]^T$$

on the limit state surface

$$\mathfrak{G}(\xi_0) = 0 \tag{3.1.3}$$

and expand $\mathfrak{G}(\xi)$ into a Taylor series about the point ξ_0 :

$$\mathfrak{G}(\xi)=\sum_{k=0}^{\infty} \frac{1}{k!} \left\{ \sum_{i=1}^{n} \Delta x_i^0 \frac{\partial}{\partial x_i} \right\}_0^k \mathfrak{G}(\xi) \tag{3.1.4}$$

where $\Delta x_i^0 = x_i - x_i^0$ and the partial derivatives of the current order, k , are calculated at ξ_0 . The choice of ξ_0 should be restricted to points for which the normal to the limit state surface is not parallel to any of the coordinate axes in order to avoid any partial derivatives becoming equal to infinity.

If we neglect in the right hand side of Equation (3.1.4) the nonlinear terms ($k \geq 2$), we obtain the equation of a hyperplan that is tangent to the limit state surface in ξ_0 . The linear approximation $\mathfrak{G}_0$ of the limit state function $\mathfrak{G}$ can be written using the scalar product of two vectors:

$$\mathfrak{G}_0 = \Delta \xi_0^T G_0 \tag{3.1.5}$$

where

$$\Delta \xi_0 = [\Delta x_1^0 \Delta x_2^0 ... \Delta x_n^0] \tag{3.1.6}$$

$$G_0=\left[\left(\frac{\partial \mathfrak{G}}{\partial x_1}\right)_0 \left(\frac{\partial \mathfrak{G}}{\partial x_2}\right)_0 ... \left(\frac{\partial \mathfrak{G}}{\partial x_n}\right)_0\right]^T \tag{3.1.7}$$

We calculate the mean and standard deviation of $\mathfrak{G}_0$ recalling that the mean value of x_i is 0 and the standard deviation of x_i is 1.

$$E[\mathfrak{G}_0] = -\xi_0^T G_0 \tag{3.1.8}$$

$$\sigma_{\mathfrak{G}_0} = (G_0^T G_0)^{\frac{1}{2}} \tag{3.1.9}$$

According to the definition

$$\beta_{HL,0} = \frac{E[\mathfrak{G}_0]}{\sigma_{\mathfrak{G}_0}} = -\frac{\xi_0^T G_0}{(G_0^T G_0)^{\frac{1}{2}}} \tag{3.1.10}$$

The point ξ_* on the limit state surface that produces the minimum value of $\beta_{HL,0}$ is called "design point" and the corresponding β_{HL} is the Hasofer-Lind Reliability Index. It can be shown (Shinozuka, 1983) that β_{HL} is the minimum distance between the origin of the coordinates in the space of the standardized variables x_i (i.e. the expected value of the limit state function) and the limit state surface. Rackwitz and Fiessler (1978) proposed an iterative algorithm to determine the design point and the Hasofer-Lind Reliability Index.

The original papers by Cornell and Hasofer-Lind used the term reliability index. Hereafter we will call this term the safety index which is the preferred term in current structural masonry code development.

3.2 GENERALIZATION FOR THE MULTISTATE SPACE

When the ultimate limit state is conditioned by the previous occurrence of one or more other limit states, the safety index can not be found using the classical First Order Second Moment solution (Hasofer-Lind). Instead of one limit state surface in the space of normalized random variables, each condition introduces a new surface characterizing a particular limit state. Each "conditional surface" splits the ultimate limit state surface in two regions: a region where the respective condition is fulfilled and one where it is not. If the design point (the closest point from the origin) is found in an undesirable region of the ultimate surface, then this design point is considered to be a "false solution". The "true solution" is to be found on the n-dimensional curve resulting from the intersection of the ultimate and conditional surfaces. The problem then becomes to find the point on the intersection curve that is closest to the origin of the space of normalized coordinates.

In some engineering problems, the ultimate limit state can not be described by an equation. Instead, the failure can be obtained through a certain sequence of conditional limit states. An example is the reinforced concrete masonry wall subjected to bending and compression. Since the brittle failure has to be avoided, the yielding of the tension steel has to occur before the crushing of the concrete masonry. The first conditional surface (G_1) is represented by the equation f_y-f_s=0, while the second (G_2) is ϵ_{mu}-ϵ_c=0. If the distance to the surface G_1 is smaller than

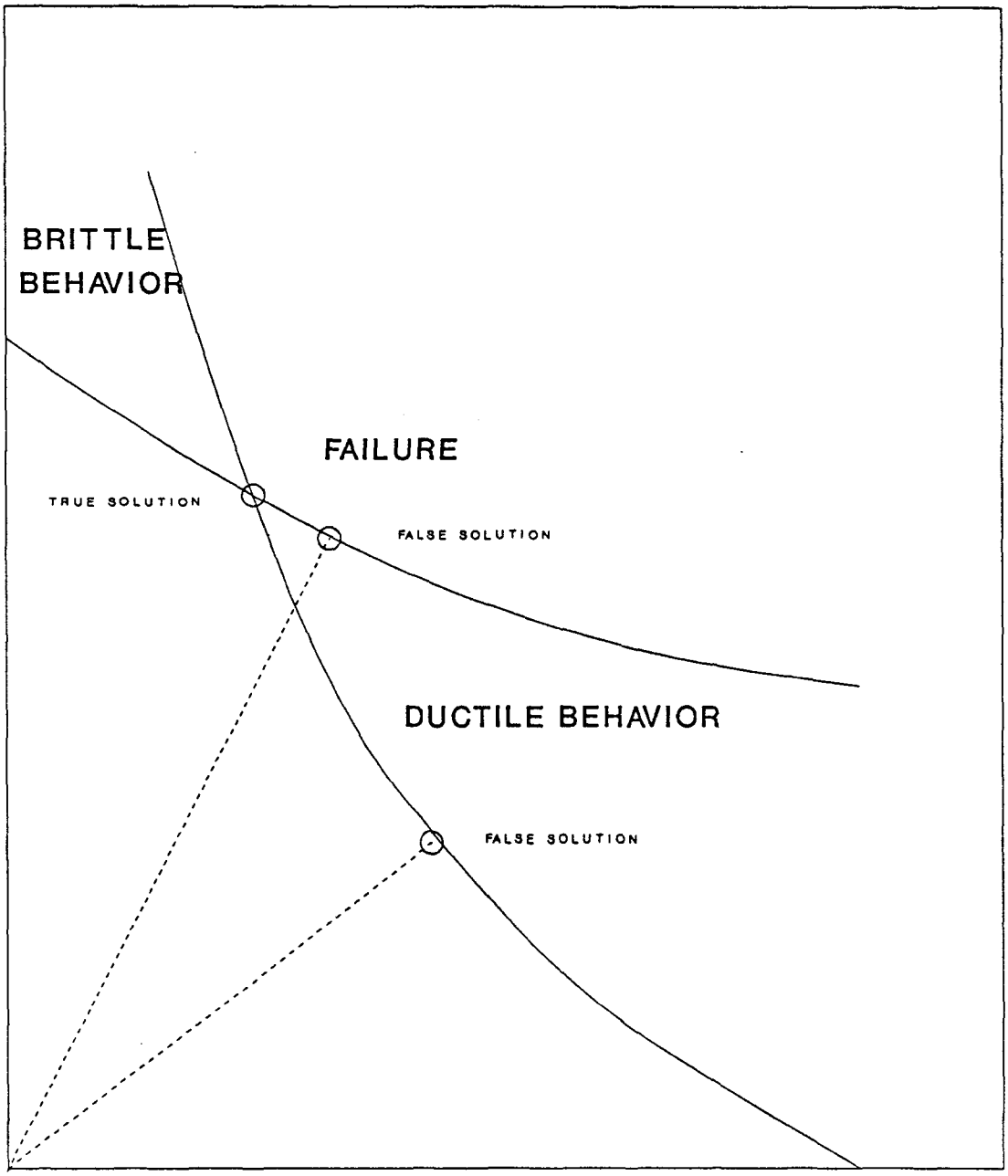

FIGURE 3.2.1 CONDITIONAL LIMIT STATES:
G1 CLOSEST TO THE ORIGIN

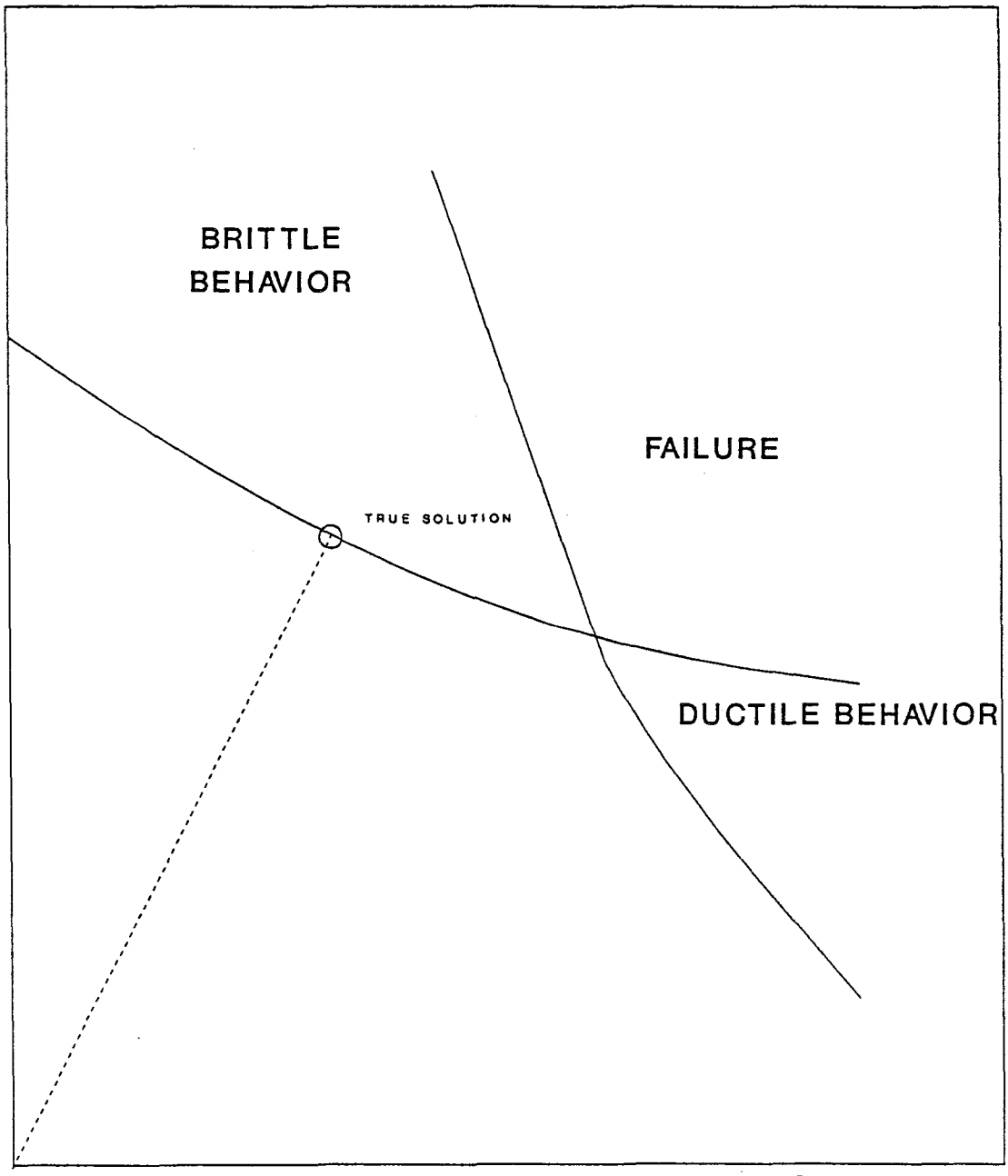

FIGURE 3.2.2 CONDITIONAL LIMIT STATES:
G2 CLOSEST TO THE ORIGIN

the distance to the surface G_2 and the closest point to the surface G_2 is found in the region where $f_s > f_y$, then this is a "false solution" because there is no concern associated with a ductile failure (see Figure 3.2.1). The "true solution" is likely to be found on the curve produced by the intersection of the two surfaces. If the distance to the surface G_2 is smaller than the distance to the surface G_1 (see Figure 3.2.2), the true solution can be found easily on G_2.

In Appendix E, the problem of the failure conditioned by several limit states is identified. Then, a new iterative algorithm that uses Lagrange Multipliers to obtain the design point and the safety index is proposed.

3.3 THE SAFETY INDEX OF DUCTILE BEHAVIOR

In Section 3.2, an example of safety index in a multistate space problem was given for the concrete masonry wall subjected to bending and compression. Since brittle failure has to be avoided, the yielding of the tension steel has to occur before the crushing of the compressed concrete. The first conditional surface is represented by the limit state equation f_s-f_y=0, while the second surface is ϵ_{mu}-ϵ_c=0. Unfortunately, the two equations can not be written as a function of the input random variables in a closed form because of the complexity created by the distribution of the reinforcing bars along the wall section. It is best to solve the problem is to use the results of a Monte Carlo simulation. This is the purpose of the next Chapter of this study.

There is a temptation to simplify the problem by overlooking its multistate character. This can basically be done by considering the unique limit state equation

$$P - P_{balanced} = 0 \qquad (3.3.1)$$

where

P = axial load in the wall

$P_{balanced}$ = axial balanced load in the wall

Equation (3.3.1) can be written as a function of the input parameters if the following series of simplifications are adopted: neglecting the compression steel; lumping the tension steel at a single location; neglecting the randomness of the shape of the strain-stress curve, etc. The Rackwitz-Fiessler algorithm can then be used to obtain the Hasofer - Lind safety index β_{HL}. For illustrative purposes, two similar approaches are developed in Appendix C.

However, this over-simplification by violating the multistate character of the problem can not be done without paying a heavy price. Equation (3.3.1) is written for the situation when the steel yields simultaneously with the concrete masonry reaching its maximum usable strain at the extreme fiber. In most cases, the strain in the extreme steel bar is greater than the yield strain when the concrete masonry crushes. For this reason, the two approaches in Appendix C produce grossly overestimated safety indices. This overestimation may exceed one unit of β.

3.4 COMPARISON BETWEEN THE DISPLACEMENT DEMAND PRODUCED BY GROUND MOTION AND THE YIELD DISPLACEMENT FOR CONCRETE MASONRY WALLS

The characterization of the seismic hazard for a specific building site is usually done using response spectra whose ordinates are associated with a given probability of exceedance during a chosen exposure time. The exposure time commonly used is 50 years because it corresponds to the expected lifetime of typical buildings. The response spectra used for the design of new buildings are usually associated with a probability of exceedance of 10 percent during the 50 years exposure time. However, a better picture of the seismic hazard is obtained by considering a "probable" expected level of response spectra during the same exposure time. Since the probability distribution of response spectra ordinates is not symmetrical, the extreme values at the upper end of the scale exert a strong influence on the mean value. For this reason the median estimator is often preferred resulting in response spectra with ordinates associated with 50 percent probability of exceedance.

The percent of critical damping usually associated with reinforced concrete masonry structures varies from 5 percent for small amplitudes of building motion to 10 percent for response amplitudes at or near yielding.

The fundamental period for the structure in Appendix A can be calculated using formulas (12-3) and (12-4) in the 1988 Edition of the Uniform Building Code

(ICBO, 1988). Such a calculation results in a period approximately equal to 0.6 seconds. If soil structure interaction is considered as well as a certain amount of stiffness degradation due to small cracking in the concrete masonry, it is reasonable to believe that this period can reach 0.9 seconds before any yielding may occur in the wall. Hart, Thurston and Englekirk (1989) have calculated the fundamental period for the prototype structure located in Whittier using several assumption for the stiffness degradation and found values between 0.9 and 1.1 seconds.

For the purpose of comparison we will consider in this research response spectrum ordinates corresponding to 0.6 seconds and a damping value equal to 5 percent critical, and spectral ordinates corresponding to 1.1 seconds and 10 percent of critical damping. The displacement response spectra used in this research were developed for a location in downtown Los Angeles by Woodward - Clyde Consultants and the response spectra ordinates are presented in Table 3.4.1.

Table 3.4.1 Displacement Response Spectra Ordinates for downtown Los Angeles

Probability of Exceedance for the Spectral Ordinate	Spectral Ordinates (inches)	
	T = 0.6 sec Damping = 5%	T = 1.1 sec Damping = 10%
50% in 50 years	1.25	1.73
10% in 50 years	2.56	3.53

To estimate the displacement demand at the top of the wall for the response spectra ordinates considered in Table 3.4.1, a participation factor of 1.4 was considered (Englekirk and Hart, 1984). The seismic displacements demands on the wall are presented in Table 3.4.2.

Table 3.4.2 Top of Wall Displacement Demand for a site in downtown Los Angeles

Probability of Exceedance for the Spectral Ordinate	Top Displacement (inches)	
	T = 0.6 sec Damping = 5%	T = 1.1 sec Damping = 10%
50% in 50 years	1.75	2.42
10% in 50 years	3.58	4.94

The expected value of the displacement of the top of the wall corresponding to the first yield of the reinforcement in the wall can be estimated using the results presented in Chapter 2. For the wall under study with a vertical load equal to $0.1A_g f'_m$ the expected value of the top displacement at yield is 2.25 inches (See Table 2.2.2 and Figure 2.2.5).

Hart and Jaw (1991) have calculated the expected top displacement at yield for the following three types of reinforced concrete masonry walls that have approximately the same height as the wall studied in Chapter 2:

(1) 22'-8" long rectangular wall (like in Chapter 2);

(2) 30'-8" T-shaped wall;

(3) 45'-4" L-shaped wall;

The longitudinal reinforcement ratio for these walls was approximately twice that used for the wall in Chapter 2. Because of the non-symmetrical section of the last two walls, the force-displacement relationship is strongly dependent on the direction of the horizontal force. The wall yields at a smaller load when the wall flange is in compression compared to the case when the horizontal force is reversed and the wall flange is in tension. The displacement at the top of each wall at yield are presented in Table 3.4.3.

Table 3.4.3 Top Displacement at Yield (in inches) for three types of Reinforced Concrete Masonry Walls (after Hart and Jaw, 1991)

Wall Type	Displacement at Top of Wall at Yield	
	Stress in Wall Flange	Deflection (in)
Rectangular		2.9
T-Shape	Compression	1.6
	Tension	2.8
L-Shape	Compression	1.2
	Tension	1.6

Hart and Jaw have also estimated the fundamental period of the building that contains the above mentioned walls to be in the range of 1.3 to 1.5 seconds. This would result in even greater displacement demands than those presented in Table 3.4.2.

Comparing the expected values of the displacement demands (Table 3.4.2) to the expected values of the deflection at yield for different walls we can conclude that:

* For rectangular walls, the yield displacement (2 to 3 inches) is in the same range with the displacement demand during the *expected* strong motion earthquake. However, the yield displacement is less than the displacement demand from a *design* strong motion earthquake.
* For flanged walls, the yield displacement (1 to 2 inches) is expected to be exceeded during the *expected earthquake*.

These findings as well as the high uncertainty associated with the characteristics of a future strong motion lead to the conclusion that a reinforced concrete masonry flexural wall can not withstand a major earthquake without ductility. Consequently, we must consider the ductile behavior as a *limit state* in assessing the safety of reinforced concrete masonry structures. This finding has to be construed as a strong motivation for the approach proposed in the previous section. The following sections of this chapter will study the influence of the variation of input parameter to the frequency of the brittle behavior and will define a "Ductility Index" as the safety index of ductile behavior.

CHAPTER 4

RELIABILITY ANALYSIS OF A SINGLE FLEXURAL WALL.

4.1 GENERAL

The theoretical framework introduced in Chapter 3 allows for a restatement of the reliability of a flexural wall subjected to strong ground motion excitations. Since an estimate of the first and second moments for the parameters of future ground motion at a certain site can not be done at this time with an acceptable degree of confidence, an ultimate limit state equation that contains the load can perhaps be viewed as an exercise in futility. Therefore, a reasonable way to approach the problem must be in line with the current seismic design philosophy that is to provide a structural element with a ductile behavior and then require limits on available ductility. From this prospective, the reliability of the wall is viewed as the conditional probability that ductility demand will be less than ductility capacity, given that the wall will behave in a ductile manner. This concept leads to a two step approach and it enables the structural problem to be separated from the engineering seismology problem. The problem is formulated as two steps which are as follows:

Step (1) Determine the probability of ductile behavior and define the associated safety index.

Step (2) Determine the probability that the ductility demand will be less than the ductility capacity.

The limit state equation linking the ductility demand to the ductility capacity should be written at the structural system level. The present approach permits this desideratum by splitting the first step in two tasks:

Task (1) Estimating the probabilistic distribution of the ductility capacity and the associated safety index for individual walls;

Task (2) Estimating the probabilistic distribution of the available ductility and the associated safety index for the structural system as a whole.

This chapter will be devoted to the first task while the next chapter will use the results of this chapter in order to fulfill the second task.

The second step of the problem constitutes a formidable task in itself and it is beyond the scope of this research. However, in conceiving the format for the safety index to be produced within the first step, one has to bear in mind the need for compatibility to the second step product. A comprehensive representation of the probabilistic information regarding the available ductility should be correlated to a similar index describing the seismic activity of a site or region.

4.2 INFLUENCE OF THE AXIAL FORCE ON THE BRITTLE BEHAVIOR OF THE WALL.

The simplest measure of the brittleness of a reinforced concrete masonry wall for a certain combination of the input random variables is given by the frequency of the brittle behavior, i.e. the number of realizations that result in brittle behavior divided by the total number of realizations in a Monte Carlo simulation. According to the results of the Monte Carlo simulation presented in Chapter 2, when the axial force on the wall is $0.2A_g f'_m$ of the maximum force or less, there are no cases of brittle behavior among the 750 realizations for each parameter combination.

When the axial force is $0.4A_g f'_m$, the frequency of brittle behavior is 8.3 percent. The sensitivity of the frequency of brittle behavior to a 20% increase in each statistical parameter of the input variables is presented in Table 4.2.1. This sensitivity is expressed as a percent variation of the relative frequency with respect to that of the "central case". For example, a 20 percent change in the mean value of ϵ_{mu} results in a frequency of brittle behavior equal to 2.4 percent and this represents a 71 percent reduction from the central case (i.e. (8.3-2.4)/8.3 = 0.71).

We performed another sensitivity study considering one standard deviation as a reasonable variation for each random variable mean instead of 20%. The results are presented in Table 4.2.2.

Table 4.2.1 Variation of the Frequency of Brittle Behavior when $P=0.4A_g f'_m$ and the Base Parameters are increased by 20% from the Central Case

Base Parameter Statistic Changed	Frequency of Brittle Behavior (%)	Variation with respect to the Central Case* (%)
Mean of ϵ_{mu}	2.4	-71
Coefficient of Variation of ϵ_{mu}	9.3	+13
Mean of f'_m	1.3	-84
Coefficient of Variation of f'_m	9.6	+16
Mean of f_y	20.1	+143
Coefficient of Variation of f_y	8.4	+1

* The central case frequency of brittle behavior is 8.3%

Table 4.2.2 Variation of the Frequency of Brittle Behavior when $P=0.4A_g f'_m$ and the Mean Values of Base Parameters are increased One Standard Deviation from the Central Case

Base Parameter Statistics Changed	Percent Change from Central Case	Frequency of Brittle Behavior (%)	Variation with respect to the Central Case* (%)
Mean of ϵ_{mu}	15	4.8	-42
Mean of f'_m	10	4.7	-43
Mean of f_y	8.3	13.2	+60

* The central case frequency of brittle behavior is 8.3%

The trend of the sensitivity displayed in Tables 4.2.1 and 4.2.2 was expected (i.e. an increase in brittleness will exist when the mean of f_y increases and a decrease in brittleness will exist when the mean values of f'_m and ϵ_{mu} increase). However, the magnitude of this sensitivity was not expected:

* the decrease in brittleness was three to four times greater than the increase in mean of the maximum concrete masonry strain and strength; and
* the increase in brittleness was seven times greater than the increase in the mean value of the steel strength variable.

The sensitivity to the coefficients of variation of the input variables is much smaller:

* the sensitivity to the variation of the C.O.V. of the steel strength (f_y) is not significant; and
* the increase of the C.O.V. of the concrete masonry strength parameters (ϵ_{mu} and f'_m) results in a smaller increase in brittleness.

4.3 RANDOM AXIAL LOADING

The axial force in all of the research to this point was considered a deterministic input variable. In order to examine the influence of the randomness of the axial force on the brittleness of the wall, a new sensitivity study has been performed. The mean value of the axial force was varied between 20% and 40%

of the maximum axial force in 5% and then 2% increments while the coefficient of variation was varied from 0% to 25% in 5% increments. The other input variables were set at the "central case" values. The frequencies of brittle behavior obtained in this sensitivity study are presented in Table 4.3.1 and Figure 4.3.1.

Table 4.3.1 Variation of the Frequency of Brittle Behavior with the Axial Load

Mean Axial Load / $A_g f'_m$ (%)	Coefficient of Variation of the Axial Load					
	0%	5%	10%	15%	20%	25%
20	0.00%	0.00%	0.00%	0.00%	0.13%	0.13%
25	0.13%	0.13%	0.13%	0.13%	0.27%	0.53%
30	0.27%	0.27%	0.27%	0.67%	1.20%	2.80%
32	0.40%	0.40%	0.80%	1.33%	2.80%	4.93%
34	1.20%	1.20%	1.60%	2.67%	3.87%	7.60%
36	2.00%	2.13%	3.20%	4.93%	8.67%	8.40%
38	4.00%	4.67%	6.13%	9.47%	11.33%	10.53%
40	8.27%	8.13%	11.47%	13.33%	13.47%	15.07%

From Table 4.3.1 and Figure 4.3.1 the following conclusions can be drawn:

* Small coefficients of variation of the axial force (up to 10%) do not produce a significant increase in the frequency of the brittle behavior.
* For values of the mean axial force equal to 30% of the maximum axial force the increase in the C.O.V of the axial force from 0 to 25% produces a ten fold increase in the frequency of brittle behavior. This compares with a two fold increase for values of the mean axial force equal to 40% of the maximum axial force.

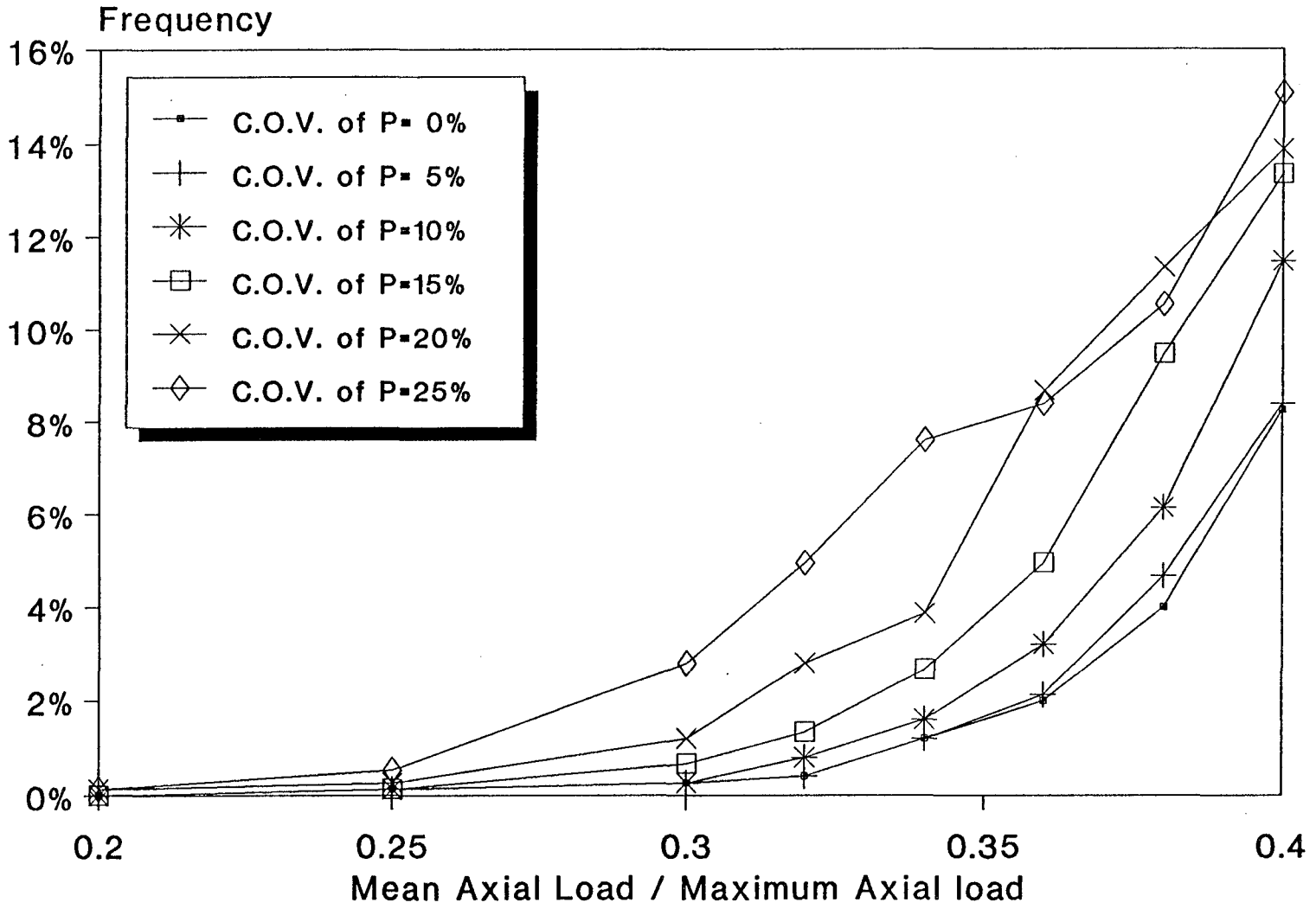

FIGURE 4.3.1 FREQUENCY OF BRITTLE BEHAVIOR

* Since a reasonable increase in f_y produces less than a doubling of brittleness, the coefficient of variation of the axial force has the greatest impact on the frequency of the brittle behavior.

The study of the frequency of brittle behavior is very important for a more deep understanding of the "balanced design axial load". When the basic parameters involved in the flexural wall problem are random, it appears that the "balanced axial load" concept requires a probabilistic definition. A possible definition is "the expected value of the axial load for which the corresponding frequency of brittle behavior is 50%." Examination of Figure 4.3.1 suggests that the balanced design axial load thus defined will be a function of the coefficient of variation of the axial load. That is, the larger the coefficient of variation of the axial load, the smaller the balanced load. This happens because the larger coefficient of variation of the axial load will produce a larger frequency of brittle behavior and the 50% frequency mark will be reached for a lower value of the mean axial load. To estimate the balanced design axial load for a given value of the coefficient of variation of the axial load, Monte Carlo runs should be performed for increasing mean values of the axial load until the obtained frequency of the brittle behavior reaches 50%.

4.4 LIMIT STATE EQUATIONS FOR THE DUCTILE BEHAVIOR

As concluded in Section 3.4, we must consider the ductile behavior as a "conditional limit state" in assessing the safety of reinforced concrete masonry structures. It was shown in Chapter 3 and Appendix E that an exact solution to this problem by considering the stress and strain equation in one wall section is impractical. This difficulty can be circumvented by using the results of a Monte Carlo analysis obtained for the curvature ductility (μ_ϕ) and displacement ductility (μ_d). The limit state equation can be written for curvature ductility as

$$F = \mu_\phi - 1 \tag{4.4.1}$$

where failure exists when F = 0.

For displacement ductility it similarly follows that

$$F = \mu_d - 1 \tag{4.4.2}$$

The mean value of F in Equations (4.4.1) and (4.4.2) is $\bar{\mu}_\phi$-1 and $\bar{\mu}_d$-1, respectively. The standard deviation of F is equal to the standard deviations of the corresponding ductility. Under the assumption that the limit state surfaces described by Equation (4.4.1) or (4.4.2) are smooth enough in the neighborhood of their design point, the safety index, or hereafter called the *ductility index*, can be estimated using the Cornell definition:

$$\beta_{\phi} = \frac{\overline{\mu_{\phi}} - 1}{\sigma_{\phi}} \qquad (4.4.3)$$

or

$$\beta_{d} = \frac{\overline{\mu_{d}} - 1}{\sigma_{d}} \qquad (4.4.4)$$

We acknowledge the fact that the adoption of the Cornell definition will produce a safety index that will be dependent to the particular choice of the failure function, namely Equation (4.4.1) or (4.4.2). However, this is the price to pay for avoiding the complications of the invariant approach described in Chapter 3 and Appendix E. Bearing in mind the fact that the safety index, even if invariant, has a notional character, and its practical value is for comparison only, we can accept this shortcoming.

Two problems arise in conjunction with estimating the safety index. The first problem is to chose between curvature ductility and displacement ductility as a basis parameter when defining the ductility index. The curvature ductility is always greater than displacement ductility and the difference may be significant if the axial force is kept at low values. Consequently, the ductility index as defined by Equation (4.4.3) will be greater than the one defined using Equation (4.4.4), although the risk of brittle behavior is the same. This inconsistency is due to the lack of invariance of the Cornell Safety Index.

The second problem lies with quantifying the "ductility" in the case of brittle behavior. In Chapter 2, the statistics on ductility were performed by assigning the value 1 to either curvature or displacement ductility when the brittle failure occurred. For this reason, the estimates of mean and standard deviation of both ductilities are accurate only for axial forces equal to or lower than 20% of the maximum axial force, when no brittle behavior occurred. For higher axial forces, these ductilities will be reevaluated in the next sections, after establishing a definition for the ductility value (smaller than 1) to be assigned to each case of brittle behavior.

The next two sections will be devoted to solving these two problems.

4.5 COMPARISON BETWEEN A DUCTILITY INDEX BASED ON CURVATURE DUCTILITY AND A DUCTILITY INDEX BASED ON DISPLACEMENT DUCTILITY

In order to compare the value for Ductility Index obtained using Equation (4.4.3) with the value obtained from Equation (4.4.4), we use the statistics of the parameters for the curvature ductility and displacement ductility obtained in Chapter 2. The comparison is made for the cases where the axial force was zero or 20% of the maximum axial force. In these cases, the lack of brittle behavior allows for a straightforward use of the statistics presented in Tables 2.2.2 and 2.2.3. Table 4.5.1 presents the values of Ductility Index obtained from curvature

ductility using Equation (4.4.3) and displacement ductility using Equation (4.4.4). Table 4.5.1 presents the sensitivity of the Ductility Index to a 20% increase in each statistical parameter of the input variables. This sensitivity is expressed in percent variation of the Ductility Index with respect to that of the "central case". We recall that the mean and coefficient of variation of the random variables for the "central case" are presented in Table 2.2.1.

Table 4.5.1 Sensitivity of Ductility Index calculated for Curvature and Displacement Ductility when the Base Parameters are increased by 20%

Base Parameter Statistics Changed	Axial Force = 0				Axial Force = 20% P_{max}			
	Curvature		Displ.		Curvature		Displ.	
	β_ϕ	Var. (%)	β_d	Var. (%)	β_ϕ	Var. (%)	β_d	Var. (%)
Central Case	10.32		3.80		3.84		2.89	
Mean ϵ_{mu}	10.34	0	3.81	0	4.08	6	3.00	5
C.O.V. ϵ_{mu}	10.13	-2	3.80	0	3.39	-12	2.69	-6
Mean f'_m	10.24	-1	3.78	-1	3.85	0	2.90	1
C.O.V. f'_m	10.30	0	4.13	9	3.76	-2	2.92	2
Mean f_y	10.06	-2	3.81	0	3.62	-6	2.80	-2
C.O.V. f_y	8.47	-18	3.93	3	3.81	-1	2.92	2

Based on the results in Table 4.5.1, the following observations can be made:

* In absence of an axial force, the Curvature Ductility Index (β_ϕ) results in unrealistically high values. This is because the high values for the mean curvature ductility produce a significant distortion to the Cornell Safety Index that relies on the mean value of the original safety margin rather than the mean value of the standard-space-mapped safety margin in the Hasofer-Lind Safety Index. The use of the displacement ductility Index (β_d) minimizes this distortion because the displacement ductility is much smaller for low values of the axial load.

* With one exception (the increase in coefficient of variation of f'_m) β_ϕ is more sensitive than β_d to variations in the statistical parameters of the input random variables.

The two conclusions obtained from the results in Table 4.5.1 can justify the choice of β_d over β_ϕ for defining the Ductility Index. However, there is a more important reason to prefer a displacement based Ductility Index. Displacement ductility for individual walls can be directly used at the structural system level for different purposes like:

* estimation of the system ductility;

* comparison between walls of different length in the same building;

* the possibility of constraining different walls in a building to undergo the same displacement at a floor level; and

* comparison between the displacement ductility capacity and the displacement ductility demand generated by a strong earthquake motion.

The curvature based Ductility Index does not have a physical meaning beyond the section level and can not be used for comparison with walls of different size. For all these reasons we define the Ductility Index as the safety index with respect to brittle behavior, based on displacement ductility and calculated with Equation (4.4.4). This Ductility Index (DI) will be used extensively in the further research in this chapter.

4.6 QUANTIFICATION OF DISPLACEMENT DUCTILITY CAPACITY IN THE CASE OF A BRITTLE BEHAVIOR

In Section 2.3.10, we discussed the probability density function for the displacement ductility. The shape of the frequency histogram appears to indicate a log-normal model. Figure 2.3.10 presents histograms for displacement ductility obtained for different levels of mean axial force. For small values of axial force practically all ductility values are greater than 1. However, for large values of axial force, the left tail of the distribution is squeezed at $\mu_d=1$ and the distribution appears truncated. The possible representation for cases that result in brittle failure is an additional Dirac Delta Function shifted to $\mu_d=1$. This research proposes an analytical extension of the distribution that will spread the Dirac lump

over the interval (0,1). This means that for each case of brittle behavior, a value between 0 and 1 will be assigned to the displacement ductility in order to obtain a smooth probability density function. Since in design we only are interested in ductility values equal to or greater than one this approach seems reasonable.

Four different definitions for the analytical extension have been proposed and tested before selecting the definition to be used in this study. One of the definitions assumes a log-normal distribution for the displacement ductility while the other three definitions do not impose any particular distribution.

Definition 1.

If the displacement ductility (μ_d) is log-normally distributed, then $\ln(\mu_d)$ will be normally distributed. The values assigned to brittle cases will be mapped from the interval (0,1) to the interval($-\infty$, 0). Based on the symmetry of the normal distribution, the analytical extension can be constructed using the median of the normal distribution as an axis of symmetry. We selected the median rather than mean value because the former can be determined independent of the analytical extension.

If there are "n" cases of brittle behavior within the sample, the analytical extension is constructed as follows;

1. The median value of $\ln(\mu_d)$ is calculated.
2. The "n" highest values for $\ln(\mu_d)$ are selected;
3. Each selected value for $\ln(\mu_d)$ is duplicated by assigning a value that is symmetrical with respect to the median value of $\ln(\mu_d)$.

4. The analytically extended distribution is mapped back using $\exp(\ln(\mu_d)) = \mu_d$.

The shortcoming of this definition is that one or more values assigned to $\ln(\mu_d)$ can be positive due to the randomness in the right tail of the distribution. In turn, a positive value for $\ln(\mu_d)$ implies ductile behavior, in violation with the established frequency of brittle behavior.

Definition 2.

This definition attempts to mitigate the shortcoming of Definition 1. Keeping the same frequency of brittle behavior, this definition is constrained to violate the assumption of log-normality of the distribution. The construction of the analytical extension starts with the three steps of Definition 1, followed by:

4. The set of values obtained in Step 3 is shifted so that the highest value for $\ln(\mu_d)$ will be zero.
5. The analytically extended distribution is mapped back using $\exp(\ln(\mu_d)) = \mu_d$.

The violation of log-normality occurs because the distribution of $\ln(\mu_d)$ will now not be symmetrical with respect to its median value.

Definition 3.

The values μ_d assigned to the cases of brittle behavior are uniformly distributed between 0 and 1.

Definition 4.

The values μ_d assigned to the cases of brittle behavior are linearly distributed between 0 and 1. The probability density function has a zero value for $\mu_d=0$ while for $\mu_d=1$ the value is determined equating the area under the curve with the frequency of brittle behavior.

The four definitions have been tested for the case with the highest frequency of brittle behavior (Mean axial load = 40% of maximum, coefficient of variation of the axial load = 25%) where the difference between the results is expected to be a maximum. The results obtained using the different definitions are presented in Table 4.6.1.

Table 4.6.1 Comparative results for Ductility Index using different definitions for the analytical extension of the PDF of μ_d. (Mean axial load = 40% of maximum, coefficient of variation = 25%)

	Definition for the analytical extension			
	1	2	3	4
$\bar{\mu}_d$	1.57	1.57	1.53	1.56
C.O.V. μ_d (%)	67	76	71	68
DI	0.54	0.48	0.49	0.53

The difference between the values obtained for DI using the four different definitions is less than 12 percent. The second definition has been selected for the purpose of this study because it appears to be the most consistent with the main segment of the distribution.

4.7 VARIATION OF THE DUCTILITY INDEX WITH THE AXIAL LOAD

Using the convention established in Section 4.6 to quantify the displacement ductility capacity for the case of a brittle behavior, we calculated the mean value and the coefficient of variation of the displacement ductility using a Monte Carlo Simulation approach. The simulation were performed for different values of mean and coefficient of variation of the axial force while the mean and coefficient of variation of the other input parameters were kept constant. The results obtained for the mean values of the displacement ductility capacity are presented in Table 4.7.1. Figure 4.7.1 presents the variation of the mean value of the ductility capacity against the mean value of the axial force varying from 20% to 40% of the maximum axial force, for different coefficients of variation of the axial force.

The variation of mean displacement ductility capacity with the deterministic axial force was discussed in Section 2.3.8. Based on the results in Table 4.7.1 and Figure 4.7.1 for a random axial force, several observation can be made.

* The mean ductility capacity decreases when the mean axial force increases, as observed in Section 2.3.8.
* The influence of the coefficient of variation of the axial force is small and is more significant for larger mean axial force when the mean ductility is small.

Table 4.7.1 Mean Displacement Ductility as a Function of the Expected Value and the Coefficient of Variation of the Axial Load

Mean Axial Load / $A_g f'_m$ (%)	Coefficient of Variation of the Axial Load					
	0%	5%	10%	15%	20%	25%
0	22.2	22.2	22.2	22.2	22.2	22.2
2.5	17.3	17.2	17.2	17.2	17.2	17.1
5	10.4	0.4	10.5	10.6	10.8	11.0
10	5.5	5.5	5.6	5.6	5.8	6.0
20	2.7	2.7	2.8	2.8	2.9	3.0
25	2.2	2.2	2.2	2.3	2.3	2.4
30	1.8	1.8	1.8	1.9	1.9	2.0
32	1.7	1.7	1.7	1.7	1.8	1.9
34	1.6	1.6	1.6	1.6	1.7	1.8
36	1.5	1.5	1.5	1.5	1.6	1.7
38	1.4	1.4	1.4	1.5	1.5	1.8
40	1.3	1.3	1.3	1.4	1.5	1.6

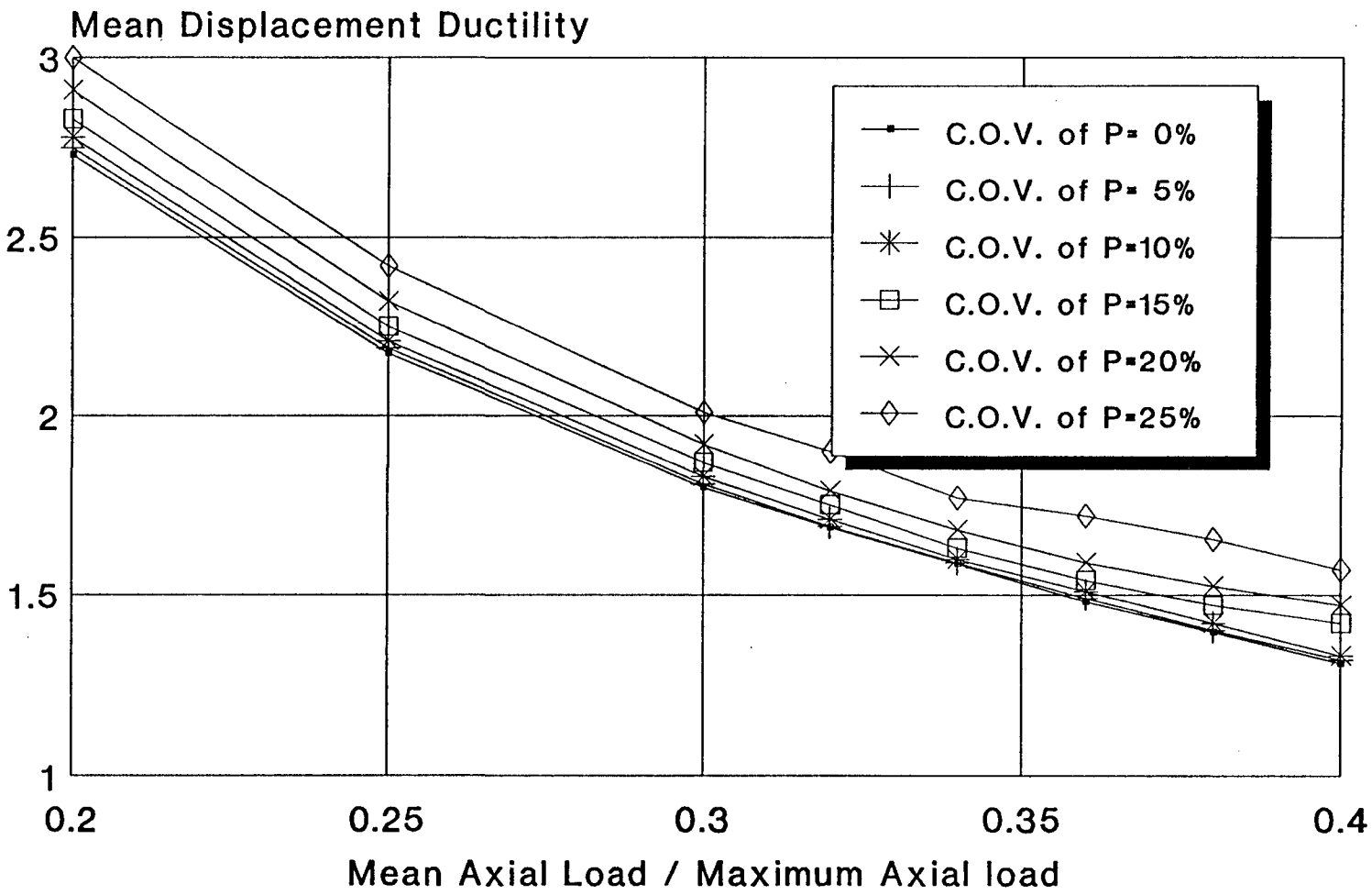

FIGURE 4.7.1 MEAN VALUE OF DISPLACEMENT DUCTILITY

Table 4.7.2 Coefficient of Variation of Displacement Ductility as a Function of the Expected Value and the Coefficient of Variation of the Axial Load

Mean Axial Load / $A_g f'_m$ (%)	Coefficient of Variation of the Axial Load					
	0%	5%	10%	15%	20%	25%
0	25.1	25.1	25.1	25.1	25.1	25.1
2.5	27.9	28.0	28.2	28.6	29.2	29.8
5	28.7	29.4	30.8	33.0	35.8	38.8
10	26.3	27.1	29.1	32.3	37.4	43.6
20	21.9	23.0	25.5	29.5	36.2	49.4
25	19.9	21.0	23.7	28.2	35.3	53.2
30	18.0	19.4	22.4	27.2	34.8	57.6
32	17.4	18.9	22.0	27.2	34.8	65.8
34	17.1	18.5	21.7	26.6	34.7	63.4
36	16.9	18.2	21.7	26.8	35.9	66.7
38	17.2	19.1	21.7	32.3	44.1	73.9
40	16.8	18.3	23.0	50.9	64.2	76.2

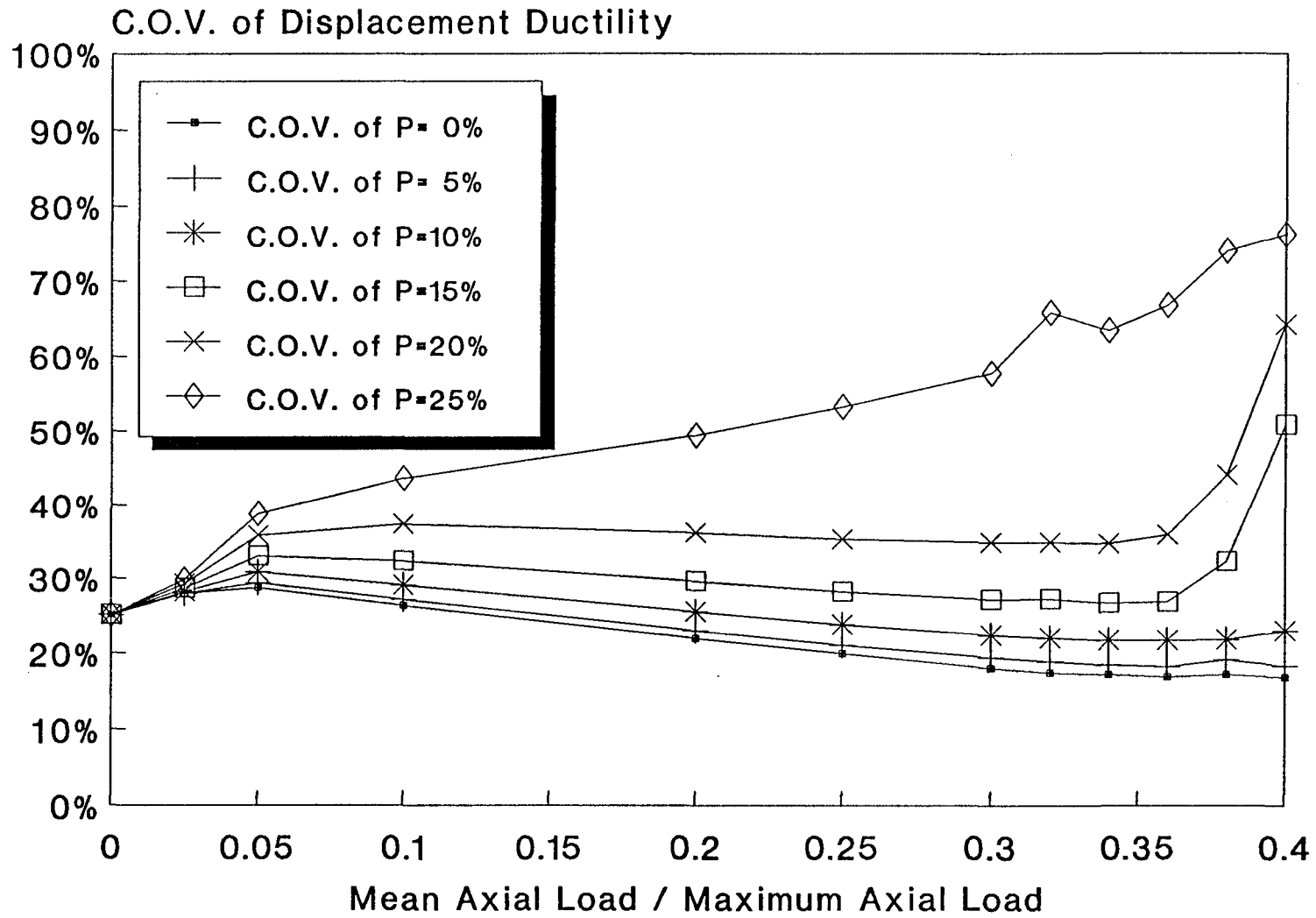

FIGURE 4.7.2 COEFF. OF VARIATION OF DISPLACEMENT DUCTILITY

* The mean ductility capacity increases slightly when the coefficient of variation of the axial force increases.

The results obtained for the coefficient of variation of the displacement ductility capacity are presented in Table 4.7.2. Figure 4.7.2 presents this coefficient of variation of the ductility capacity against the mean value of the axial force for different coefficients of variation of the axial force.

Based on the results in Table 4.7.2 and Figure 4.7.2, several observation can be made.

* For low coefficients of variation of the axial force, the coefficient of variation of ductility capacity decreases slightly when the mean axial force increases.
* For coefficients of variation of the axial force between 15% and 20% the coefficient of variation of ductility capacity remains almost constant up to a mean axial force equal to 36% of the maximum, and then increases steeply with the mean axial force.
* For a 25% coefficient of variation of the axial force, the coefficient of variation of ductility capacity increases constantly when the mean axial force increases.
* The influence of the coefficient of variation of the axial force is minimal for values between 0% and 10% but becomes significant for values larger than 15%.

* The coefficient of variation of the ductility capacity increases with the increasing coefficient of variation of the axial force.

The Ductility Index calculated using Equation (4.4.4) from the values in Tables 4.7.1 and 4.7.2 is presented in Table 4.7.3 and Figure 4.7.3. Several observations can be made.

* A comparison with the results obtained for the frequency of brittle behavior (Figure 4.3.1) reveals more clear trends for the Ductility Index. The two lines corresponding to 20% and respectively 25% coefficient of variation of the axial force do not cross any more, indicating that the Ductility Index is not as sensitive to the sampling of the input parameters. At the same time, there is a clearer distinction between the curves corresponding to 0% and respectively 5% coefficient of variation of the axial force than it is for the frequency of brittle behavior.
* The Ductility Index is decreasing with the increasing mean axial force.
* The Ductility Index is decreasing with the increasing coefficient of variation of the axial force.
* The impact of the coefficient of variation of the axial force is a maximum when the mean value of the axial force is between 20% and 30% of the maximum axial force. For this range, the Ductility Index decreases approximately 1.5 units when the coefficient of variation of the axial force increases from 0 to 25%.

Table 4.7.3 Ductility Index as a Function of the Expected Value and the Coefficient of Variation of the Axial Load

Mean Axial Load / $A_g f'_m$ (%)	Coefficient of Variation of the Axial Load					
	0%	5%	10%	15%	20%	25%
0	3.8	3.8	3.8	3.8	3.8	3.8
2.5	3.4	3.4	3.3	3.3	3.2	3.2
5	3.2	3.1	2.9	2.7	2.5	2.3
10	3.1	3.0	2.8	2.5	2.2	1.9
20	2.9	2.8	2.5	2.2	1.8	1.3
25	2.7	2.6	2.3	2.0	1.6	1.1
30	2.4	2.3	2.0	1.7	1.4	0.9
32	2.3	2.2	1.9	1.6	1.3	0.7
34	2.1	2.0	1.7	1.4	1.2	0.7
36	1.9	1.8	1.5	1.3	1.0	0.6
38	1.6	1.5	1.4	1.0	0.8	0.5
40	1.4	1.3	1.1	0.6	0.5	0.5

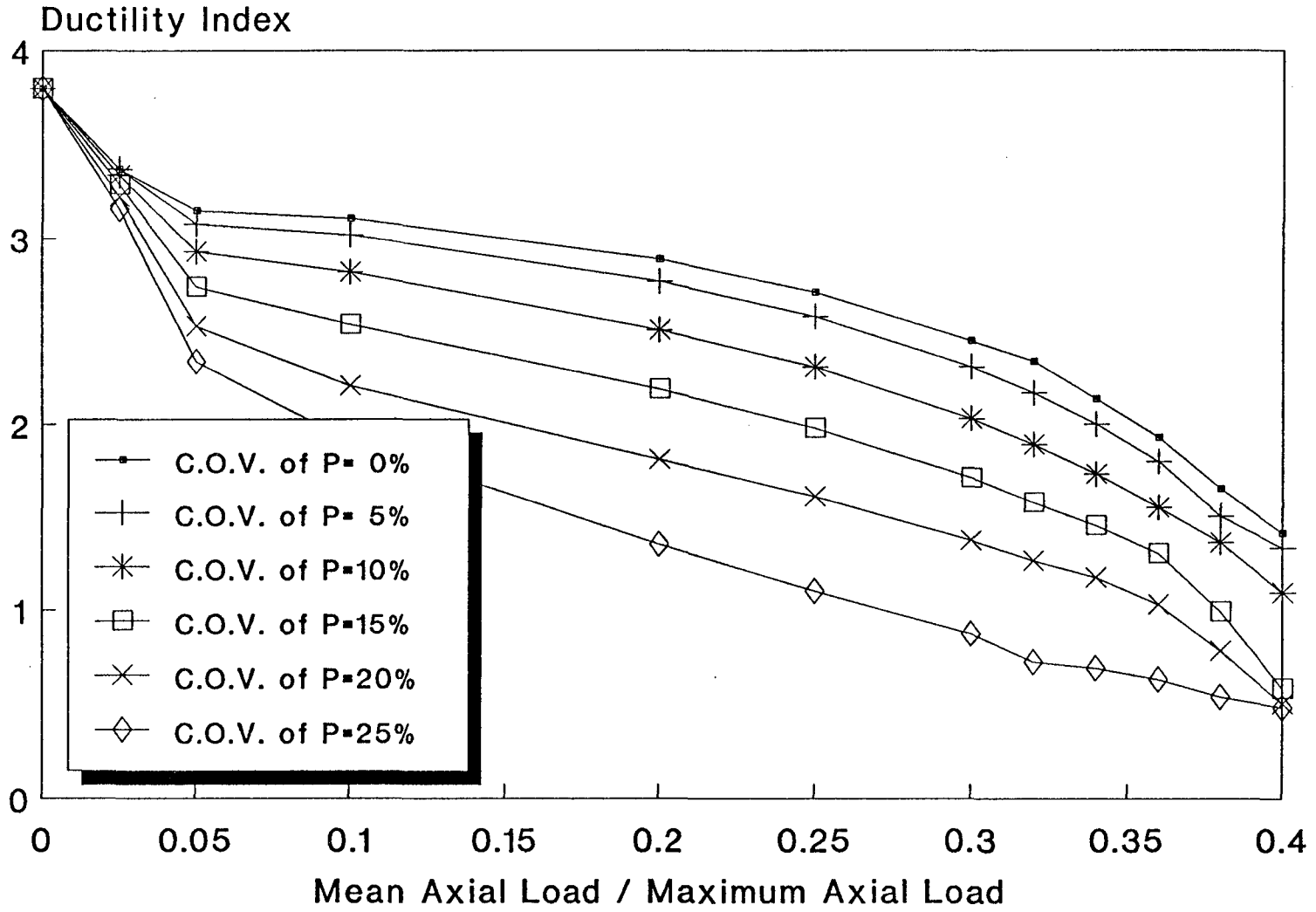

FIGURE 4.7.3 DUCTILITY INDEX

4.8 THE DUCTILITY INDEX AND THE FREQUENCY OF BRITTLE BEHAVIOR

Since an analytical approach to the problem of wall reliability with respect to the brittle behavior is impractical, the only available tool remains the Monte Carlo analysis. This analysis can produce, for a wall of given geometric characteristics and steel reinforcing, the expected frequency of brittle behavior as well as the statistics of the curvature ductility and the displacement ductility.

The previous section presented the variation of the Ductility Index with the axial force for a reinforced concrete masonry wall. A powerful feature of any Safety Index is the ability to circumvent the lack of knowledge relative to the probabilistic distribution of the safety margin. Moreover, the Ductility Index contains more information than the Frequency of Brittle Behavior. However, it is interesting to establish a link between the two values since the latter is easier to understand because of its physical meaning.

A relationship between the two values can be established only if the probability distribution is known. If the frequency of brittle behavior is normally distributed, then it can be shown (Shinozuka, 1983) that:

$$f_{brittle} \geq 1 - \Phi(\beta) \tag{4.8.1}$$

$$\beta \geq \Phi^{-1}(1 - f_{brittle}) \tag{4.8.2}$$

where:

$f_{brittle}$ = Frequency of Brittle Behavior

$1-f_{brittle}$ = Frequency of Ductile Behavior

$\Phi(\beta)$ = Standardized Gaussian Distribution Function

β = The Safety Index obtained under the assumption that $f_{brittle}$ is normally distributed

The right hand side of Equation (4.8.1) represents the integral of the joint density function of the random variable over the domain bounded by the hyper-plan tangent to the limit state surface at the design point. Equation (4.8.2) shows that the Safety Index based on the Gauss distribution (β) is slightly underestimated when calculated using the Inverse Standardized Gaussian Function as in Equation (4.8.2). Approximating the limit state surface in the neighborhood of the design point with the tangent hyper-plan, Equation (4.8.2) becomes:

$$\beta = \Phi^{-1}(1 - f_{brittle}) \qquad (4.8.3)$$

An alternate safety index can be defined using Equation (4.8.3). However, the Ductility Index has more credibility because no assumption on the distribution has been implied. The only sources of distortion are equally present in the Inverse Gauss Safety Index: the approximation of the limit state surface by the tangent hyper-plan and the variability of the Monte-Carlo samples. Consequently, the difference between the two indices has to be construed as the amount of departure of the real distribution of the $f_{brittle}$ from the Gauss distribution.

The Inverse Gauss Safety Index has been computed from the values of $f_{brittle}$ in Table 4.3.3 using Equation (4.8.3) and the results are presented in Table 4.8.1

and Figure 4.8.1 as a function of the mean value and the coefficient of variation of the axial load.

Table 4.8.1 Inverse Gauss Safety Index

Mean Axial Load / $A_g f'_m$ (%)	Coefficient of Variation of the Axial Load					
	0%	5%	10%	15%	20%	25%
20	N/A	N/A	N/A	N/A	3.0	3.0
25	3.0	3.0	3.0	3.0	2.8	2.5
30	2.8	2.8	2.8	2.5	2.3	1.9
32	2.6	2.6	2.4	2.2	1.9	1.6
34	2.3	2.3	2.1	1.9	1.8	1.4
36	2.0	2.0	1.8	1.6	1.4	1.4
38	1.7	1.7	1.5	1.3	1.2	1.2
40	1.4	1.4	1.2	1.1	1.1	1.0

Figure 4.8.2 compares the safety index defined with the Inverse Gauss Function (4.8.3) with the Ductility Index (4.4.4) for a deterministic axial load and for an axial load that has a 25% coefficient of variation. Several observations can be made:

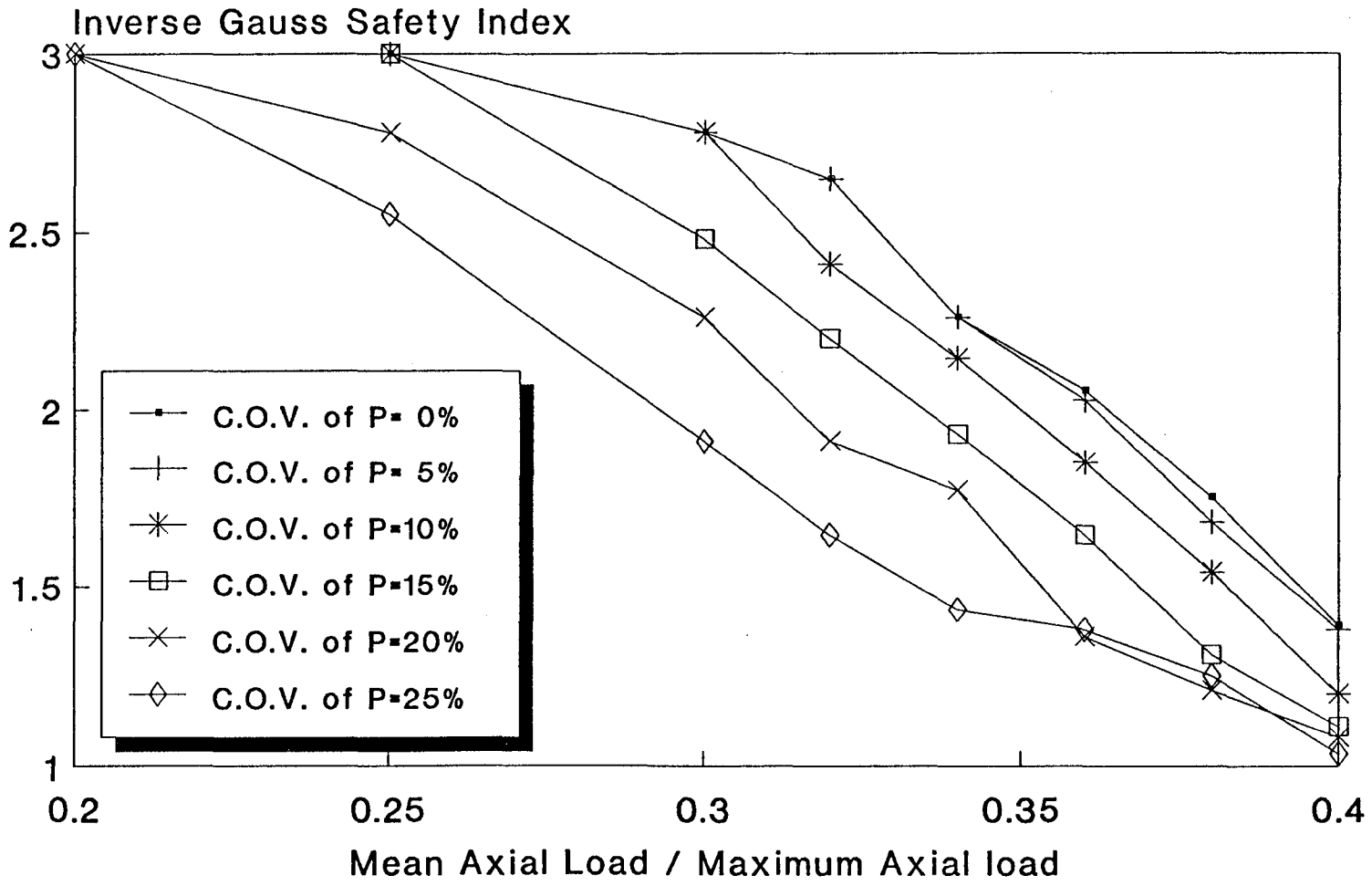

FIGURE 4.8.1 INVERSE GAUSS SAFETY INDEX

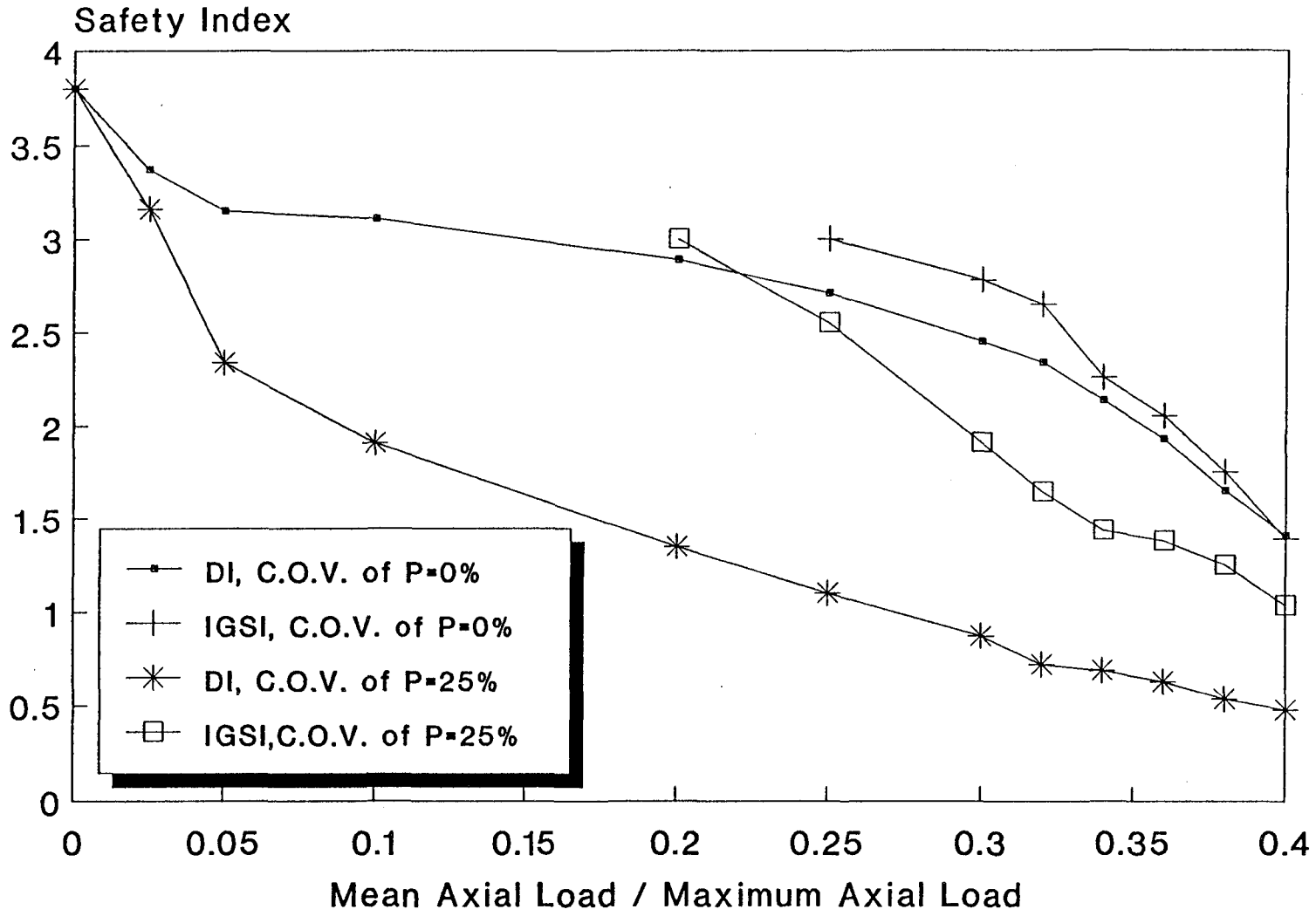

FIGURE 4.8.2 DUCTILITY INDEX AND INVERSE GAUSS SAFETY INDEX

* In order to obtain values for the Inverse Gauss Safety Index when the mean axial force is lower than 25% of the maximum, thousands of realizations are required for each Monte Carlo simulation.
* The Inverse Gauss Safety Index overestimates the Ductility Index.
* For low coefficients of variation of the axial force (smaller than 5%) the two indices present very close values. However, when the coefficient of variation of the axial force increases, the error of considering a Gauss distribution for $f_{brittle}$ becomes significant.

4.9 CONCLUSIONS

The following conclusions can be drawn for the research in this chapter:

(1) Ductile behavior is considered to be a "conditional limit state" that is important in assessing the structural safety.

(2) A Monte Carlo simulation study can be used to calculate a safety index (Cornell type) of ductile behavior.

(3) A Ductility Index based on displacement ductility is preferred to an index based on curvature ductility because:

- for small values of axial force, the values for the index based on curvature ductility are unrealistically high;

- the index based on curvature ductility is more sensitive to variations in the statistical parameters of the input variables than the index based on displacement ductility;
- using an index based on displacement ductility, the transition from a single-wall safety problem to the safety problem at the structural system is easier.

(4) An alternate Safety Index can be defined if we assume that the frequency of brittle behavior is normally distributed. This index, although more easy to understand, is impractical and inaccurate.

(5) The Ductility Index decreases when the mean value or the coefficient of variation of the axial force increases.

(6) The Ductility Index defined in this chapter presents several advantages:

- Unlike the classical reliability index, tributary to an extremely uncertain load, this index can be estimated with reasonable accuracy;
- It can be used to calibrate the design prescriptions for flexural walls;
- Since it is a comprehensive representation of the probabilistic information regarding the available ductility, chances are that it may be directly correlated with a similar index describing the seismic activity of a site or region.

CHAPTER 5

RELIABILITY OF CONCRETE MASONRY FLEXURAL WALL SYSTEMS

5.1 GENERAL

In Chapter 4 we studied the ductility capacity of a single flexural wall and defined a ductility index. In this chapter we will expand the study to structural systems composed of several flexural walls. The ductility of the structural system as well as the corresponding safety index will be defined and studied. A measure for the redundancy of the structural system will be proposed. Then, the complementary roles of ductility and redundancy in shaping a global quality of the system - *robustness* - will be explored.

Structures composed of reinforced concrete masonry flexural walls can be very diverse as far as the plan layout and building elevation are concerned. Herein, we limit our study to a particular class of structures consisting of several (two to eight) ten-story rectangular walls connected in the horizontal plane with rigid diaphragms. The walls are parallel and have statistically identical geometrical and material properties.

When this structure is subjected to a set of static lateral forces applied at the story levels where one wall reaches its yield load, a redistribution of forces among the remaining elements results. In a seismic base excitation, the

successive yielding and/or failure of walls leads to a decrease in the level of total force input in the structure. Hence, a masonry multiple wall seismic resisting system is not characterized by a redistribution of load like a Daniels System. For example, highrise masonry buildings composed of flexural walls and rigid floor diaphragms can have a significant increase in the effective fundamental natural period of vibration when compared to the period in the elastic range. During strong ground motion, the stiffness degradation in the structure can increase this period by values up to two seconds. In this situation, the structural response is governed by displacement rather than acceleration. If we treat this problem using an equivalent static approach, the structure is subjected to imposed displacements rather than inertial forces. Under a monotonic increasing displacement imposed equally to all of the participating walls, the walls will reach consecutively their ultimate capacity until the system reaches the ultimate structural limit state.

In Section 2.2.1 we discussed the three limit states that describe the behavior of individual walls. Within the structure, walls may fail according to different limit states. For example, when the mean axial load is high, some walls may exhibit a brittle behavior while the others remain ductile. If at least one wall behaves ductile before the structure reaches its ultimate displacement, we consider the structural system limit state to be ductile. There are two reasons for such a definition:

(1) for an individual wall, the yielding of one steel bar before the concrete masonry crushes is enough to qualify the wall as having ductile behavior.

(2) the single ductile wall performs, on behalf of the whole structure, the task of dissipating energy and reducing the structural response to the ground motion.

On the other hand, if all the walls exhibit a brittle behavior, the structural system limit state is brittle. When the mean axial load is small, some walls may fail according to the first limit state while the other fail according to the second limit state. For similar reasons, we consider that this structure fails according to the second limit state. We now define the three *structural system* limit states as follows:

Structural System Limit State (1): when all the walls fail according to the First Limit State as defined in Section 2.2.1.

Structural System Limit State (2): if at least one wall behaves according to the Second Limit State as defined in Section 2.2.1 before the structure reaches its ultimate displacement.

Structural System Limit State (3): when all the walls fail according to the Third Limit State as defined in Section 2.2.1.

Besides the parameters that govern the ultimate capacity of one wall (as described in Chapter 2) there are additional factors that have an influence on the

system ductility, redundancy and robustness: the size of the system (the number of walls), the covariance matrix corresponding to each material parameter distributed among walls, and the distribution and correlation of axial load among walls.

A "balanced system" is defined to be a structural system composed by statistically identical elements that are subjected to statistically identical loads and all elements work in parallel (De, Karamchandani, and Cornell, 1989).

The structural system studied in this research fits the definition of a "balanced system" when the axial load corresponding to each wall has the same mean value and coefficient of variation. The variation of axial load among the walls is mainly due to the randomness in live load distribution across the floor. In the case when cross walls are present, the simultaneous excitation on the direction perpendicular to the walls under study may induce compression in some walls and tension in the other. This structural system is "unbalanced".

The Monte Carlo simulation is performed in this chapter for structures consisting of two to eight walls. Each statistical sample contains 750 structures. Consequently, for each sample, the number of generated walls is 750 multiplied by the number of walls in the structure. Because of the increased complexity created by the larger number of variables as well as the necessity of controlling their correlation, the generation of random values requires a special attention. This problem will be discussed in Section 5.2.

Section 5.3 will be devoted to the statistical definition of the axial loads in the walls and the coefficient of variation of the axial loads in balanced systems. The covariance matrix of the axial loads in unbalanced system will be evaluated.

Section 5.4 defines and studies the system ductility of balanced and unbalanced systems of walls, while Section 5.5 attempts to clarify the extremely difficult notion of system redundancy and quantify the redundancy effects for the flexural wall systems.

In Section 5.6, the two attributes of the system - ductility and redundancy - are merged into a new quality of the system: *robustness*. The robustness is quantified as the System Ductility Index. The beneficial contributions of system ductility and redundancy to the robustness of the system are discussed. Section 5.7 presents the conclusions regarding the reliability of the systems composed of concrete masonry flexural walls.

5.2 PROBLEMS REGARDING THE MONTE CARLO SIMULATIONS FOR STRUCTURAL SYSTEMS

5.2.1 Generation of Correlated Variables

The generation of random vectors with a specified multivariate distribution and a target correlation matrix is a difficult, often unsolvable problem. In general, the generation of correlated variables is accomplished in two steps:

(1) generation of independent components according to the marginal distributions that result from the multivariate distribution.

(2) derivation of the desired random vectors through combination (usually linear) of independent components.

There are two possible pitfalls associated with this procedure:

(1) The combination of independent components may alter the initial distributions.

(2) The mean vector and the covariance matrix can be insufficient for completely defining the multivariate distribution.

In order to avoid both pitfalls, the normal multivariate distribution is adopted in this research. A linear combination of normally distributed variables results in a normally distributed variable. At the same time, the normal distribution is completely defined by the mean vector and the covariance matrix. From the inception of this research, we made the normality assumption at the expense of physical realism. The possible shortcoming of this assumption, namely the occurrence of negative values for the variables, is completely remote. In exchange, the normality assumption pays off handsomely by the possibility of controlling the covariance.

Rubinstein and Rosen (1968) used a particular Cholesky matrix decomposition for facilitating the structural analysis computations:

$$[A] = [L][D][L]^T \tag{5.2.1}$$

where A is a symmetric, positive definite matrix, L is a lower diagonal matrix, and D is a diagonal matrix. This decomposition is known in the Systems Control Theory as the "LDLT decomposition" (Mortensen, 1987). Hart (1982) uses the LDLT decomposition to find the lower diagonal matrix L that can transform an uncorrelated random vector {Y} associated with a diagonal covariance matrix S_Y into the correlated vector {X} with the target covariance matrix S_X. If

$$[S_X] = [L][S_Y][L]^T \tag{5.2.2}$$

then the mean vector $\{\overline{X}\}$ can be found as

$$\{\overline{X}\} = [L]\{\overline{Y}\} \tag{5.2.3}$$

The LDLT decomposition is a particular case of the Cholesky decomposition because it provides unique solutions for the diagonal and the lower diagonal matrices. If the uncorrelated vector {Y} is the standard normal multivariate (all mean values equal to 0 and all variances equal to 1), the diagonal matrix is the unit matrix E

$$[S_X] = [L][E][L]^T = [L][L]^T \tag{5.2.4}$$

In this case, the requirement of uniqueness of the Cholesky decomposition becomes unnecessary and the last product in Equation (5.2.4) represents the

general Cholesky decomposition that has an infinity of solutions. Then, the correlated vector {X} can be obtained (Liebetrau and Doctor,1987) as:

$$\{X\} = [L]\{Y\} + \{\bar{X}\} \qquad (5.2.5)$$

The general Cholesky decomposition, easier to perform as compared to the LDLT decomposition has been used in this research in order to generate the correlated input random vectors.

5.2.2 Minimization of the Sample Bias and Instability

We supposed in Section 5.2.1 that the vector {Y} is perfectly uncorrelated. This seldom happens in practice, because the univariates that are separately generated posses a random, non-zero correlation (some coefficients of correlation may reach 20%-30%). These input samples may produce a severe bias and instability in the output results. The higher the number of variables and the complexity of the problem, the higher the instability. Research has been devoted to eliminate this instability. Several methods gained notoriety among the Monte Carlo practitioners.

The Importance Sampling Method (Hammersley and Handscomb, 1964) selects more samples in regions of the space of input variables that can produce significant contribution to the probability of exceeding a certain limit state. A correction is applied to the final results in order to reduce the bias. Unfortunately,

this method can produce extremely biased results without the possibility of knowing it (Cornell, 1988 a).

The Latin Hypercube Sampling (McKay, Conover, and Beckman, 1979), uses a partition of the range of each variable into a number of equiprobable intervals and then selects the elements of the random vector so that they belong to subranges of different order. In fact, the intent of the method is to insure that the space of the variables is uniformly covered according to the target multivariate distribution.

So far, no attempt has been made to avoid the undesired correlations that occur when the sampling is not controlled.

The problem can be solved by eliminating these correlations. In order to perform this elimination, the following steps are taken:

(1) A number of realizations for the standard normal vector {Y} are generated.

(2) The mean vector {Y} and the covariance matrix S_Y of the generated sample are calculated.

(3) Using the Cholesky decomposition, the matrix S_Y is expressed as a product $[L][L]^T$.

(4) A new vector $\{Y_1\}$ is calculated using the transform:

$$\{Y_1\} = [L]^{-1}\{Y\} - \{\overline{Y}\} \qquad (5.2.6)$$

(5) Repeat steps (2) through (4) until the greatest nondiagonal element of the covariance matrix falls below a target tolerance.

The final vector {Y} obtained through this iteration process has a markedly improved representation throughout the variables' space. Thus, the aim sought when using the Latin Hypercube Sampling is accomplished too. As a consequence, {Y} is free of bias and can be used in generating the input vector {X} according to Equation (5.2.5). For random vectors up to eight components, three iterations are usually enough to reduce the value of the highest coefficient of correlation below 0.1%.

5.3 STATISTICAL DEFINITION OF AXIAL LOADS

5.3.1 Axial Loads in Balanced Systems

The typical layout for a balanced system of walls is presented in Figure 5.3.1(a). The walls are parallel and have statistically identical geometrical and material properties. The axial loads in the walls of the structure are mainly produced by dead loads, live loads, and earthquake loads. The purpose of this section is to evaluate a global coefficient of variation for the axial loads. This coefficient of variation will be used in this study.

The coefficient of variation of the dead load (C_{DL}) varies between 6% and 13% (Hart, 1982). We adopt in this research the value: $C_{DL} = 12\%$.

The live load is composed of sustained live load (or "arbitrary point-in-time" load) and additional load due to extraordinary crowding. As we do not consider

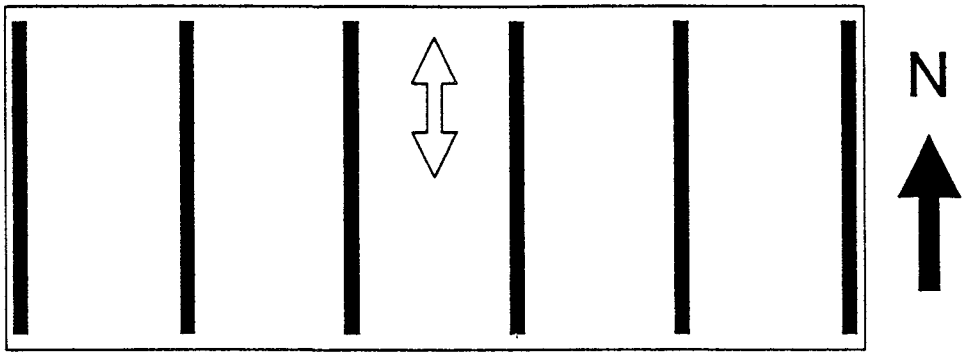

(a) Balanced System

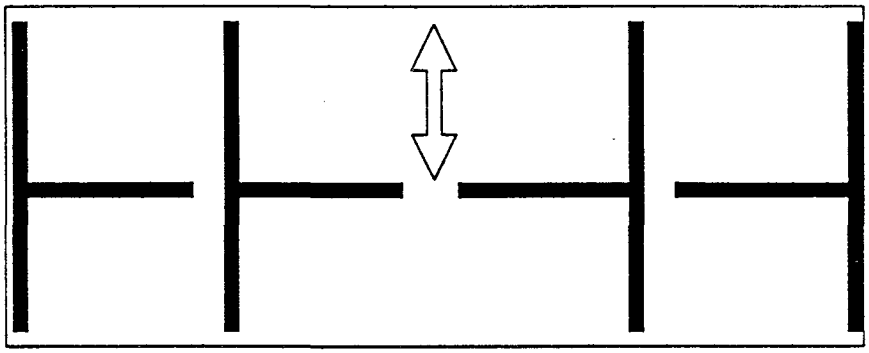

(b) Unbalanced System

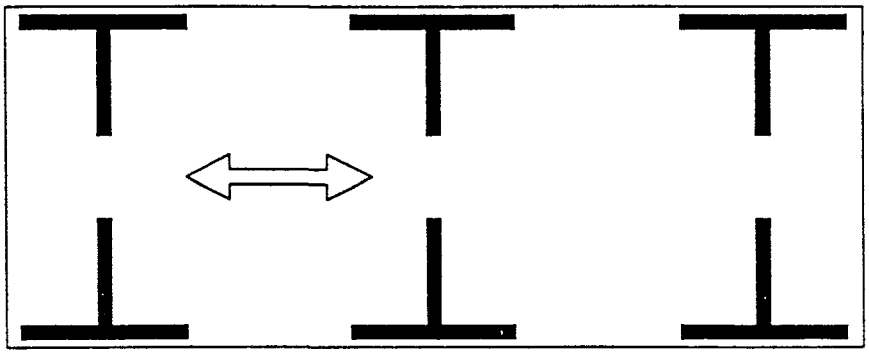

(c) Unbalanced System

FIGURE 5.3.1 TYPICAL PLAN LAYOUTS FOR MASONRY WALL SYSTEMS

earthquake occurrence simultaneously with crowding, the coefficient of variation of live load will be the coefficient of variation of the sustained live load (C_{SLL}). A recent study indicate that, for a tributary area of 1500 to 2500 square feet, the coefficient of variation of the sustained live load is approximatively equal to 15% (Kanda and Yamamura, 1989). Since the particular distribution of the load across the tributary area produces additional scatter in the load effect (Culver, 1976) we adopt in this research a value of 30% for C_{SLL}. Because the expected sustained live load is approximatively 20% of the expected dead load, the standard deviation of the sustained live load is:

$$\sigma_{SLL}=0.3\overline{SSL}=0.06\overline{DL} \tag{5.3.1}$$

where

$$\overline{SSL}=0.2\overline{DL}$$

The horizontal components of the strong motion earthquake excitation do not induce axial loads in the balanced systems of walls. The vertical component has no effect on the mean axial force, but produces additional variance of the axial load in the individual walls as well as the covariance of the axial load among the walls. The standard deviation of the earthquake-induced axial load is dependent on the severity of the ground motion. We consider:

(1) a peak ground acceleration of 0.60 g for the horizontal components;

(2) a ratio of 2/3 between the peak ground acceleration of the vertical and horizontal components; and

(3) a ratio of 2 between the peak and the standard deviation of the vertical ground acceleration.

With these assumptions, the standard deviation of the earthquake-induced axial load is:

$$\sigma_{EQ}=(0.6\overline{DL})(\frac{2}{3})(\frac{1}{2})=0.2\overline{DL} \qquad (5.3.2)$$

Considering all the three components as being normally distributed, the global coefficient of variation of axial load is:

$$C = \frac{\sqrt{\sigma_{DL}^2+\sigma_{SLL}^2+\sigma_{EQ}^2}}{\overline{DL}+0.2\overline{DL}+0} = 20\% \qquad (5.3.3)$$

where 0 in the denominator is the mean value of the earthquake-induced axial load.

A constant value of 20% for the coefficient of variation of axial load will be used in this chapter.

5.3.2 Axial Loads in Unbalanced Systems

Two possible layouts for unbalanced systems of walls are presented in Figures 5.3.1(b) and (c). The walls under study are parallel to the main direction of ground motion excitation (indicated by the double, hollow arrow). Because of the presence of cross walls, the simultaneous earthquake excitation in the direction perpendicular to the arrow will induce compression in some walls and tension in

others'. If the mean axial force in the walls of the balanced system is $\overline{P}$, the unbalance adds $\alpha\overline{P}$ to the each compressed wall and $-\alpha\overline{P}$ to each tensioned wall, where the random variable α is the unbalance coefficient. The unbalance affects the correlation of the axial loads of different walls in the structure. The purpose of this section is to find the mean values and the covariance matrix of the axial loads associated with the walls of the unbalanced system.

The random axial loads in the unbalanced system are derived from the random axial loads in the balanced system and the unbalance coefficient:

$$\wp_I = P_I + \alpha\overline{P} \tag{5.3.4}$$

$$\wp_J = P_J - \alpha\overline{P} \tag{5.3.5}$$

Where

i , k	=	indices associated with compressed walls in Equations (5.3.4) through (5.3.15)
j	=	index associated with a tensioned wall
P_i, P_j	=	random axial loads in the balanced system
$\wp_I$, $\wp_J$	=	random axial loads in the unbalanced system

Equations (5.3.4) and (5.3.5) can be used to derive the mean values of the axial loads associated with the compressed and tensioned walls:

$$\overline{\rho_i} = \overline{P}(1 + \overline{\alpha}) \tag{5.3.6}$$

$$\overline{\rho_j} = \overline{P}(1 - \overline{\alpha}) \tag{5.3.7}$$

The covariance between ρ_i and ρ_j is the ij term in the covariance matrix and is equal to

$$cov(\rho_i,\rho_j)=E<(P_i+\alpha\overline{P}-\overline{P}-\overline{\alpha}\,\overline{P})(P_j-\alpha\overline{P}-\overline{P}+\overline{\alpha}\,\overline{P})> \tag{5.3.8}$$

It follows that

$$cov(\rho_i,\rho_j)=cov(P_i,P_j)-\overline{P}^2\sigma_\alpha^2 \tag{5.3.9}$$

where σ_α is the standard deviation of the unbalance coefficient. Similarly, for the term of index ik in the covariance matrix we obtain

$$cov(\rho_i,\rho_k)=cov(P_i,P_k)+\overline{P}^2\sigma_\alpha^2 \tag{5.3.10}$$

If we consider the axial loads corresponding to the walls of the balanced system to be independent random variables then it follows that we obtain

$$cov(\rho_i,\rho_j) = -\overline{P}^2\sigma_\alpha^2 \tag{5.3.11}$$

$$cov(\rho_i,\rho_k) = \overline{P}^2\sigma_\alpha^2 \tag{5.3.12}$$

This assumption of independence produces the most interesting case for the effects of unbalance.

To obtain the diagonal terms of the covariance matrix, we calculate the standard deviation of the axial load for the walls of the unbalanced system

considering that the coefficient of variation of the axial load for the walls of the balanced system is 20%, as established in Section 5.3.1.

$$\sigma_{\rho} = \sigma_{[P_f + \alpha \bar{P}]} = \sigma_{[P_f - \alpha \bar{P}]} = \bar{P}\sqrt{0.04 + \sigma_{\alpha}^2} \tag{5.3.13}$$

The correlation coefficients for the axial loads among the walls of unbalanced system then become:

$$\rho_{ij} = -\frac{\sigma_{\alpha}^2}{0.04 + \sigma_{\alpha}^2} \tag{5.3.14}$$

$$\rho_{ik} = \frac{\sigma_{\alpha}^2}{0.04 + \sigma_{\alpha}^2} \tag{5.3.15}$$

The correlation coefficients of the axial loads are a function of the standard deviation of the unbalance coefficient only. On the other hand, the mean value of the unbalance coefficient is primarily a function of the severity of the ground motion in the direction perpendicular to the walls, whereas the coefficient of variation of the unbalance coefficient is a function of the coefficient of variation of material properties of the walls in both directions. This means that the correlation coefficients the axial loads are function of the coefficient of variation of the material properties and the coefficient of variation of the axial load on individual walls.

5.4 SYSTEM DUCTILITY

5.4.1 Ultimate Displacement

A wall is considered to have reached its Ultimate Limit State when the top displacement reaches its ultimate displacement. This happens when the compression strain at the base of the wall exceeds the maximum usable strain in concrete masonry. In this research, the ultimate displacement for a *structural system* occurs when all but the last wall have reached their individual wall ultimate limit states. For example, a structure composed of eight walls is considered to have reached its Ultimate Limit State when seven walls have reached their ultimate top displacement. The primary reasons for this definition of a structural system Ultimate Limit State are:

(1) The end walls are the least likely to fail. These walls are more ductile because the expected axial load is typically one half the axial load of the interior walls.

(2) With both end walls not yet reaching their Ultimate Limit State, the structural system is still stable. However, when one of the end walls reaches its Ultimate Limit State, the torsional response of the building will become large.

Because of the randomness of the displacement at the ultimate limit state of each wall, the expected value of the displacement at the system ultimate limit state will increase with the number of walls. It is expected that the ultimate

displacement of the structure is greater than the ultimate displacement of an individual wall. However, when the structure has only two walls, the displacement of one wall at its Ultimate Limit State will not be less than the Ultimate System Displacement. This is a consequence of the particular character of the structural system failure definition: the structure fails when the first wall fails. According to a well known fact from ordered statistics, the expected value of a minimum of two realizations of the same variables is smaller than the expected value of the variable (Bury, 1975).

5.4.2 Yield Displacement

To quantify the structural system ductility, we need to provide a definition for the structural system yield displacement. In Section 2 we defined the yield displacement of an individual wall as the displacement at the top of the wall when the vertical steel first yields.

Figure 5.4.1 presents the load-deflection response (the overturning moment at the base against the displacement at the top) for:

(1) three statistically identical walls; and

(2) the structure consisting of these three walls.

The load-deflection curve for the structure is obtained by summing the ordinates of the curves corresponding to each of the three walls.

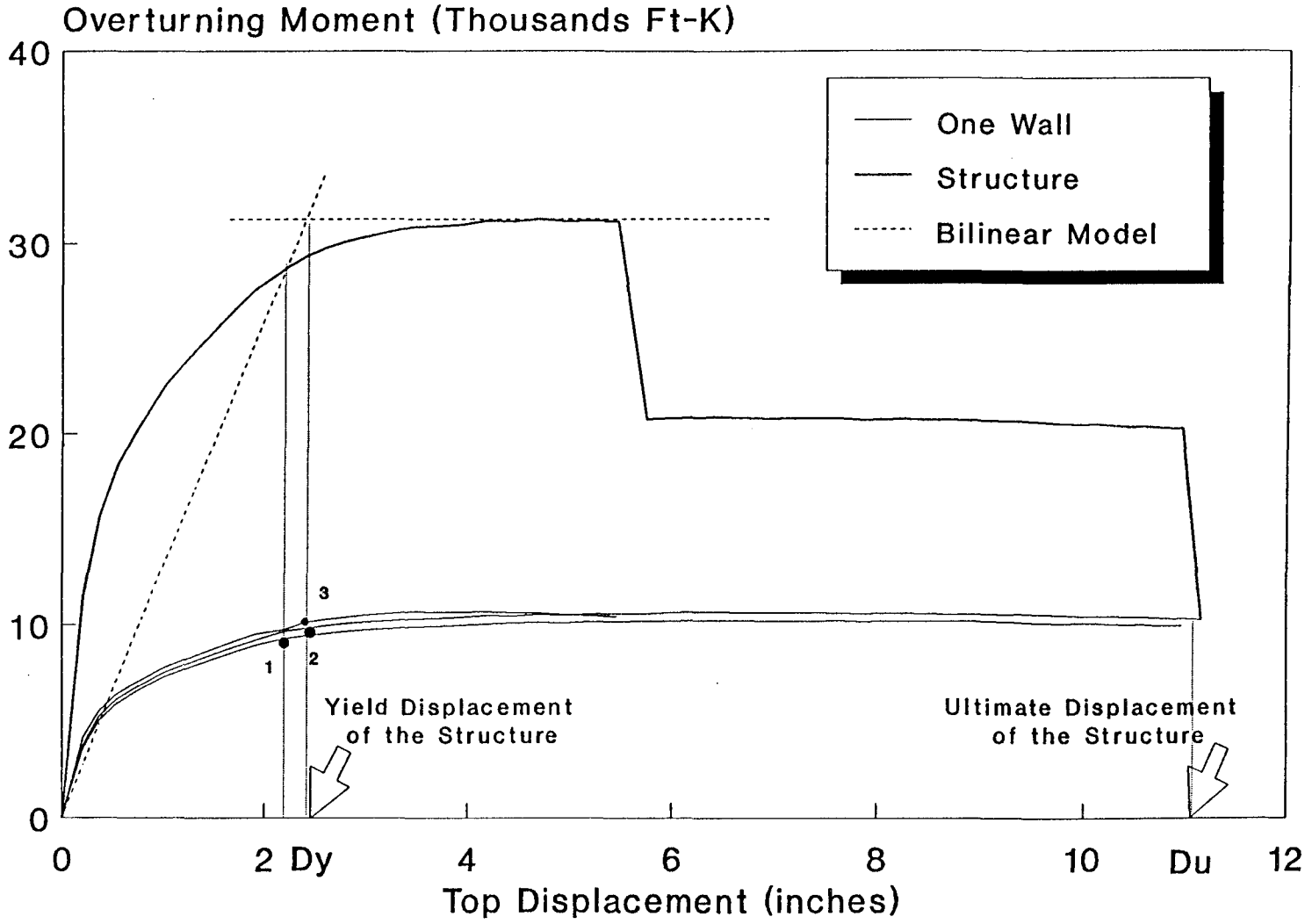

FIGURE 5.4.1 LOAD-DEFLECTION RESPONSE OF A 3-WALL STRUCTURE

The yield displacement of the structure should be defined consistently with the yield displacement of the bilinear model. To achieve this, the load-deflection curve for the structure is "stylized" as follows:

(1) The elastic branch of the bilinear model is obtained by joining the origin to the point on the curve corresponding to the first yielding of a wall.

(2) The plateau of the bilinear model is a parallel to the displacement axis and corresponds to the sum of the yield moments of the walls. If one or more walls have a brittle behavior, the ultimate moment is considered instead of the yield moment.

(3) The yield displacement of the structure is the point on the displacement axis corresponding to the intersection of the two branches of the bilinear model.

The determination of the yield displacement of several structures generated through Monte Carlo simulations revealed that this value is very close to the average of the smallest and the largest yield displacements of the individual walls of the structure.

5.4.3 The Variation of the System Ductility with the Number of Walls

We define the system ductility (SD) as the ratio between the ultimate displacement of the structural system and the yield displacement of the structural

system. Monte Carlo simulations have been performed on samples of structures in order to study the variation of the statistics of SD when the number of walls in the structure varies from two to eight and the mean axial load varies from 0 to 40% of the maximum axial load. The material properties are considered independent among the different walls. In order to guarantee this independence, we used the procedure described in Section 5.2.1. The coefficient of variation of the axial load was selected to be 20% in accordance with the conclusion presented in Section 5.3.1. For each case corresponding to a certain number of walls and a certain mean axial load, we generated 750 structures. For each structure so generated we calculated the yield displacement, the ultimate displacement and system ductility.

In structures where all but one wall exhibited a brittle behavior (Third Structural Limit State according to the definition in Section 5.1), a SD smaller than one was assigned according to the rule established in Section 4.6. Consistently with the definition in Section 4.3, we define the frequency of the brittle structural system behavior as the number of brittle structures divided by 750. These frequencies have been calculated and are presented in Table 5.4.1.

For reasons explained in Section 5.4.1 the frequency of brittle structural system behavior for two-wall buildings is greater than the frequency of brittle behavior for a single wall (see Table 4.3.3). It is remarkably that cases of brittle structural behavior were encountered only for two-wall and three-wall structures.

Table 5.4.1 The Frequency of Brittle Structural Behavior as a Function of the Number of Walls and the Axial Load

Number of Walls	Axial Load / Maximum Axial Load	
	30%	40%
2	1.6%	20.5%
3	0.0%	6.0%

For each sample of 750 structures, the mean and standard deviation of the SD have been estimated for each case associated with a number of walls and a value of the axial load. The results are presented in Tables 5.4.2 and 5.4.3 and in Figures 5.4.2 and 5.4.3.

Table 5.4.2 Mean System Ductility as a Function of the Number of Walls and the Axial Load

Number of Walls	Axial Load / Maximum Axial Load				
	0%	10%	20%	30%	40%
2	18.9	4.7	2.4	1.6	1.3
3	22.0	5.5	2.7	1.8	1.4
4	22.9	5.9	2.9	1.9	1.7
5	23.7	6.2	3.1	2.0	1.7
6	23.9	6.5	3.2	2.0	1.8
7	24.4	6.7	3.3	2.1	1.9
8	25.1	7.0	3.4	2.2	1.9

Table 5.4.3 Coefficient of Variation of the System Ductility as a Function of the Number of Walls and the Axial Load

Number of Walls	Axial Load / Maximum Axial Load				
	0%	10%	20%	30%	40%
2	25%	27%	23%	19%	38%
3	15%	21%	19%	16%	28%
4	13%	19%	17%	15%	22%
5	12%	17%	15%	14%	20%
6	11%	16%	14%	12%	18%
7	9%	15%	14%	12%	17%
8	8%	14%	13%	12%	17%

As shown in Table 5.4.2 and Figure 5.4.2, the mean SD exhibits the following features:

(1) The mean SD increases from 30% to 50% when the number of walls increases from two to eight.

(2) The mean SD decreases dramatically when the axial force increases.

As shown in Table 5.4.3 and Figure 5.4.3, the coefficient of variation of SD exhibits the following features:

(1) The coefficient of variation of SD decreases when the number of walls increases from two to eight. The smaller the axial load, the greater is the rate of decrease in the coefficient of variation of SD.

(2) The coefficient of variation of SD increases when the axial load increases from zero to 10% of the maximum axial load. For axial

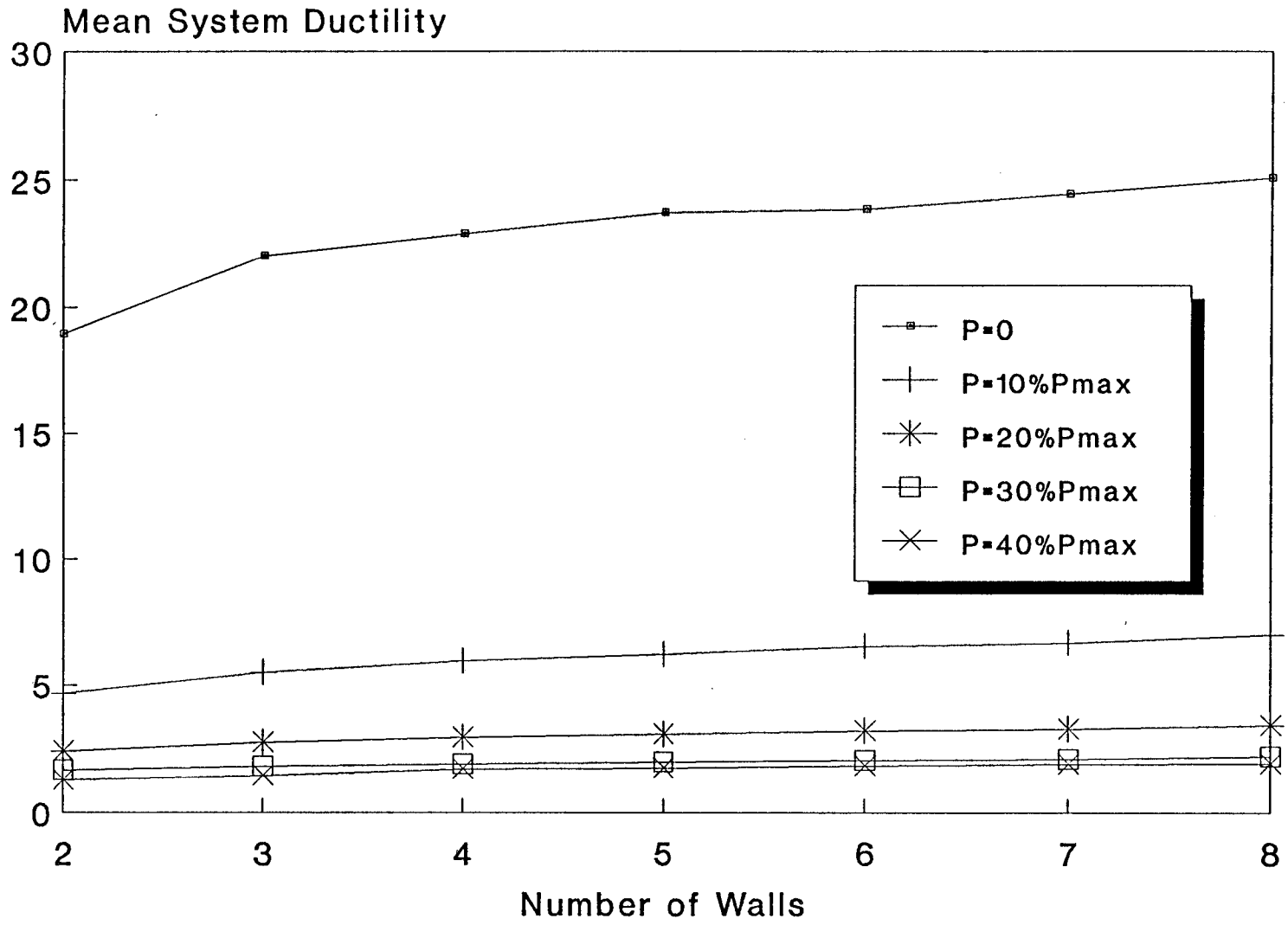

FIGURE 5.4.2 MEAN SYSTEM DUCTILITY VERSUS NUMBER OF WALLS

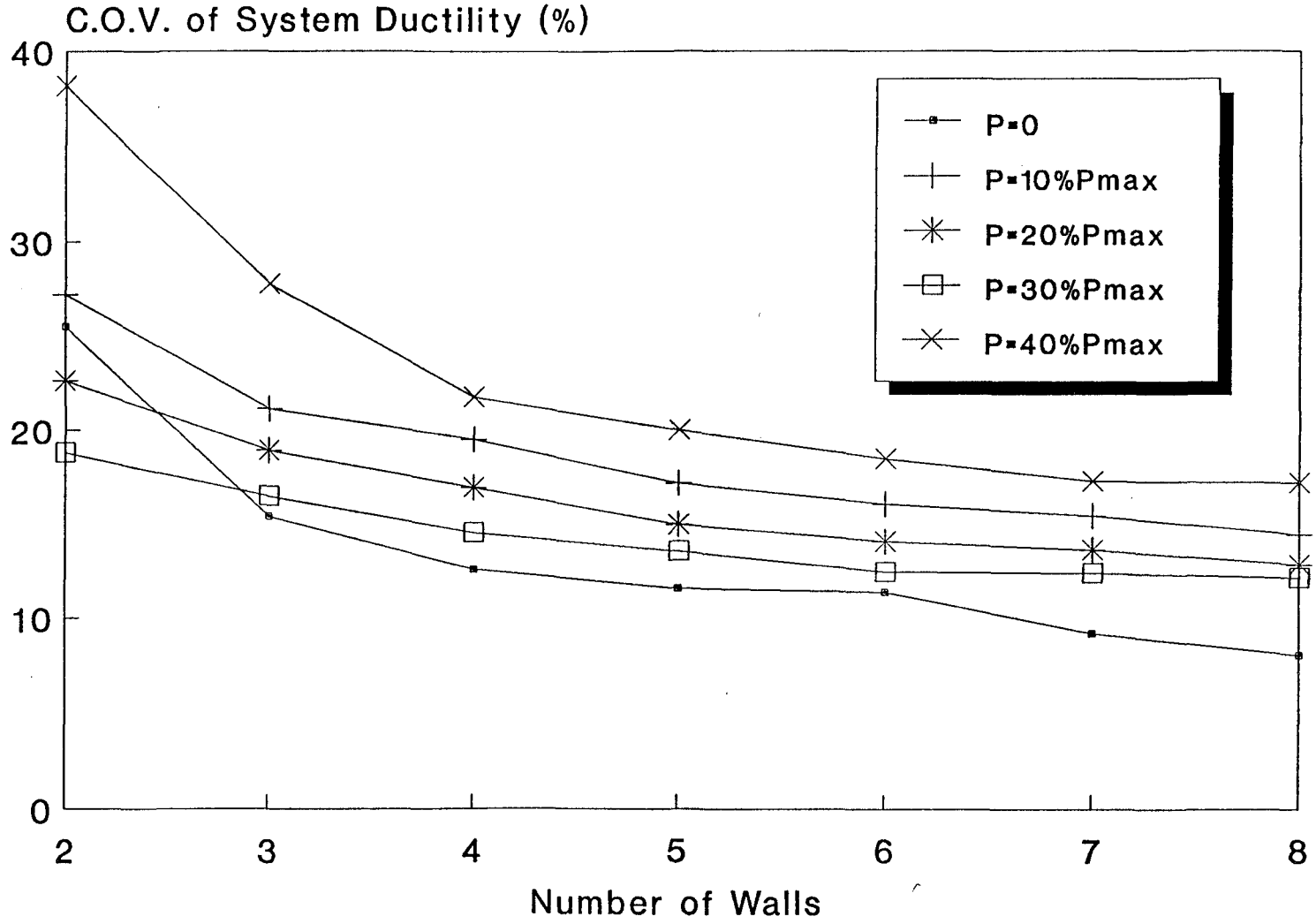

FIGURE 5.4.3 COV OF SYSTEM DUCTILITY VERSUS NUMBER OF WALLS

load between 10% and 30% of the maximum axial load, the coefficient of variation of SD is practically constant, but increases for the 40% axial load case.

The mean system ductility is less sensitive than the coefficient of variation of system ductility to an increase in the number of walls but it is more sensitive to an increase in the axial load.

5.4.4 The Variation of the System Ductility with the Correlation of Material Properties among Walls

Monte Carlo simulations were performed using a building with five walls in order to study the variation of the statistics of system ductility when we vary the coefficient of correlation of material properties (f'_m, ϵ_{mu}, and f_y) and the mean axial load varies from 0 to 40% of the maximum load. All the nondiagonal terms of the three covariance matrices (corresponding to each of the three input variables) have been set up to the same value. This value was, consecutively, 0, 0.0625, and 0.25, and 0.5625 corresponding, respectively, to 0, 0.25, 0.50, and 0.75 values for the correlation coefficient. For instance, the covariance matrices corresponding to a value of the correlation coefficient equal to 0.5 were

$$S_{f'_m} = S_{\epsilon_{mu}} = S_{f_y} = \begin{bmatrix} 1 & 0.25 & 0.25 \\ 0.25 & 1 & 0.25 \\ 0.25 & 0.25 & 1 \end{bmatrix}$$

The coefficient of variation of the axial load was set to 20% based on the conclusion reached in Section 5.3.1. For each case corresponding to a certain correlation coefficient and mean axial load, 750 Monte Carlo simulations were generated and we calculated the mean and standard deviation of the system ductility. The results are presented in Tables 5.4.4 and 5.4.5 and in Figures 5.4.4 and 5.4.5.

Table 5.4.4 Mean System Ductility as a Function of the Correlation Coefficient of Material Properties for a Five-Wall Structure

Correlation Coefficient	Axial Load / Maximum Axial Load				
	0%	10%	20%	30%	40%
0.00	23.7	6.2	3.1	2.0	1.7
0.25	23.6	6.3	3.1	2.0	1.7
0.50	23.6	6.4	3.2	2.0	1.7
0.75	23.6	6.5	3.2	2.1	1.7

As shown in Table 5.4.4 and Figure 5.4.4, the mean SD remains practically constant when the correlation coefficient increases from zero to 75%.

Table 5.4.5 Coefficient of Variation of System Ductility as a Function of the Correlation Coefficient of Material Properties for a Five-Wall Structure (in %)

Correlation Coefficient	Axial Load / Maximum Axial Load				
	0%	10%	20%	30%	40%
0.00	12	17	15	14	20
0.25	12	17	16	15	22
0.50	12	19	18	16	26
0.75	13	22	20	19	35

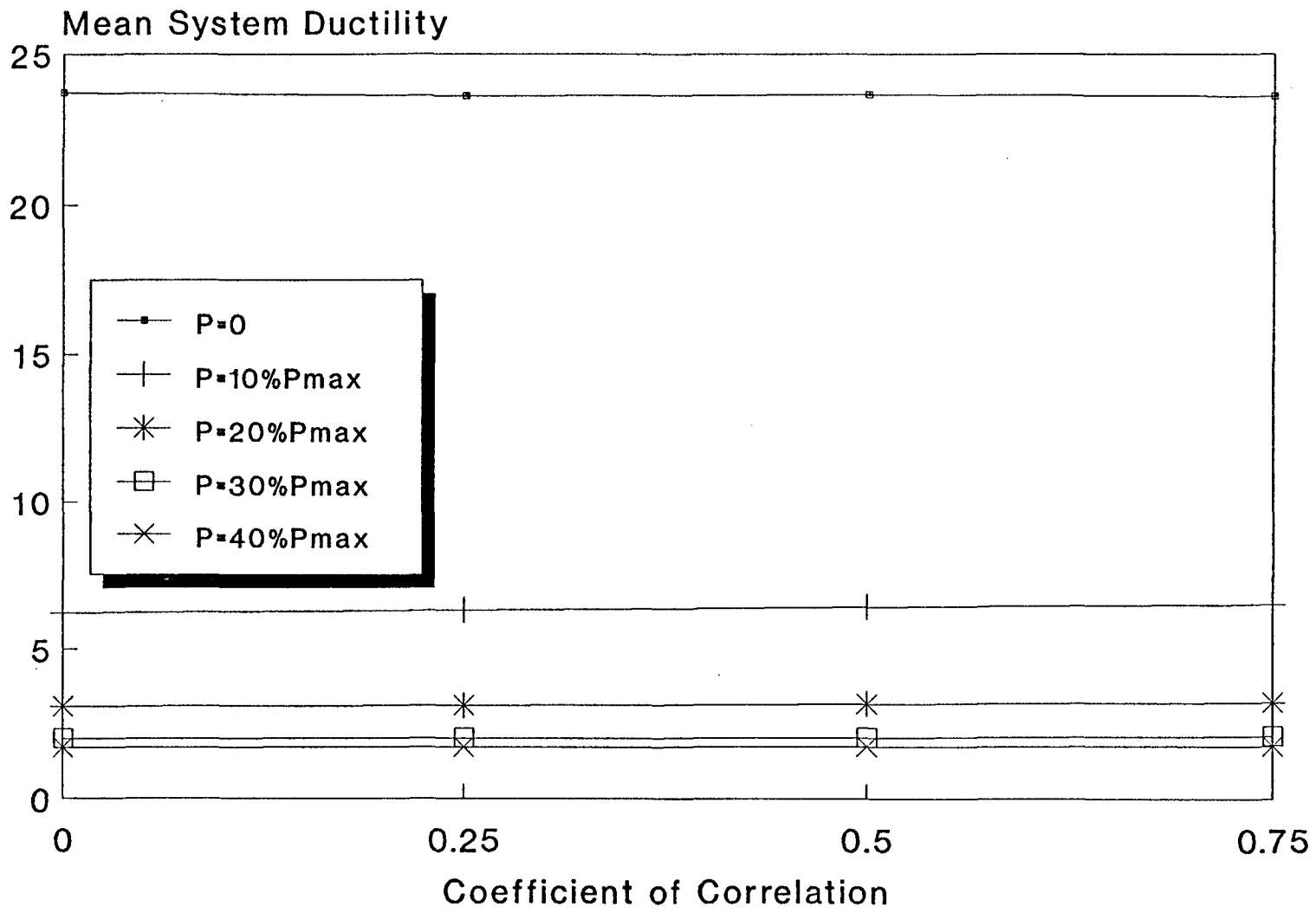

FIGURE 5.4.4 MEAN SD VS. CORRELATION OF MATERIAL PROPERTIES

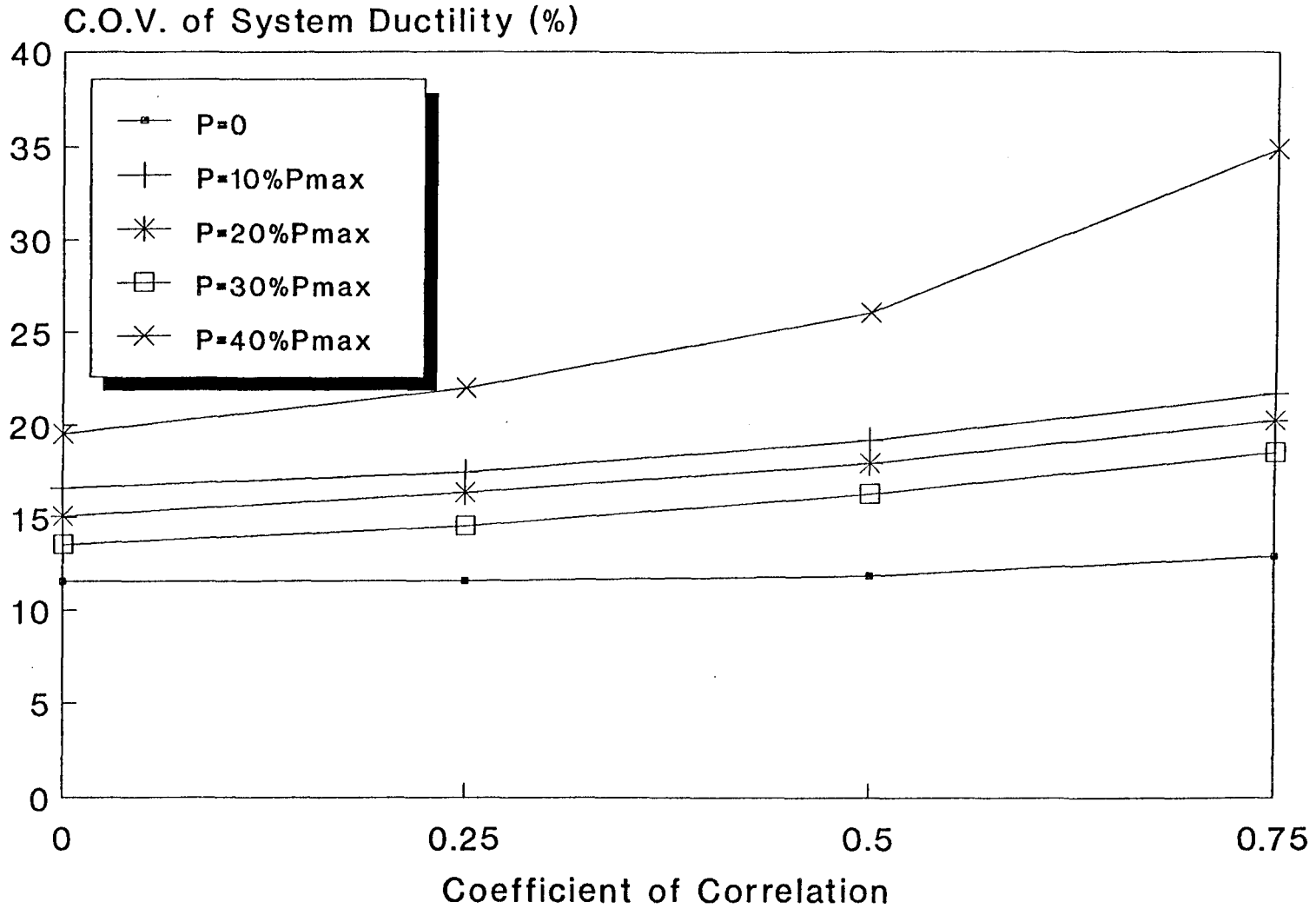

FIGURE 5.4.5 COV OF SD AS A FUNCTION OF CORRELATION

As shown in Table 5.4.5 and Figure 5.4.5, there is, in most cases, an approximately 40% increase in the coefficient of variation of SD when the correlation coefficient increases from zero to 0.75. There are two exceptions:

(1) for zero axial load, the increase is small; and

(2) for the 40% axial load case there is a larger increase in coefficient of variation of SD.

The estimation of the correlation coefficient of the concrete compressive strength f'_c among the walls of an actual structure was performed. This separate study is presented in Appendix D. The estimation resulted in a correlation coefficient of approximately 0.5.

In conclusion, the coefficient of variation of system ductility increases with increasing correlation coefficient while the mean system ductility is almost insensitive to the correlation between the material properties.

5.4.5 System Ductility of the Unbalanced Systems of Walls

Monte Carlo simulations have been performed on samples of six-wall structures of the type presented in Figures 5.3.1 (b) and (c) in order to study the variation of the statistics of the system ductility when the mean unbalance coefficient $\bar{\alpha}$ varies from 0.5 to 1.0 , the correlation coefficient of the axial loads among walls ρ varies between 0.3 and 0.9, and the mean axial load varies from 10

to 20% of the maximum load. For reasons mentioned in Section 5.4.4, all the correlation coefficients of material properties among walls are considered equal to 0.5. The coefficient of variation of the axial load remains 20% for the reasons presented in Section 5.3.1. For each case corresponding to a certain value of $\bar{\alpha}$ (0.5, 0.75 or 1), a certain value of ρ (0.3, 0.5, 0.7, and 0.9), and a certain mean axial load (10% or 20% of the maximum load), 750 structures have been generated. For each structure within one sample, the system ductility has been calculated. The mean and standard deviation of the system ductility have been estimated for each of the 750 structures of the Monte Carlo Simulation. The results are presented in Tables 5.4.6 and 5.4.7 and in Figures 5.4.6 and 5.4.7.

Table 5.4.6 Mean System Ductility for a Six-Wall Unbalanced System

ρ	Axial Load = 10% of Maximum			Axial Load = 20% of Maximum		
	$\bar{\alpha}$=0.5	$\bar{\alpha}$=0.75	$\bar{\alpha}$=1	$\bar{\alpha}$=0.5	$\bar{\alpha}$=0.75	$\bar{\alpha}$=1
30%	9.9	12.7	10.3	4.9	7.0	5.8
50%	9.8	12.0	10.2	5.0	6.5	5.3
70%	9.7	11.5	10.0	5.1	6.0	4.8
90%	9.4	9.5	9.1	4.9	4.9	5.3

The mean SD of this unbalanced system is approximate double the SD of a six-wall balanced system. This can be explained according to the results obtained in Section 2.2.1 and presented in Figure 2.2.3:

(1) The less compressed walls yield earlier;

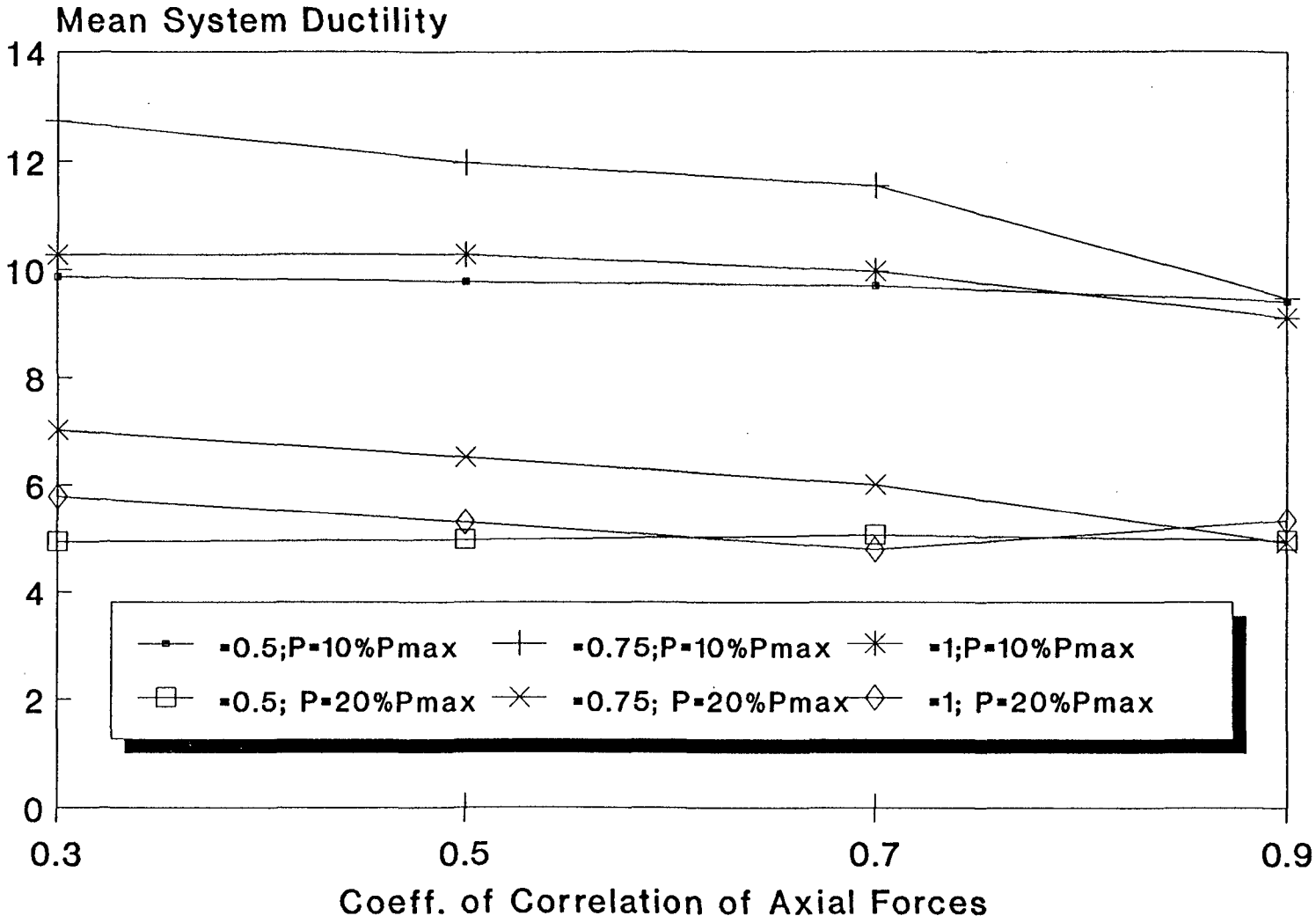

FIGURE 5.4.6 MEAN SD FOR A 6-WALL UNBALANCED SYSTEM

(2) The yield moments of these walls are much smaller than those of the more compressed walls and, consequently, the horizontal branch of the bilinear model as defined in Section 5.4.2 is lowered;

(3) Items (1) and (2) above contribute to a substantial decrease in the yield displacement of the structural system;

(4) the ultimate displacement of the structural system is again governed by walls with small compressive loads and may reach much greater values than those corresponding to the mean value of the axial load.

The very large values of the coefficient of variation of SD (up to five times greater than the corresponding values of the balanced system) suggest that, in case of unbalanced systems, considering the mean SD alone would be misleading. The consequence of these findings for the reliability of the unbalanced system will be discussed in Section 5.6.

Table 5.4.7 Coefficient of Variation of System Ductility for a Six-Wall Unbalanced System (in %)

ρ	Axial Load = 10% of Maximum			Axial Load = 20% of Maximum		
	$\bar{\alpha}$=0.5	$\bar{\alpha}$=0.75	$\bar{\alpha}$=1	$\bar{\alpha}$=0.5	$\bar{\alpha}$=0.75	$\bar{\alpha}$=1
30%	31	25	54	34	41	75
50%	31	26	55	38	46	74
70%	33	31	58	44	53	71
90%	39	47	62	54	62	92

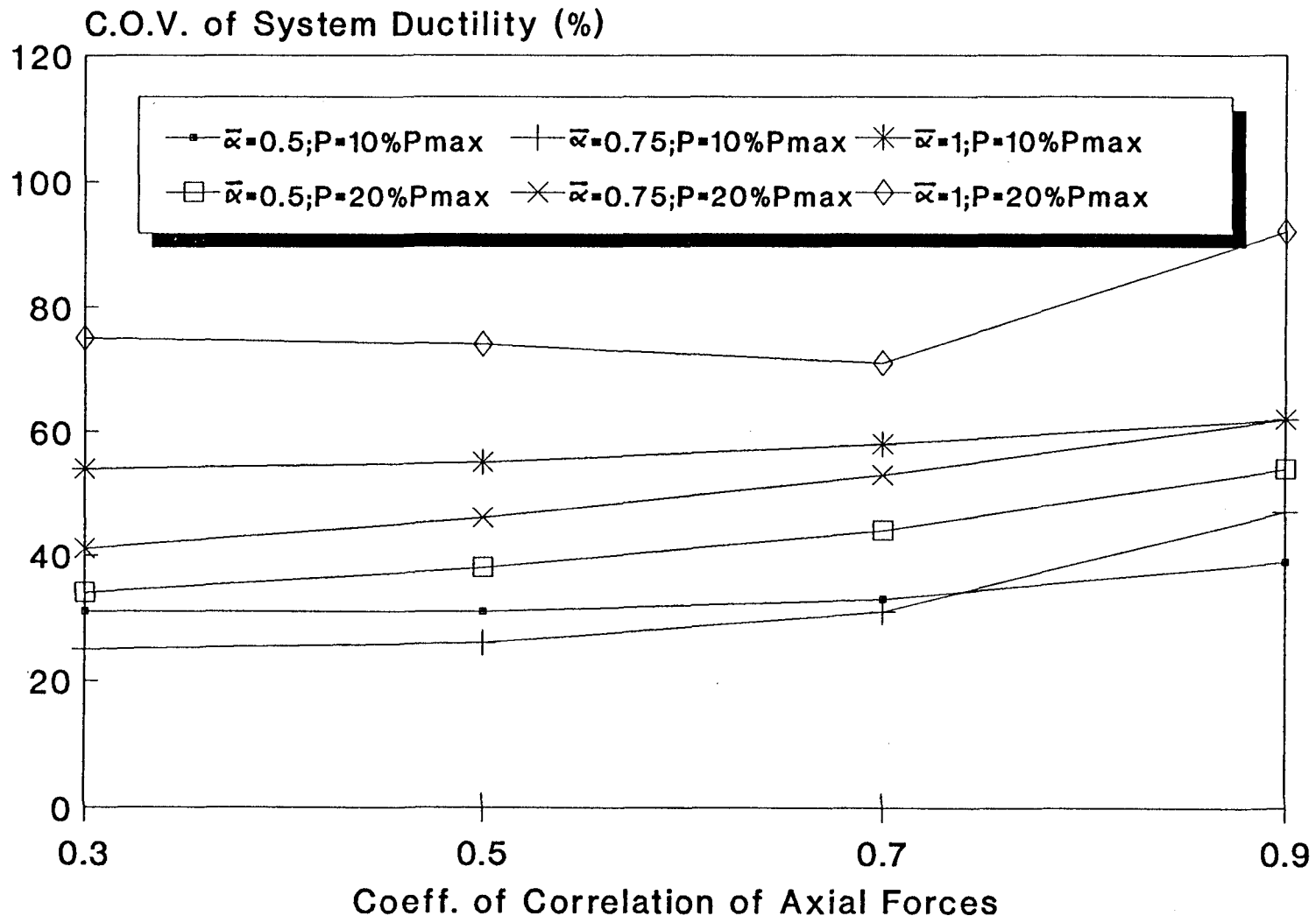

FIGURE 5.4.7 COV OF SD FOR A 6-WALL UNBALANCED SYSTEM

5.5 SYSTEM REDUNDANCY

5.5.1 General

A discussion concerning the latest developments in systems redundancy was presented in Chapter 1. Redundancy is viewed in this research as an intrinsic quality of the structural system, independent of loading, while the *redundancy effects* are different according to the type of loading. The redundancy effects are manifested when the structure is subjected to earthquake loading by the gain (or loss) in overall capacity with respect to the component capacity. An increase in capacity from the element level to the system level will imply an increase in system reliability.

In order to study the redundancy effects of a wall system, one has to acknowledge the difference between the problem statement in this research as compared to the existing literature. There are several basic differences:

(1) The horizontal loads are absent from the equation of the limit state surface. The vertical loads are present in this equation but their role in the flexural behavior of the wall is more on the side of material properties.

(2) The ductility indices at the element and structural system level reflect the necessity of preserving ductile behavior rather than outright failure like in case of reliability indices.

(3) Instead of quantifying the ultimate capacity of the structural system in terms of generalized force, we are interested in quantifying the system ductility.

(4) The structural system is subjected to imposed displacements instead of forces.

(5) After the failure of one wall there is no redistribution in the system, hence the degree of static indeterminacy is almost irrelevant.

The complexity created by these basic differences, preclude the utilization of any of the probabilistic redundancy indices existing in the literature and discussed in Chapter 1.

A structural system composed by statistically identical elements (i.e. having the same statistics for each geometrical or material property) working in parallel is defined as a "balanced system." In this case, the redundancy effect can be understood as Cornell's "probabilistic redundancy" (Cornell, 1988 b) i.e. the effect of the stochastic variations of resistance of different parallel elements about a common mean that does not permit the structure to collapse when the first member fails.

The structural system studied in this research can be best modeled as a "balanced system" when the axial load corresponding to each wall has the same mean value and coefficient of variation. One limit state of interest for the structure composed of concrete masonry walls is the ultimate displacement of each individual wall. The greater the spread of the ultimate displacement corresponding

to each wall of the structure about the common mean ultimate displacement, the greater the redundancy effect because the extreme cases will govern the ultimate displacement of the structure.

This finding would suggest that we quantify redundancy effects using the coefficient of variation of the ultimate displacement (d_u). Such a redundancy index that is a function of the coefficient of variation of d_u only would be invariant to the number of walls in a parallel system. Since this is unreasonable, we need to find a definition that involves directly the ordered statistics of the set of walls that constitute the structural system. At the same time, the definition must capture the two milestones in the load-deflection relationship of the structural system that are present in the current definitions of the redundancy index: the first wall reaching its ultimate limit state and the structural system reaching its ultimate limit state.

We define as Redundancy Ratio (RR) the ratio between the displacement corresponding to the structural system reaching its ultimate limit state and the displacement corresponding to the wall reaching its ultimate limit state. When RR has the minimum value of 1 (i.e. all the walls fail simultaneously), there are no redundancy effects in the system. As RR is a random variable, its mean and coefficient of variation characterize the *probabilistic redundancy effects* of the system. The mean and coefficient of variation of RR were calculated for each Monte Carlo sample as described in Section 5.4. The results are presented in Sections 5.5.2 and 5.5.3.

5.5.2 The Variation of the Redundancy Ratio with the Number of Walls

The series of Monte Carlo analyses described in Section 5.4.3 was used to study the variation of the Redundancy Ratio (RR) with respect to the number of walls in the structural system. The statistics of the redundancy ratio are presented in Tables 5.5.1 and 5.5.2 and in Figures 5.5.1 and 5.5.2.

Table 5.5.1 Mean Redundancy Ratio as a Function of the Number of Walls and Axial Load

Number of Walls	Axial Load / Maximum Axial Load				
	0%	10%	20%	30%	40%
2	1.0	1.0	1.0	1.0	1.0
3	1.3	1.4	1.3	1.2	1.0
4	1.5	1.6	1.4	1.3	1.1
5	1.6	1.6	1.5	1.3	1.2
6	1.7	1.8	1.6	1.4	1.3
7	1.8	2.0	1.7	1.5	1.4
8	1.8	2.0	1.7	1.5	1.4

As shown in Figure 5.5.1, the mean redundancy ratio exhibits the following features:

(1) The mean RR increases with the number of walls and levels off for more than seven walls.

(2) The mean RR increases when the axial load on the wall decreases. The only exception is observed for the zero axial load case when the

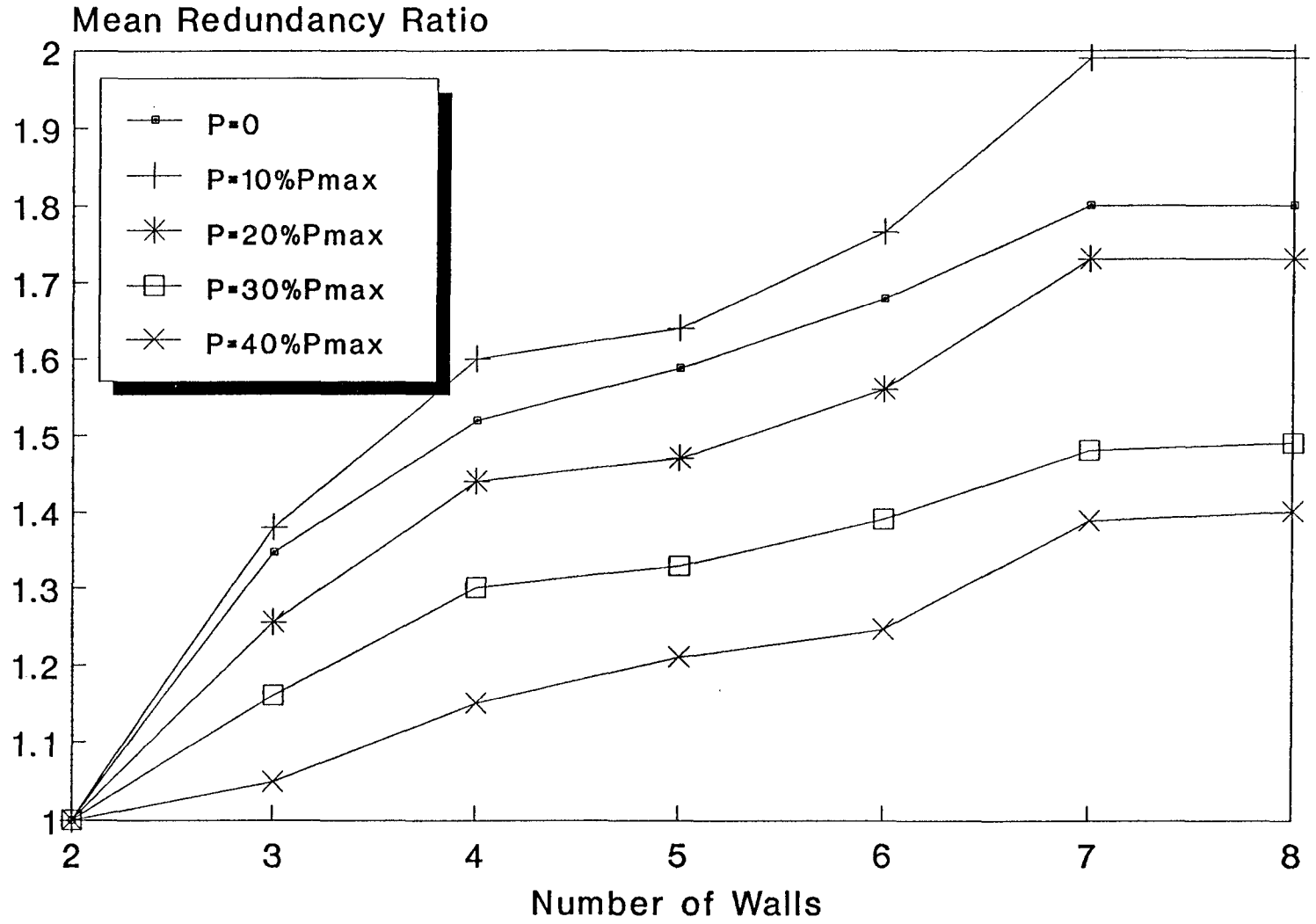

FIGURE 5.5.1 MEAN REDUNDANCY RATIO VERSUS NUMBER OF WALLS

mean RR is smaller than that corresponding to the 10% axial load case. This behavior matches closely the variation of the coefficient of variation of the ultimate displacement with the axial load as presented in Figure 2.2.5. The explanation of this behavior has been provided in Section 2.2.2. Because high axial load results in a higher potential for brittle behavior, the essence of this feature is that structural systems composed of brittle elements possess a small value of the RR. This important property of the redundancy ratio for balanced systems of walls confirms a similar finding obtained for Daniels Systems (Rackwitz and Gollwitzer, 1988).

(3) The higher the axial load, the smaller the increase in the redundancy ratio. When the number of walls increases from 2 to 8, the mean RR increases by 100% for the 10% axial load case but the increase is only 40% when the axial load is 40%.

As shown in Figure 5.5.2, the coefficient of variation of the redundancy ratio exhibits the following features:

(1) The coefficient of variation of redundancy ratio is essentially independent of the number of walls.

(2) The coefficient of variation of redundancy ratio decreases from approximatively 25% to 15% when the axial load increases from zero to 40% of the maximum axial load.

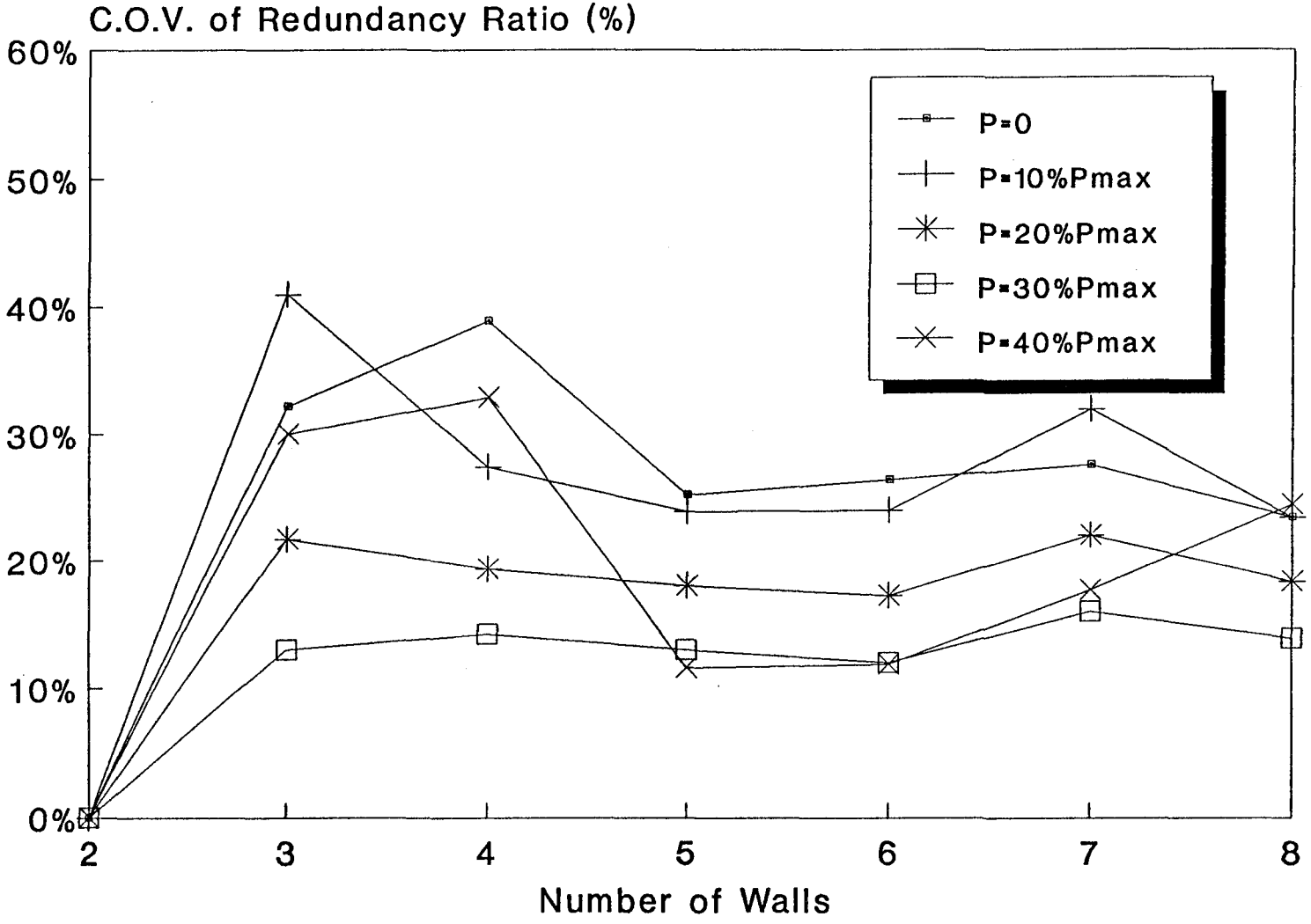

FIGURE 5.5.2 COV REDUNDANCY RATIO VERSUS NUMBER OF WALLS

Table 5.5.2 Coefficient of Variation of the Redundancy Ratio as a Function of the Number of Walls and Axial Load

Number of Walls	Axial Load / Maximum Axial Load				
	0%	10%	20%	30%	40%
2	0	0	0	0	0
3	32	41	22	13	30
4	39	27	19	14	33
5	25	24	18	13	12
6	26	24	17	12	12
7	28	32	22	16	18
8	23	23	18	14	24

It can be observed from Table 5.5.1 that the maximum values of the mean redundancy ratio, reached when the structure has a sufficient number of walls, is equal to 2 for the 10% axial load case and 1.4 for the 40% axial load case. In practice, another index of a more direct physical meaning may be useful. It is interesting to know how much additional capacity is conferred to the system through redundancy. This additional capacity can be investigated calculating the ratio between the displacement corresponding to the system reaching its ultimate structural limit state and the *expected* displacement corresponding to a single wall reaching its ultimate limit state. The mean value of this ratio has been calculated using a Monte Carlo simulation for the 7-wall system for the 40% and 10% axial load cases and it was equal to 1.08 and 1.19, respectively. This means that using a sufficient number of walls we can obtain an average increase in the capacity of the structure to withstand imposed displacements from 8% to 19%.

5.5.3 The Variation of the Redundancy Ratio with the Correlation of Material Properties among the Walls

The series of Monte-Carlo analyses described in Section 5.4.4 were performed to obtain results enabling us to study the variation of the redundancy ratio with respect to the correlation coefficient of material properties among the walls of the structure. The statistics of the redundancy ratio are presented in Tables 5.5.3 and 5.5.4 and in Figures 5.5.3 and 5.5.4.

As shown in Figure 5.5.3, the mean redundancy ratio is essentially independent of the correlation coefficient of the material properties. There is an exception for the 40% axial load case when the mean RR slightly increases with the correlation coefficient.

As shown in Figure 5.5.4, the coefficient of variation of the redundancy ratio is also very insensitive of the correlation coefficient of the material properties with an exception for the 40% axial load case. In that case, the coefficient of variation of redundancy ratio increases with the value of the correlation coefficient going from 12% to 33%.

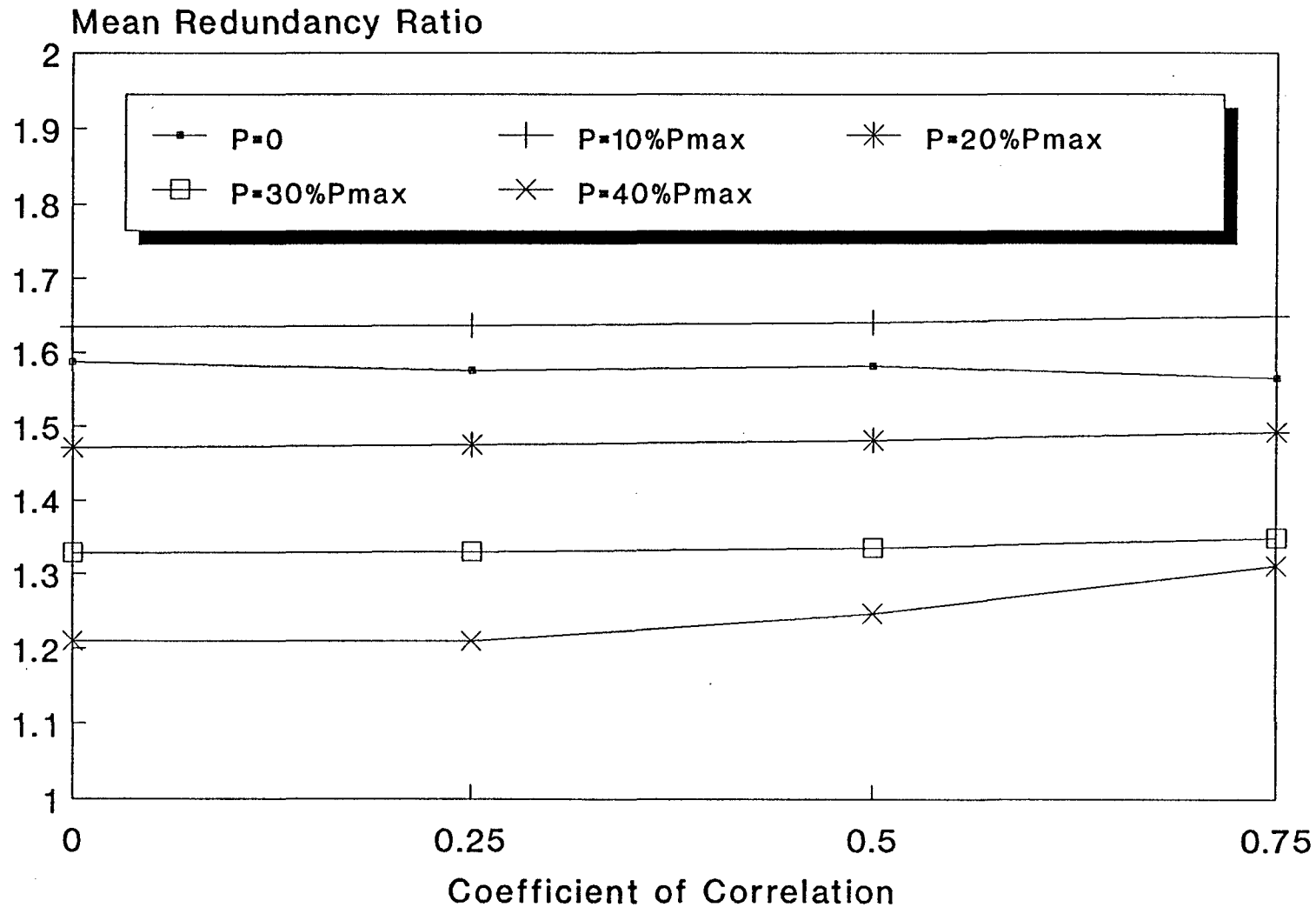

FIGURE 5.5.3 MEAN RR VS. CORRELATION OF MATERIAL PROPERTIES

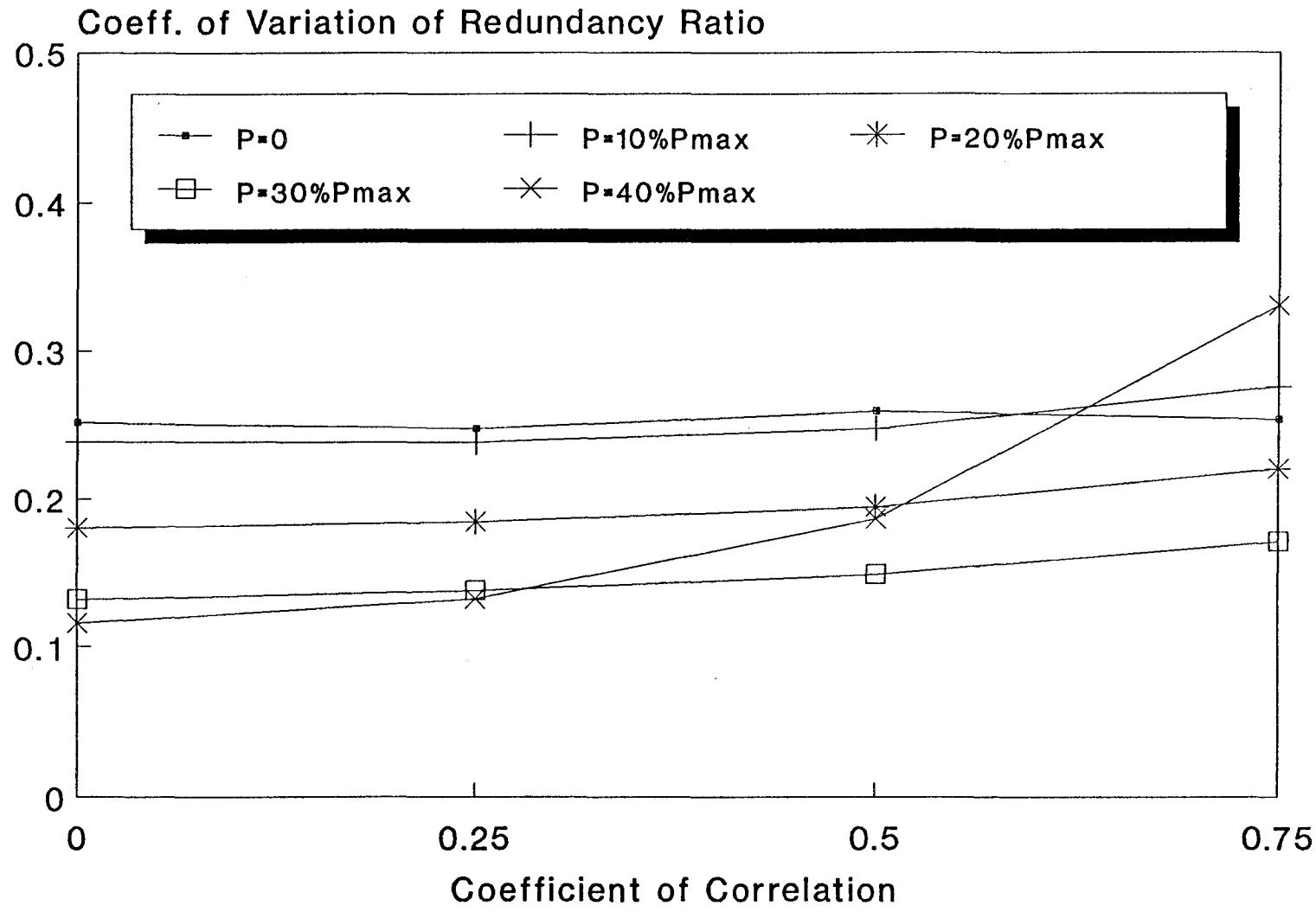

FIGURE 5.5.4 COV OF RR VS CORRELATION OF MATERIAL PROPERTIES

Table 5.5.3 Mean Redundancy Ratio as a Function of the Correlation Coefficient of Material Properties

Correlation Coefficient	Axial Load / Maximum Axial Load				
	0%	10%	20%	30%	40%
0.00	1.6	1.6	1.5	1.3	1.2
0.25	1.6	1.6	1.5	1.3	1.2
0.50	1.6	1.6	1.5	1.3	1.2
0.75	1.6	1.6	1.5	1.3	1.2

Table 5.5.4 Coefficient of Variation of the Redundancy Ratio as a Function of the Correlation Coefficient of Material Properties (%)

Correlation Coefficient	Axial Load / Maximum Axial Load				
	0%	10%	20%	30%	40%
0.00	25	24	18	13	12
0.25	25	24	18	14	13
0.50	26	25	19	15	19
0.75	25	28	22	17	33

5.5.4 Redundancy Effects of the Unbalanced Systems of Walls

As stated in Section 5.5.1, the probabilistic redundancy in parallel systems is meaningful for balanced systems. In case of a slight unbalance in the system due to differences in wall geometry or axial load the redundancy ratio can still be defined as in Section 5.5.1. However, in case of strongly unbalanced systems as

that studied in Section 5.4.5 the definition introduced in Section 5.5.1 can not be used. Because of the unbalance, the coefficient of variation of the ultimate displacement of the six walls in the system is high, but this does not provide an additional resistance capacity. Due to cyclic nature of the earthquake loads, the walls that are highly compressed will fail during one cycle and the other three walls can fail in a subsequent cycle when the strong motion component perpendicular to the walls changes the direction. This suggests a split of the unbalanced system into two balanced subsystems. It appears that the redundancy effects of the unbalanced system studied in Section 5.4.3 is governed by the redundancy effects of the weakest subsystem (i.e. the subsystem with the highest axial load). The presence of a much stronger balanced system does not help the overall redundancy effects of the unbalanced system.

5.5.5 Discussion on Redundancy Effects versus System Ductility for the Wall Structures

It is interesting to compare the conclusions obtained in Section 5.5 for redundancy ratio with those obtained in Section 5.4 for the system ductility. For the balanced systems, the two properties appear to have a contradictory character as it results from the two main conclusions:

(1) The mean redundancy ratio increases with the number of walls at a much higher rate than the mean system ductility increases.

(2) Unlike the coefficient of variation of system ductility that decreases when the number of walls increases, the coefficient of variation of redundancy ratio is independent of the number of walls.

These features are summarized in Table 5.5.5.

Table 5.5.5 The Variation of System Ductility and Redundancy Ratio with an Increasing Number of Walls

	System Ductility	Redundancy Ratio
Mean Value	Almost Constant	Increases
Coefficient of Variation	Decreases	Constant

According to its definition, the mean value of the redundancy ratio mirrors the scatter in the system ductility and, apparently, it should exhibit similar features to the coefficient of variation of the system ductility. Then, why does the mean redundancy ratio increase when the coefficient of variation of system ductility decreases ? The explanation resides with the rapport between scatter and uncertainty.

When the uncertainty in system ductility increases because the uncertainty in material properties or axial loads increases, the redundancy ratio increases. However, an increase in the number of walls without changing the statistics of the material properties or axial load does not increase the uncertainty. The increase in the number of walls is similar to increasing the size of a statistical sample. This produces a more confident estimate associated with a smaller sampling variance. This decrease in uncertainty is revealed by the decrease in the coefficient of

variation of system ductility. At the same time, the ratio of the two extremes of the sample increases. This increase is not a consequence of an increase in uncertainty; in a larger sample the expected maximum is greater and the expected minimum is smaller according to the properties of the ordered statistics (Bury, 1975). This explains why the scatter in system ductility reflected by the redundancy ratio increases, while the overall uncertainty in the system decreases. Hence, both system ductility and redundancy ratio, although apparently contradictory, provide their beneficial effects to the system behavior.

5.6 SYSTEM ROBUSTNESS

5.6.1 General

It was recognized that the ability of the structural system to survive the loading is better represented by a new quality that has been called "robustness" (Corotis et al, 1988). We define as "robustness" the system quality that combines the beneficial effects of the system ductility and redundancy to the advantage of the balanced system. An index that can quantify robustness must fulfill the conditions outlined in Section 5.5.5:

(1) Increases with the mean value of SD; and

(2) Increases when the scatter of SD decreases.

In Section 4.5 we have defined the Ductility Index for a wall (DI) as the safety index based on displacement ductility and calculated with Equation (5.6.1):

$$DI = \frac{\overline{\mu_d} - 1}{\sigma_d} \tag{5.6.1}$$

Using the same theoretical background, we define the System Ductility Index (SDI) as a function of the statistics of the System Ductility (SD):

$$SDI = \frac{\overline{SD} - 1}{\sigma_{SD}} \tag{5.6.2}$$

where:

$\overline{SD}$ = the mean value of the System Ductility

σ_{SD} = the standard deviation of the System Ductility

For the reasons similar to those delineated in Section 4.4, SDI is the safety index of ductile structural behavior. Similar to DI, the SDI is not invariant to different mappings of the limit state equation.

Besides the quantification of safety with respect to ductile behavior, the System Ductility Index fulfills the conditions outlined above for measuring the system robustness. That is:

(1) The SDI increases with the mean value of SD and this is the beneficial effect provided by the SD.

(2) The SDI increases when the scatter of SD decreases; this decrease in uncertainty is attributed to the increase in the number of walls, and consequently to increased redundancy effects.

5.6.2 The Variation of the System Ductility Index with the Number of Walls

The series of Monte Carlo analyses described in Section 5.4.3 were performed and they produced results on the variation of the system ductility index with respect to the number of walls in the structure. The results are presented in Table 5.6.1 and in Figure 5.6.1.

Table 5.6.1 System Ductility Index as a Function of the Number of Walls and Axial Load

Number of Walls	Axial Load / Maximum Axial Load				
	0%	10%	20%	30%	40%
2	3.72	2.89	2.59	2.10	0.56
3	6.20	3.87	3.37	2.73	1.10
4	7.60	4.27	3.90	3.26	1.89
5	8.29	4.89	4.50	3.67	2.14
6	8.44	5.28	4.89	4.12	2.47
7	10.42	5.51	5.10	4.23	2.76
8	11.98	5.95	5.52	4.51	2.79

As shown in Table 5.6.1 and Figure 5.6.1, the SDI increases substantially when the number of walls increases from two to eight. The rate of increase is dependent of the axial load, as follows:

- For the zero axial load case the SDI increases more than three times from its value for two-wall buildings.

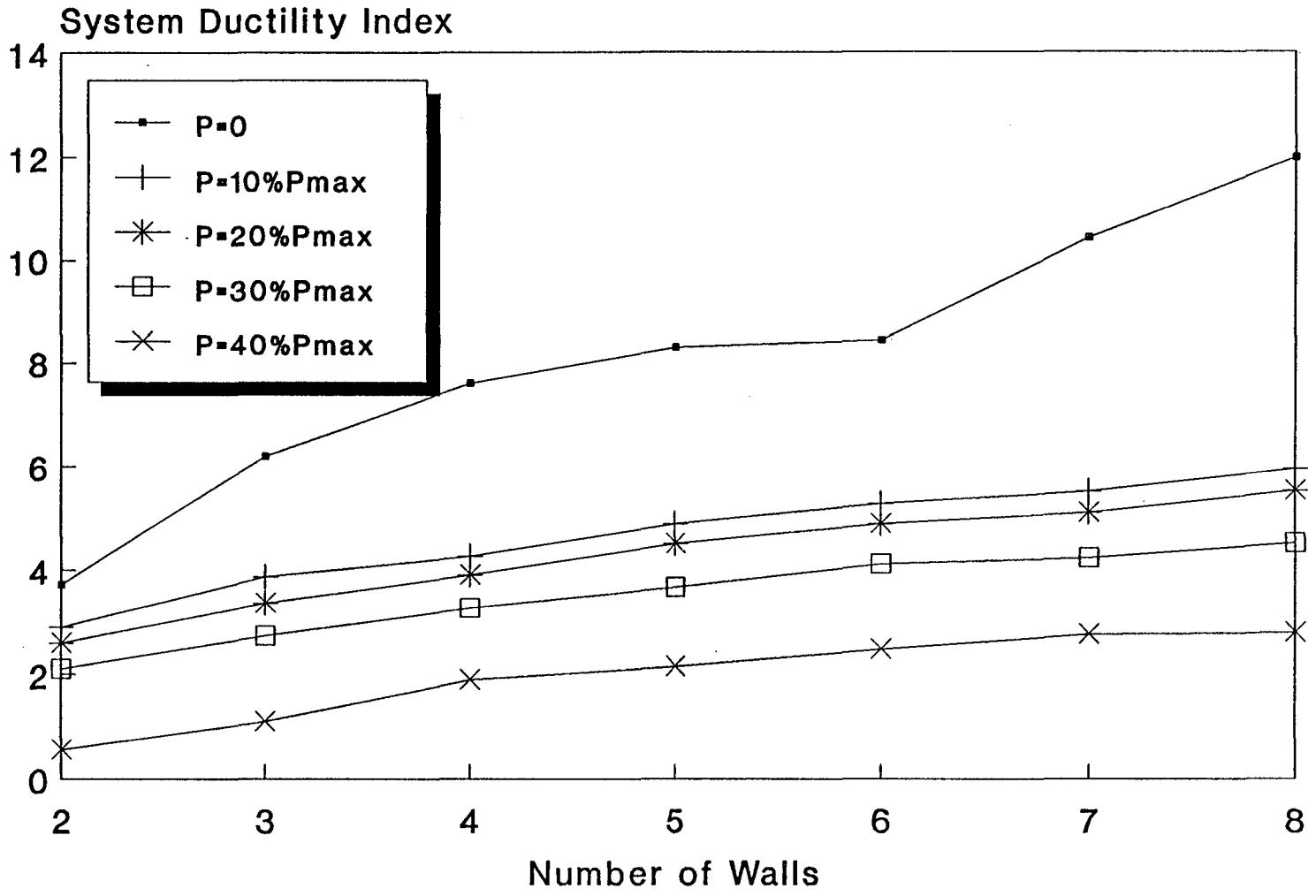

FIGURE 5.6.1 SDI AS A FUNCTION OF THE NUMBER OF WALLS

- For axial loads from 10% to 30% of the maximum, the SDI increases more than twice from its value for two-wall buildings.
- For the 40% axial load case, the SDI increases five times from its value for two-wall buildings.

The patterns of the system ductility index increase with the number of walls is dependent of the three limit states of structural failure described in Section 5.1. For axial loads between 10% and 30% of the maximum axial load, corresponding to the second limit state, the curves in Figure 5.6.1 are almost parallel and closely spaced. The curve corresponding to the 40% axial load case is parallel to the previous curves from 4 walls to 8 walls when the system as a whole behaves according to the Second Structural Limit State. As mentioned in Section 5.4.3, two and three-wall structures may exhibit a brittle behavior for this level of axial load. The relatively small values for the frequency of brittle structural behavior presented in Table 5.4.1 are sufficient to cause the system ductility index values to be much lower than the general trend would have indicated.

5.6.3 The Variation of the System Ductility Index with the Correlation of Material Properties among Walls

The series of Monte Carlo analyses described in Section 5.4.4 were performed and they produced the results for the variation of the system ductility index with respect to the correlation coefficient of material properties among the

walls of the structure. These results are presented in Table 5.6.2 and in Figure 5.6.2.

Table 5.6.2 System Ductility Index as a Function of the Correlation Coefficient of Material Properties

Correlation Coefficient	Axial Load / Maximum Axial Load				
	0%	10%	20%	30%	40%
0.00	8.29	4.89	4.50	3.67	2.14
0.25	8.28	4.82	4.15	3.44	2.33
0.50	8.09	4.40	3.81	3.13	2.13
0.75	7.40	3.89	3.39	2.79	1.20

As shown in Table 5.6.2 and Figure 5.6.2, the SDI decreases when the correlation coefficient of material properties increases from zero to 0.75. The rate of decrease is practically independent of the axial load. As an average, when the correlation coefficient increases from zero to 0.75, the SDI decreases by 25%. The only exception is the larger decrease for the highest correlation coefficient combined with the highest value of the mean axial load. The low value of SDI exhibited by this case (1.20) shows how the advantages of structural behavior with respect to the individual wall behavior can be annihilated when the high axial load is combined with a high (but not unreasonable) correlation coefficient of the material properties.

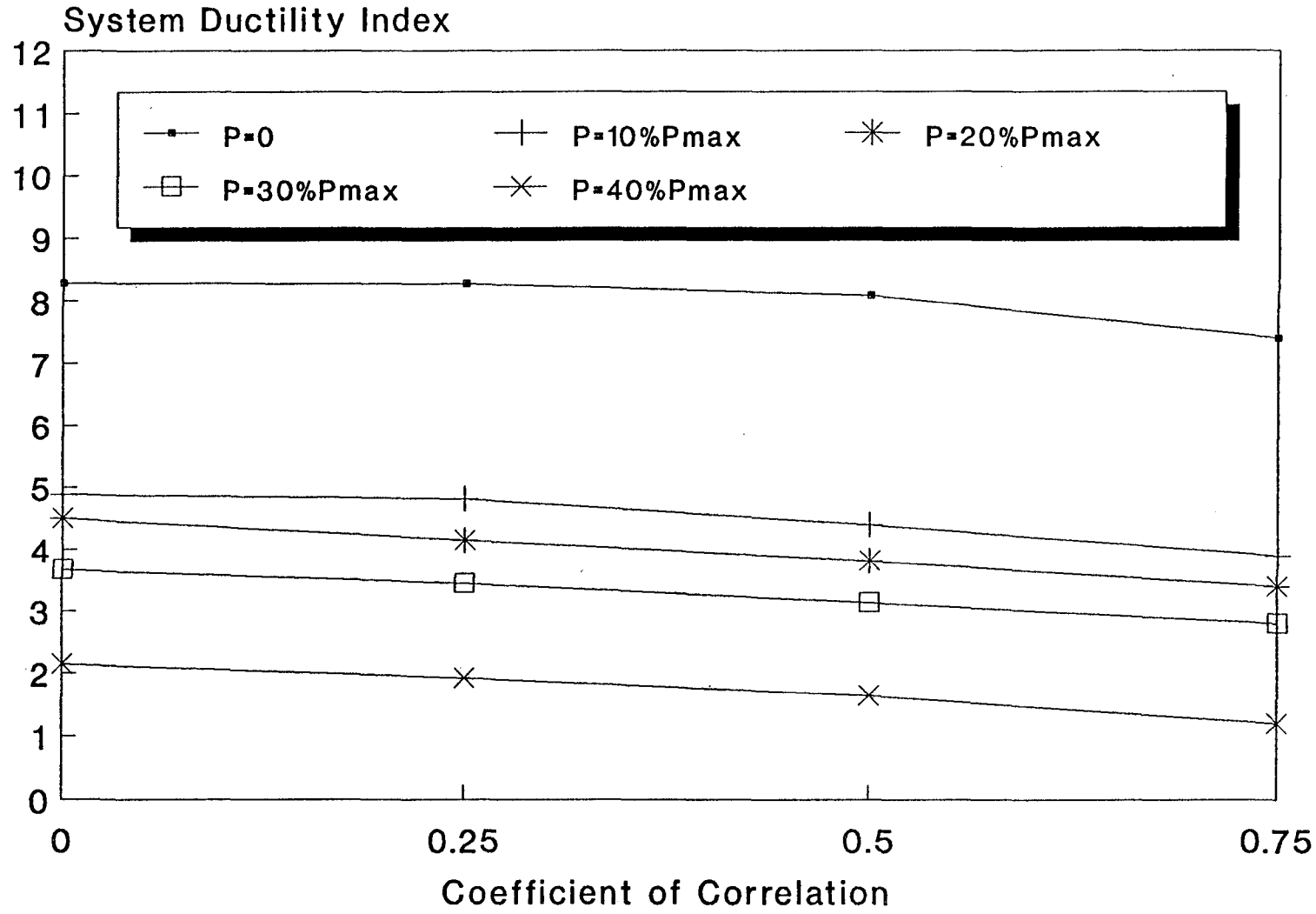

FIGURE 5.6.2 SDI AS A FUNCTION OF COEFFICIENT OF CORRELATION

5.6.4 The System Ductility Index of the Unbalanced Systems of Walls

The series of Monte Carlo analyses described in Section 5.4.5 were performed and they produced the results showing the variation of the system ductility index with respect to the variation of the mean unbalance coefficient $\bar{\alpha}$, the correlation coefficient of the axial loads among walls ρ, and the mean axial load $\bar{P}$. These results are presented in Table 5.6.3 and in Figure 5.6.3.

Table 5.6.3

System Ductility Index for a Six-Wall Unbalanced System

ρ	Axial Load = 10% of Maximum			Axial Load = 20% of Maximum		
	$\bar{\alpha}$=0.5	$\bar{\alpha}$=0.75	$\bar{\alpha}$=1	$\bar{\alpha}$=0.5	$\bar{\alpha}$=0.75	$\bar{\alpha}$=1
30%	2.89	3.71	1.67	2.31	2.11	1.11
50%	2.84	3.44	1.64	2.11	1.83	1.09
70%	2.69	2.92	1.55	1.84	1.57	1.12
90%	2.36	1.89	1.43	1.47	1.28	0.89

Because of the complexity of the problem for the case of the unbalanced wall system, the different combinations of the values of $\bar{\alpha}$ and mean axial load produce SDI values with less conclusive and sometimes surprising trends. The only expected trend is the SDI decrease when the correlation coefficient of axial forces increases from 0.3 to 0.9. This decrease is between 15% and 50% but

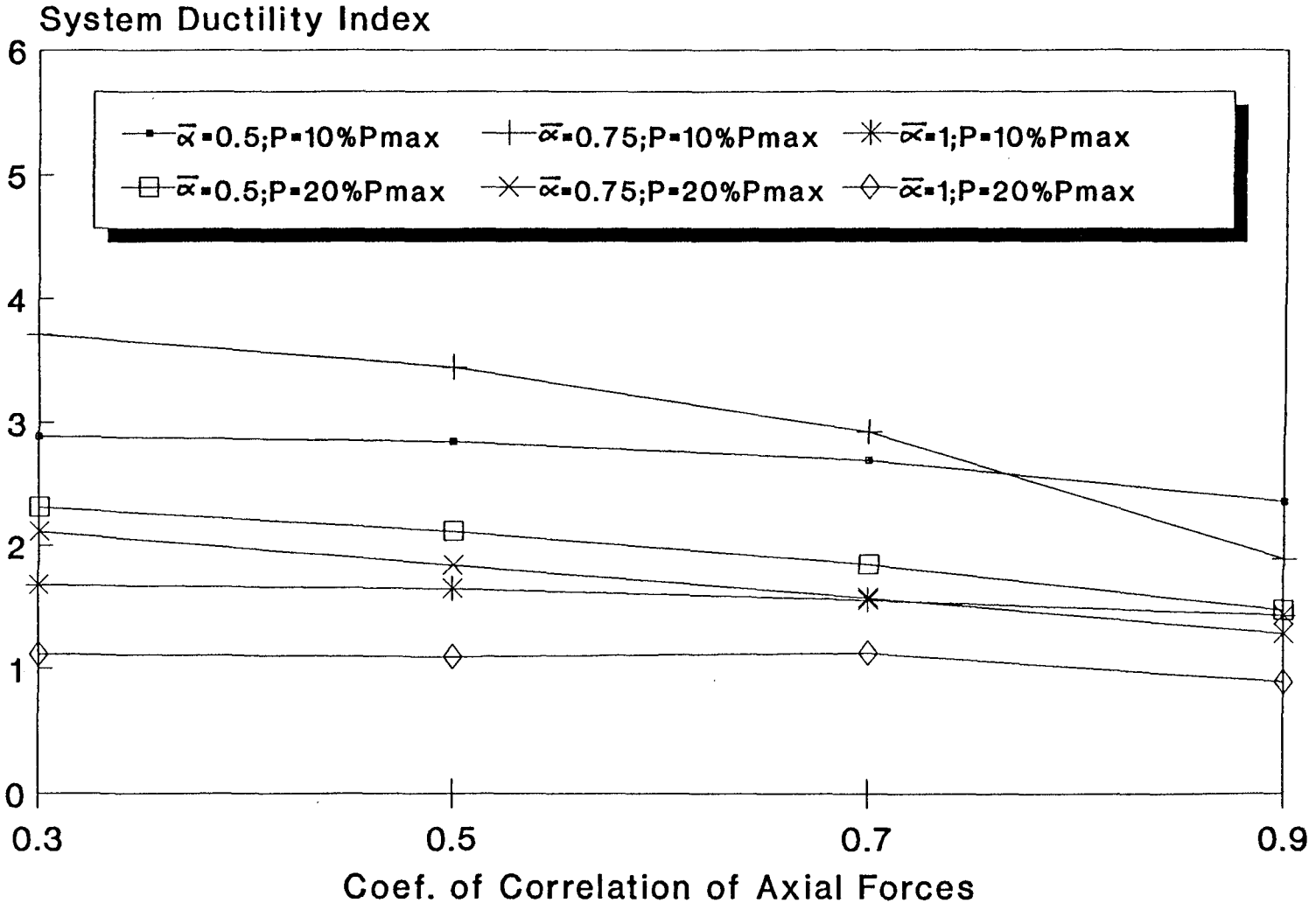

FIGURE 5.6.3 SDI FOR A 6-WALL UNBALANCED SYSTEM

there is not a clear dependence of this rate to the unbalance coefficient or the mean axial load.

It was expected that a larger mean unbalance coefficient $\bar{\alpha}$ will produce a smaller SDI. This feature was observed in most cases. The exception occurs for $\bar{\alpha}=0.75$ and 10% axial load case. However, the negative effect of a high unbalance coefficient is felt for values of correlation coefficient of axial forces below 0.5: a mean unbalance coefficient equal to 1 can push the SDI corresponding to the 10% axial load case below SDI values for 20% axial load with a smaller $\bar{\alpha}$.

It was suggested in Section 5.5.4 that the unbalanced system can be split in two balanced systems. It is interesting to compare the range of SDI values obtained for the unbalanced system with the SDI values presented in Table 5.6.1 and obtained for the component balanced subsystems. For example, the six-wall unbalanced system with $\bar{\alpha}=1$ and 20% axial load can be split into two balanced three-wall systems. The weakest system has a mean axial load equal to $(0.2*P_{maximum}+1*0.2*P_{maximum}) = 0.4*P_{maximum}$ while the strongest system has a mean axial load equal to $(0.2*P_{maximum}-1*0.2*P_{maximum})=0$. This comparison is presented in Table 5.6.4 for the cases when the mean axial loads of each subsystem result in values already studied for the balanced systems.

Table 5.6.4 Comparison Between the System Ductility Index for a Six-Wall Unbalanced System and the System Ductility Indices for the Component Three-Wall Balanced Subsystems

Six-Wall Unbalanced System			Weakest Three-Wall Balanced Subsystem	Strongest Three-Wall Balanced Subsystem
$\tilde{\alpha}$	P/Pmaximum	SDI Range	SDI	SDI
1.0	10%	1.43 to 1.67	3.37	6.20
0.5	20%	1.47 to 2.31	2.73	3.87
1.0	20%	0.89 to 1.11	1.10	6.20

As shown in Table 5.6.4, the SDI values obtained for the unbalanced system are always smaller than the corresponding SDI values of the weakest balanced subsystem. This clearly shows the difference between the system ductility and system robustness. We mentioned in Section 5.4.5 that the mean SD of the unbalanced system are much greater than the mean SD of any balanced system. However, due to the large coefficient of variation of system ductility that can not be associated with probabilistic redundancy effects, the robustness of the unbalanced system is very low.

5.7 CONCLUSIONS

In this chapter, the study of reliability of single flexural walls was expanded to structural systems composed of two to eight flexural walls. Four main properties of these systems were defined and studied:

(1) the frequency of brittle structural behavior;

(2) the system ductility;

(3) the redundancy ratio; and

(4) the system robustness quantified by the system ductility index.

The main conclusions obtained from this research are:

(1) For a Monte Carlo study using 750 structures, no cases of brittle structural behavior were observed for structures having four or more walls.

(2) The increase in the number of walls produces an increase in the mean value of the redundancy ratio and a decrease in the coefficient of variation of the system ductility.

(3) The mean value of the system ductility increases with the number of walls, but at a much slower rate as compared to the mean redundancy ratio.

(4) The coefficient of variation of redundancy ratio remains almost constant with respect to the number of walls.

(5) The system robustness, measured by the system ductility index, increases with the number of walls because it combines two beneficial effects that exhibit opposite trends with respect to the variation of the uncertainty in the system:

   (a) the decrease of coefficient of variation of the system ductility, that reduces the uncertainty; and

   (b) the increase in the spread of extreme versus expected ultimate displacement of the component walls, that increases the uncertainty.

(6) An increase in the axial load produces a decrease in the mean values of system ductility, redundancy ratio, and system ductility index.

(7) The coefficient of variation of system ductility is smallest for zero axial load and largest for the 40% axial load case. However, between 10% and 30% of the maximum axial load the coefficient of variation decreases only slightly with increasing load.

(8) In general, the coefficient of variation of redundancy ratio decreases with increasing axial load.

(9) The increase in correlation of material properties produces a slight increase in the coefficient of variation of system ductility.

(10) The increase in correlation of material properties does produces only slight variation of the mean system ductility and mean and coefficient

of variation of redundancy ratio (exception only for the 40% axial load case). However, the system ductility index decreases markedly when the material correlation increases.

(11) The mean value of the ratio between the displacement corresponding to structural system limit state and the average displacement corresponding to an individual wall ultimate limit state varies, as a function of the axial load, from 8% to 19%.

(12) The unbalanced systems present large values for both the mean value and the coefficient of variation of system ductility.

(13) The system ductility index for an unbalanced system is smaller than the system ductility index of the weakest balanced subsystem contained in the unbalanced system, and may reach dangerously low values.

CHAPTER 6

SUMMARY AND CONCLUSIONS

This research investigates the effects of system ductility and redundancy on the reliability of the concrete masonry structures. We limited our study to a particular class of wall structures. These structures can be modeled as *balanced systems*. We introduced *unbalance* into the system by using a particular pattern of vertical loading. The *structural system limit states* as well as the probabilistic measures for the *system ductility* and *redundancy effects* were defined accordingly. Then we performed Monte Carlo Simulations that used the actual geometrical and material properties in order to obtain the System Ductility Index that we propose as a probabilistic measure of the system *robustness*.

The particular class of wall structures has been chosen for the purpose of clarity only. Consequently, this approach can be used for a much larger class of building structures. For example, the walls of actual structures may have slightly different geometrical properties or vertical load patterns. A small unbalance thus created would not impose any changes in the proposed approach. For more complex structures, several of the base definitions have to be changed but the general approach remains valid.

One important finding in this research consists of revealing the fact that system ductility and redundancy require a special "chemistry" in order to

"cooperate" for improving the safety of structures when subjected to earthquake loading. The resulting conclusion is that *balancing* the structural systems should be an important desideratum for design. A first "casualty" of this requirement will be the use of flanged walls. However, the problem is more complex when considering the beneficial contributions of the flanges. It is recommended that the research presented herein be followed with an optimization study to seek out optimal wall configurations.

This research is based on the assumption that the lateral loading is *static* in nature. Such a departure from the physical reality is common to most current research in systems reliability. Although we believe that the qualitative findings of this research will remain valid under dynamic loading and nonlinearly dynamic response, there are important differences to be expected from the quantitative viewpoint. And thus, such research is recommended as the next step.

REFERENCES

Apostolakis G., 1978, "Probability and Risk Assessment: The Subjectivistic Viewpoint and Some Suggestions," Nuclear Safety, Vol 19, No. 3.

Barlow R.E., Proschan F., 1975, "Statistical Theory of Reliability and Life Testing," Holt, Rinehart and Winston, ed.

Bury K.V., 1975, "Statistical Models in Applied Science," John Wiley & Sons, Inc.

Contini S., Poucet A., 1988, "Fault Tree and Event Tree Techniques," ISPRA Courses on Major Hazard Analysis, Thessaloniki, October 10-14.

Cornell C.A., 1967, "Bounds on the Reliability of Structural Systems," J. Struct. Div., ASCE, 93, Febr. 1967.

Cornell C.A., 1969, "A Probability Based Structural Code," Journal of the American Concrete Institute, Vol. 66, No.12.

Cornell C.A., 1988 a, "Some Comments on Structural Systems Reliability," International Workshop on Structural System Reliability, Boulder, Co., September 1988, University of Colorado, Boulder, Dan M. Frangopol Editor.

Cornell C.A., 1988 b, "Discussion to Paper by Rackwitz and Gollwitzer (1988)," International Workshop on Structural System Reliability, Boulder, Co., September 1988, University of Colorado, Boulder, Dan M. Frangopol Editor.

Corotis R.B., et. al., 1988, "Position Paper of Working Group No. 1 on Concepts and Techniques," International Workshop on Structural System Reliability, Boulder, Co., September 1988, University of Colorado, Boulder, Dan M. Frangopol Editor.

Culver G.C., 1976, "Survey Results for Fire Loads and Live Loads in Office Buildings," National Bureau of Standards Building Science Series 85, U.S. Department of Commerce.

Daniels H.E., 1945, "The Statistical Theory of the Strength of Bundles of Threads," Part I, Proc. Roy. Soc., A 183.

De R.S., Karamchandani A., Cornell A.C., 1989, "Study of Redundancy in Near-Ideal Parallel Structural Systems," Proc. of 5th International Conference on Structural Safety and Reliability, San Francisco, California, August.

Der Kiureghian A., Liu P.L., 1986, "Structural Reliability under Incomplete Probability Information," J. of Eng. Mech., ASCE, 112, No. 1.

Ditlevsen O., 1973, "Structural Reliability and the Invariance Problem," Research Report No. 22, Solid Mechanics Division, University of Waterloo, Waterloo, Canada.

Ditlevsen O., 1979, "Narrow Reliability Bounds for Structural Systems," J. Struct. Mech., 7.

Ditlevsen O., 1981, "Uncertainty Modeling," McGraw Hill, Inc.

Ellingwood B., Galambos T.V., MacGregor J.G., Cornell A.C., 1980, "Development of a Probability Based Load Criterion for American National Standard A58, NBS Special Publication 577, U.S. Department of Commerce.

Englekirk R., Hart G.C. 1984, "Earthquake Design of Concrete Masonry Buildings," Prentice Hall, Inc., Englewood Cliffs, New Jersey.

Frangopol D.M., 1985, "Sensitivity Studies in Reliability-Based Analysis of Redundant Structures," Proc. of 4th International Conference on Structural Safety and Reliability, Kobe, Japan, May.

Frangopol D.M., Nakib R., 1989, "Redundancy Evaluation of Steel Girder Bridges," Proc. of 5th International Conference on Structural Safety and Reliability, San Francisco, California, August.

Frangopol D.M., Nakib R., 1991, "Effects of Damage and Redundancy on the Safety of Existing Bridges," Proc. of 3rd Bridge Engineering Conference, Denver, Colorado, March.

Frangopol D.M., Iizuka M., Yoshida K., 1991, "Redundancy Measures for Design and Evaluation of Structural Systems," Proc. of 10th International Conference on Offshore Mechanics and Arctic Engineering, Stavanger, Norway, June.

Fu G., Frangopol D., 1988, "System Reliability and Redundancy in a Multiobjective Optimization Framework," International Workshop on Structural System Reliability, Boulder, Co., September 1988, University of Colorado, Boulder, Dan M. Frangopol Editor.

Hammersley J.M., Handscomb D.C., 1964, "Monte Carlo Methods", Methuen and Co. Ltd.

Hart G.C., 1982, "Uncertainty Analysis, Loads, and Safety in Structural Engineering," Prentice Hall, Inc., Englewood Cliffs, New Jersey.

Hart G.C., Noland J.L., Kingsley G.R., Englekirk, R.E., 1987, "Confinement Steel in Reinforced Concrete Masonry Shear Walls," Proceedings of 4th North American Masonry Conference, University of California at Los Angeles, August.

Hart G.C., Basharkah M.A., Zorapapel G.T., 1987, "Limit State Design Criteria for Minimum Flexural Steel," Proceedings of 4th North American Masonry Conference, University of California at Los Angeles, August.

Hart G.C., Noland J.L., Kingsley G.R., Englekirk, R.E., Sajjad N.A., 1988, "The Use of Confinement Steel to increase the Ductility in Reinforced Concrete Masonry Shear Walls," The Masonry Society Journal, Vol. 7, No.2, July-December.

Hart G.C., Sajjad N.A., 1988, "R Values for Residential Concrete Masonry Buildings," Report for the National Concrete Masonry Association, EHI Job Number 87-G147, Los Angeles, California.

Hart G.C., Sajjad N.A., 1989, "Evaluating the Ductility of Concrete Masonry Flexural Walls," The 5th Canadian Masonry Symposium, Vancouver.

Hart G.C., Thurston S.J., Englekirk R.E., 1989, "Seismic Evaluation of a Tall Reinforced Concrete Frame Building," ASCE Spring Convention, San Francisco, May.

Hart G.C., Sajjad N.A., Basharkhah M.A., 1990, "Inelastic Masonry Flexural Shear Wall Analysis Computer Program," NSF Grant No. BCS-8722869, Ewing, Kariotis, Englekirk & Hart.

Hart G.C., Jaw J.W., 1991, "Seismic Response of a Tall Masonry Building," Proc. of the Second Conference on Tall Buildings in Seismic Regions, Los Angeles, California.

Hasofer A.M., Lind N.C., 1974, "Exact and Invariant Second-Moment Code Format," Journal of the Engineering Mechanics Division, ASCE, Vol. 100.

Hohenbichler M., Rackwitz R., 1983, "First-Order Concepts in System Reliability," Structural Safety, 1, Elsevier Ed.

Hong W.K., 1989, "Development of Analytical Methods for Reinforced Concrete Masonry Flexural Walls," Doctoral Dissertation, University of California.

International Conference of Building Officials (ICBO), 1988, "Uniform Building Code," Whittier, California.

Kanda J., Yamamura K., 1989, "Extraordinary Live Load Model in Retail Premises," Proc. of 5th International Conference on Structural Safety and Reliability, San Francisco, California, August.

Liebetrau A.M., Doctor P.G., 1987, "The Generation of Dependent Input Variables to a Performance Assessment Simulation Code," Proc. of a N.E.A. Workshop on Uncertainty Analysis for Performance Assessments of Radioactive Waste Disposal Systems, Seattle, Wa, February.

Madsen H.O., Krenk S., Lind N.C., 1986, "Methods of Structural Safety," Prentice Hall.

McKay M.D., Conover W.J., Beckman R.J., 1979, "A Comparison of Three Methods for Selecting Values of Input Variables in the Analysis of Output from a Computer Code," Technometrics, 21 (2).

Mirza S.A, McGregor J.C., 1979, "Variability of Mechanical Properties of Reinforcing Bars," J. Struct. Div., ASCE, 105, May.

Mortensen R.E., 1987, "Random Signals and Systems," John Wiley & Sons, Inc.

Park R., Pauley T., 1975, "Reinforced Concrete Structures," John Wiley & Sons.

Rackwitz R., Fiessler B., 1978, "Structural Reliability under Combined Random Load Sequences," Computer & Structures, Vol 9.

Rackwitz R., Gollwitzer S., 1988, "On the Reliability of Daniels Systems," International Workshop on Structural System Reliability, Boulder, Co., September 1988, University of Colorado, Boulder, Dan M. Frangopol Editor.

Rubinstein M.F., Rosen R., 1968, "Structural Analysis by Matrix Decomposition," Journal of the Franklin Institute, Vol 286, No.4.

Sajjad N.A., 1990, "Confinement of Concrete Masonry," Doctoral Dissertation, University of California, Los Angeles.

Shinozuka M., 1983, "Basic Analysis of Structural Safety," J. Struct. Div., ASCE, 109, March.

Vanmarcke E.H., 1971, "Matrix Formulation Of Reliability Analysis and Reliability Based Design," Comput. Struct., 13.

APPENDIX A

BUILDING DESCRIPTION

The building that presents the typical features for the structures studied in this research is located in the City of Whittier, Southern California. The lateral force resisting system in the longitudinal direction consists of concrete exterior frames from the Roof and the First Floor continued with reinforced concrete structural walls between First Floor and The Basement. Figure B.1 presents a plan view of the building. The lateral force resisting system in the transverse direction consists of cast-in place, reinforced concrete structural walls from Roof to the Basement. The end walls are weakly coupled (Lines 2 and 13). The length of the walls is 23'-4". The two central walls on lines 7 and 8 are 19'-4" long. The 6½ inch thick slabs are cast-in-place. The foundations are spread footings beneath the columns and walls.

In this research, the cast-in-place concrete walls have been replaced with reinforced concrete masonry walls. The wall studied in Chapters 2 and 4 is located on Line 2.

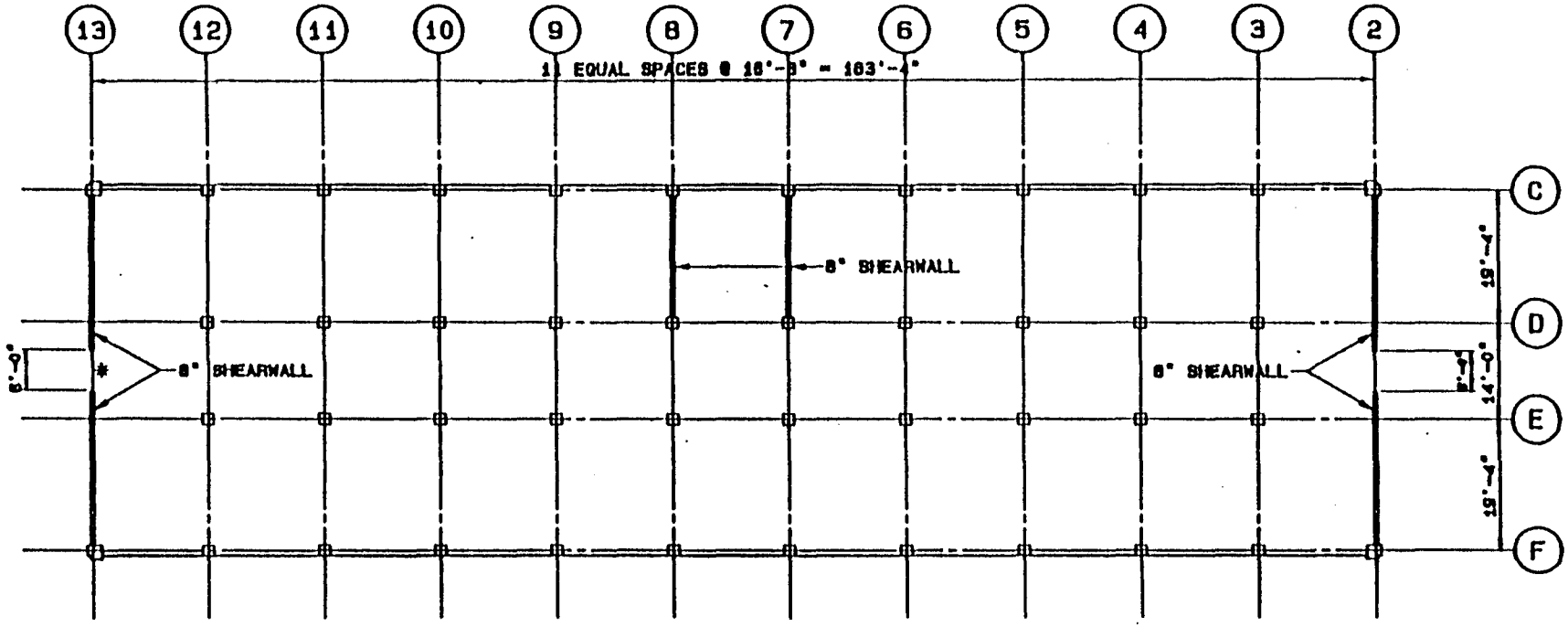

FIGURE A.1 PLAN LAYOUT OF A CONCRETE MASONRY BUILDING

APPENDIX B

RESULTS OF TESTS CONDUCTED AT THE UNIVERSITY OF COLORADO ON CONCRETE MASONRY PRISMS

An experimental program was conducted at the University of Colorado (Sajjad, 1990) to study the confinement of vertical steel in concrete masonry in a state of compression. The program was comprised of prism testing using different kinds of confinement configurations and was done in two series of tests. The present research is concerned only with the "Confinement Comb" configuration that was tested in Series B. The parameters of the concrete masonry stress-strain curve that are of interest for this research are:

f'_m = the maximum compressive stress

ϵ_u = the strain corresponding to the maximum compressive stress

ϵ_{mu} = the maximum usable strain, corresponding to 50% of the maximum compressive stress on the falling branch of the curve.

In this appendix, the pertinent data are processed in order to obtain estimates for the statistics of the above mentioned parameters. Two steps of processing were performed:

(1) Statistics for the entire sample of test results obtained from prisms with "Confinement Combs", regardless the block thickness.

(2) Statistics for sample of test results obtained from 8" thick prisms with "Confinement Combs".

Table B.1 Results of University of Colorado Series B Tests with "Confinement Combs"

Prism Series	Unit (In)	f'_m (Ksi)	ϵ_u	ϵ_{mu}
8B	6	4.09	0.00222	0.00476
		4.72	0.00268	0.00479
		4.46	0.00253	0.00350
9B	8	4.22	0.00274	0.00500
		4.22	0.00279	0.00484
		4.52	0.00293	0.00624
10B	8	4.14	0.00259	0.00686
		4.29	0.00262	0.00677
		4.32	0.00257	0.00492
11B	12	3.45	0.00193	0.00801
		3.31	0.00185	0.01361
		3.47	0.00205	0.00685
All series	Mean	4.10	0.00246	0.00635
	C.O.V.	10.56%	13.87%	39.50%
8" units only	Mean	4.28	0.00271	0.00577
	C.O.V.	2.79%	4.72%	15.15%

The results of tests and data processing (mean values and coefficients of variation) are presented in Table B.1. Sajjad (1990) presents the statistics of limit state parameters for each test series separately. His results, presented in Table

B.2, show a strong dependency of the parameter statistics on the thickness of the masonry block. Because of this conclusion as well as the fact that the wall studied in Chapters 2 and 4 is 8" thick, we used in our research the statistics for ϵ_u and ϵ_{mu} as they result from step (2) of the data processing. However, we used for f'_m the statistics that result from step (1) because the corresponding coefficient of variation (10%) is more realistic. Data presented in Table B.2 show that the coefficient of variation of ϵ_{mu} has the tendency of increasing with increasing mean value of ϵ_{mu}. This conclusion will be used in Appendix C for estimating the Capacity Reduction Factor of the Design Balanced Axial Load.

Table B.2 Statistics of Limit State Parameters for University of Colorado Series B Tests (Sajjad, 1990)

Prism Series	Unit (In)		f'_m (Ksi)	ϵ_u	ϵ_{mu}
8B	6	Mean	4.42	0.0025	0.0044
		C.O.V.	7.1%	12.0%	17.2%
9B	8	Mean	4.32	0.0028	0.0053
		C.O.V.	4.0%	3.6%	14.2%
10B	8	Mean	4.25	0.0026	0.0062
		C.O.V.	2.2%	1.0%	18.2%
11B	12	Mean	3.41	0.0020	0.0095
		C.O.V.	2.5%	5.9%	38.3%

It is important to establish the correlation between the different limit state parameters. We consider that the f'_m, ϵ_u and ϵ_{mu} values associated with each test

are the components of a random vector X. Thus, each test generates a realization of X. The correlation matrix of the vector X can provide information on the correlation coefficients of the three limit state parameters. This matrix was calculated for both steps (1) and (2). The correlation matrices corresponding to steps (1) and (2) are, respectively

$$\begin{bmatrix} 1.00 & 0.89 & -0.75 \\ 0.89 & 1.00 & -0.64 \\ -0.75 & -0.64 & 1.00 \end{bmatrix}$$

$$\begin{bmatrix} 1.00 & 0.62 & 0.06 \\ 0.62 & 1.00 & -0.14 \\ 0.06 & -0.14 & 1.00 \end{bmatrix}$$

The first correlation matrix indicates that f'_m and ϵ_u are approximately linearly related while ϵ_{mu} has a tendency to decrease when f'_m and ϵ_u increase. The second correlation matrix, corresponding to 8" units only provides more credible results; it shows a relatively strong correlation between f'_m and ϵ_u and a lack of correlation between ϵ_{mu} and the other two parameters. The conclusions obtained from the second correlation matrix supports the assumption of independence between f'_m and ϵ_{mu} used in generating the values of the input parameters for the Monte Carlo simulations.

APPENDIX C

THE AXIAL LOAD ON A WALL

C.1 GENERAL

Desirable performance criteria for concrete masonry flexural walls is achieved when yielding of the steel occurs before the masonry crushes in compression. This behavior allows the wall to develop a significant ductility capacity. When the axial force acting on the section is large, the yielding of the tension steel will not occur prior to the masonry crushing and thus the element fails immediately after reaching its maximum strength.

A "balanced" design limit state occurs when the tension steel yields at the same time the masonry crushes. The axial force corresponding to this balanced design limit state represents the upper limit of compression that a section can bear without the danger of the element failing in a brittle limit state. This axial force (P_b) is derived with the following assumptions:

(1) The tension and compression steel produces forces which cancel and thus produce a net axial force of zero.

(2) The compressive force on the wall can be modelled using a Whitney Equivalent Compression Stress Block.

(3) A linear distribution of strain exists on the cross section.

With these assumptions, the balanced axial load (P_b) is a function of the maximum usable strain (ϵ_{mu}), the maximum compressive force ($f'_m bd$), the steel yield stress (f_y), and the steel modulus of elasticity (E_s). The equation for the random variable Pb is:

$$P_b = 0.72 f_m bd \frac{\epsilon_{mu}}{\epsilon_{mu} + \frac{f_y}{E_s}} \qquad \text{(C.1.1)}$$

The geometric variables b and d as well as the steel modulus of elasticity E_s have small coefficients of variation relative to the other variables and thus can be considered to be deterministic. Thus, f'_m, f_y, and ϵ_{mu} are herein considered to be independent and normally distributed random variables.

The expected value of the maximum axial capacity of the wall is

$$P_{max,e} = f'_{me} bd \qquad \text{(C.1.2)}$$

where

f'_{me} = mean, or expected value, of the maximum compressive stress.

If we divide both sides of Equation (C.1.1) by the expected value of $P_{max,e}$ we obtain

$$\frac{P_b}{P_{max,e}} = 0.72 \frac{f'_m}{f'_{me}} \frac{\epsilon_{mu}}{\epsilon_{mu} + \frac{f_y}{E_s}} \qquad \text{(C.1.3)}$$

Let us now define the new random variable

$$f_b = 0.72 \frac{f'_m}{f'_{me}} \frac{\epsilon_{mu}}{\epsilon_{mu} + \frac{f_y}{E_s}} \qquad \text{(C.1.4)}$$

The random variable f_b is a function of three basic random variables (f_y, f'_m/f'_{me} and ϵ_{mu}). The coefficient of variation of f_b is equal to the coefficient of variation of P_b.

The investigation consists of three steps:

(1) Establish the most likely values for the mean and coefficients of variation of each of the three basic random variables. Perform a Monte Carlo simulation for this "central case" and determine the frequency histogram of f_b as well as its mean value and coefficient of variation.

(2) Study the sensitivity of the mean and coefficient of variation of f_b to the increase in means and coefficients of variation of f_y, f'_m/f'_{me}, and ϵ_{mu}.

(3) Establish the relationship between the capacity reduction factor ϕ and the target reliability index β, based on the sensitivity analysis performed in Step (2).

C.2 THE "CENTRAL CASE"

The probabilistic distributions and the values for the mean and coefficient of variation of f_y and ϵ_{mu} that are used in this "Central Case" are presented in Table 2.2.1. The variable f'_m/f'_{me} is considered to be normally distributed with mean 1 and coefficient of variation equal to 10%.

A Monte Carlo simulation for 5,000 realizations of each basic random variable was performed for the Central Case. The frequency histogram obtained from this study suggest a distribution for f_b very close to a Normal distribution. The mean value of f_b was 0.51 and the coefficient of variation of f_b was 11.3%.

C.3 THE SENSITIVITY OF THE MEAN VALUE OF f_b

The mean value of f_b is an important parameter that governs the ductility of the walls. Thus, a sensitivity study is performed to evaluate the key statistics that influence it. As a first step, the values of the mean and coefficient of variation of the three random variables in Section C.2 were independently increased by 10%. The increase was performed, one at a time, while keeping the other parameters constant. The parameter f'_m/f'_{me} is theoretically constant and equal to 1. The percent variation in the mean value of f_b due to each parameter variation is shown in Table C.3.1.

Table C.3.1
Percent Change in the Mean Value of f_b due to a 10% Increase in Basic Parameter Statistics.

Basic Parameter Statistic Changed	% Change in Mean f_b
Mean f_y	-2.8
Coefficient of Variation of f_y	-0.1
Coefficient of Variation of f'_m/f'_{me}	-0.1
Mean ϵ_{mu}	2.7
Coefficient of Variation of ϵ_{mu}	-0.1

It can be observed from Table C.3.1 that the mean value of f_b exhibits:

(1) a reduced sensitivity (2.7 or 2.8% change for a 10% change) to the variation of mean values of steel yielding stress and maximum usable strain;

(2) no engineeringly significant sensitivity to variations of the coefficients of variation of the three random variables.

In reality, the ranges of variation of the statistics parameters are different and it is possible that the mean value of the maximum usable strain may double the 10% change, while the assumed 10% variation in the mean value of f_y is unlikely. For this reason, a sensitivity study for the *possible* range of values of each of the three random variables was performed as a second step. The ranges of values are presented in Table C.3.2.

Table C.3.2
Range of Values Considered for Studying the Sensitivity of f_b

Variable	Range of Mean	Range of Coefficient of Variation
f_y	65 to 69 Ksi	4% to 15%
f'_m/f'_{me}	1.0	5% to 25%
ϵ_{mu}	0.003 to 0.016	5% to 25%

When the range of values for one statistics parameter was swept, the other parameters were set equal to the "Central Case" values. Monte Carlo runs for samples of 5,000 realizations were performed for each case. The only parameter that produces a significant variation of this mean *when varying within likely limits* is the mean value of the maximum usable strain (Figure C.3.1). The mean value of f_b increases with an increasing mean maximum usable strain and tends to stabilize for large values of the mean of ϵ_{mu}. The lower limit of the mean value is 0.4 for a mean value of the maximum usable strain of 0.003. When the maximum usable strain exceeds 0.012, the mean value of f_b reaches 0.6. For larger values of the mean ϵ_{mu}, the mean value of f_b tends to stabilize around the value 0.65. The following formula is proposed for this variation:

$$\overline{f_b} = 0.68e^{-\frac{0.0016}{\overline{\epsilon_{mu}}}} \qquad \text{(C.3.1)}$$

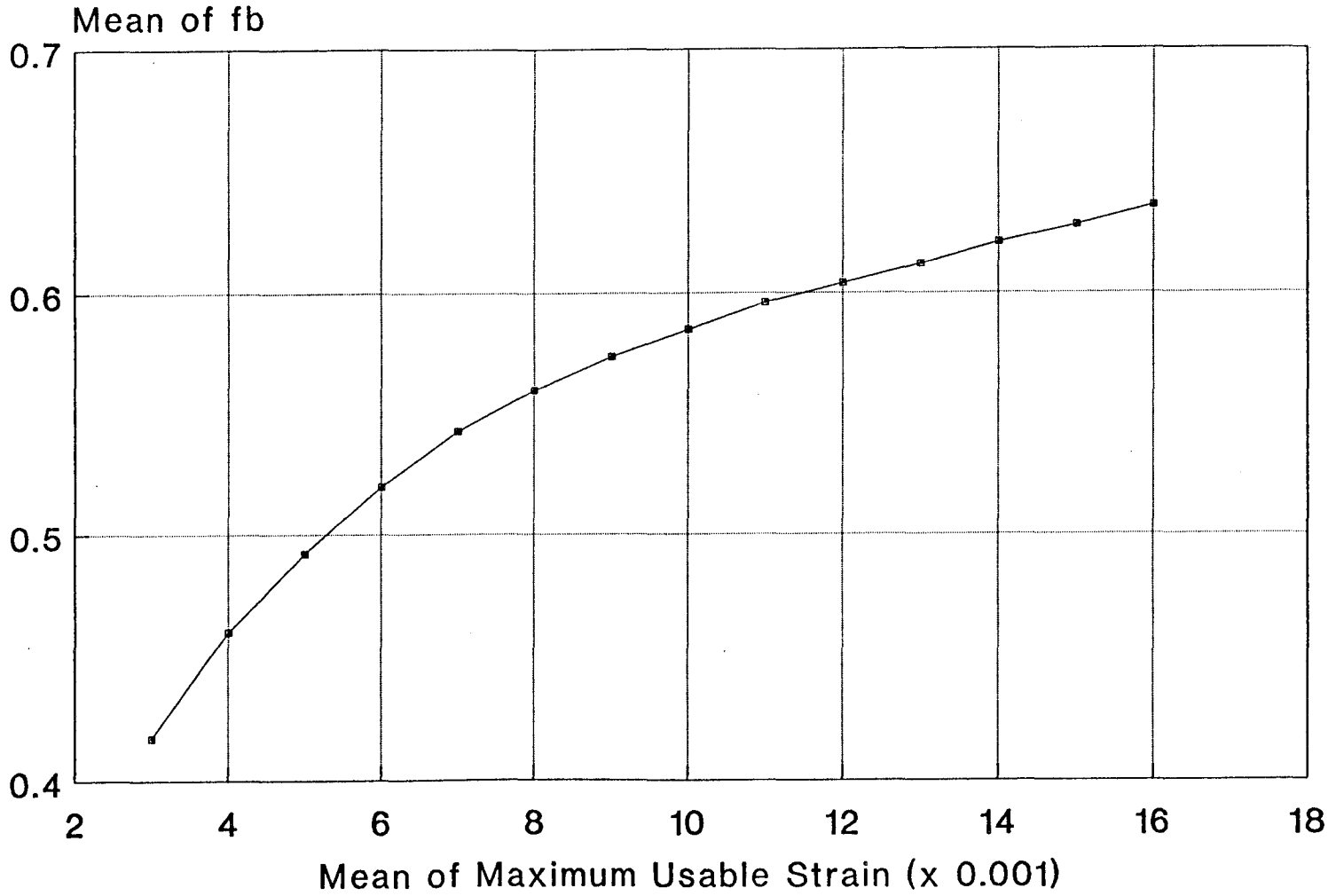

FIGURE C.3.1 MEAN fb AS A FUNCTION OF MAXIMUM USABLE STRAIN

C.4 THE SENSITIVITY OF THE COEFFICIENT OF VARIATION OF f_b

The capacity reduction factor is a function of the coefficient of variation of f_b and thus a sensitivity study was performed. As a first step, the values of mean and coefficient of variation of the three random variables of the "Central Case" were independently increased by 10%. The percent change of the coefficient of variation of f_b due to each parameter variation is shown in Table C.4.1.

Table C.4.1
Percent Change in the Coefficient of Variation of f_b due to a 10% Increase in Basic Parameter Statistics

Basic Parameter Statistics Changed	% Change in Coefficient of Variation of f_b
Mean f_y	1.3
Coefficient of Variation of f_y	0.1
Coefficient of Variation of f'_m/f'_{me}	7.9
Mean ϵ_{mu}	-1.3
Coefficient of Variation of ϵ_{mu}	1.8

It can be observed from Table C.4.1 that the coefficient of variation of f_b exhibits:

(1) A significant sensitivity to the change in the coefficient of variation of the variable f'_m/f'_{me}.

(2) A little sensitivity (less than 2% for a 10% change) to mean values of steel yielding stress and maximum usable strain as well as to the coefficient of variation of the maximum usable strain.

(3) A very small sensitivity to the change of the coefficient of variation of the steel yielding stress.

Similar to the sensitivity study performed for the mean value of f_b, the second step was carried out. The same ranges of values (presented in Table C.3.2) were used for the statistics of the parameters. Monte Carlo simulations for samples of 5,000 realizations were performed for each case. The only parameter that produces a significant change in the coefficient of variation of f_b is the coefficient of variation of f'_m. As it can be seen from Figure C.4.1, the coefficient of variation of f_b (V_{f_b}) increases almost linearly with an increasing coefficient of variation of f'_m ($V_{f'_m}$) . The following linear expression was fitted to this variation:

$$V_{f_b} = 0.94 V_{f'_m} + 0.02 \qquad \text{(C.4.1)}$$

According to the results of Monte Carlo simulations, a change in the coefficient of variation of the maximum usable strain from 5% to 25% produces a change in the coefficient of variation of f_b from 10.3% to 13.4%. A change in the mean value of the maximum usable strain from 0.003 to 0.016 produces a decrease in the coefficient of variation of f_b from 12.6% to 10.3%.

As described in Appendix B, the coefficient of variation of ϵ_{mu} has a tendency of increasing with the increasing mean value of ϵ_{mu}. A regression analysis based upon the Least Square Method was performed and the following analytical model was obtained:

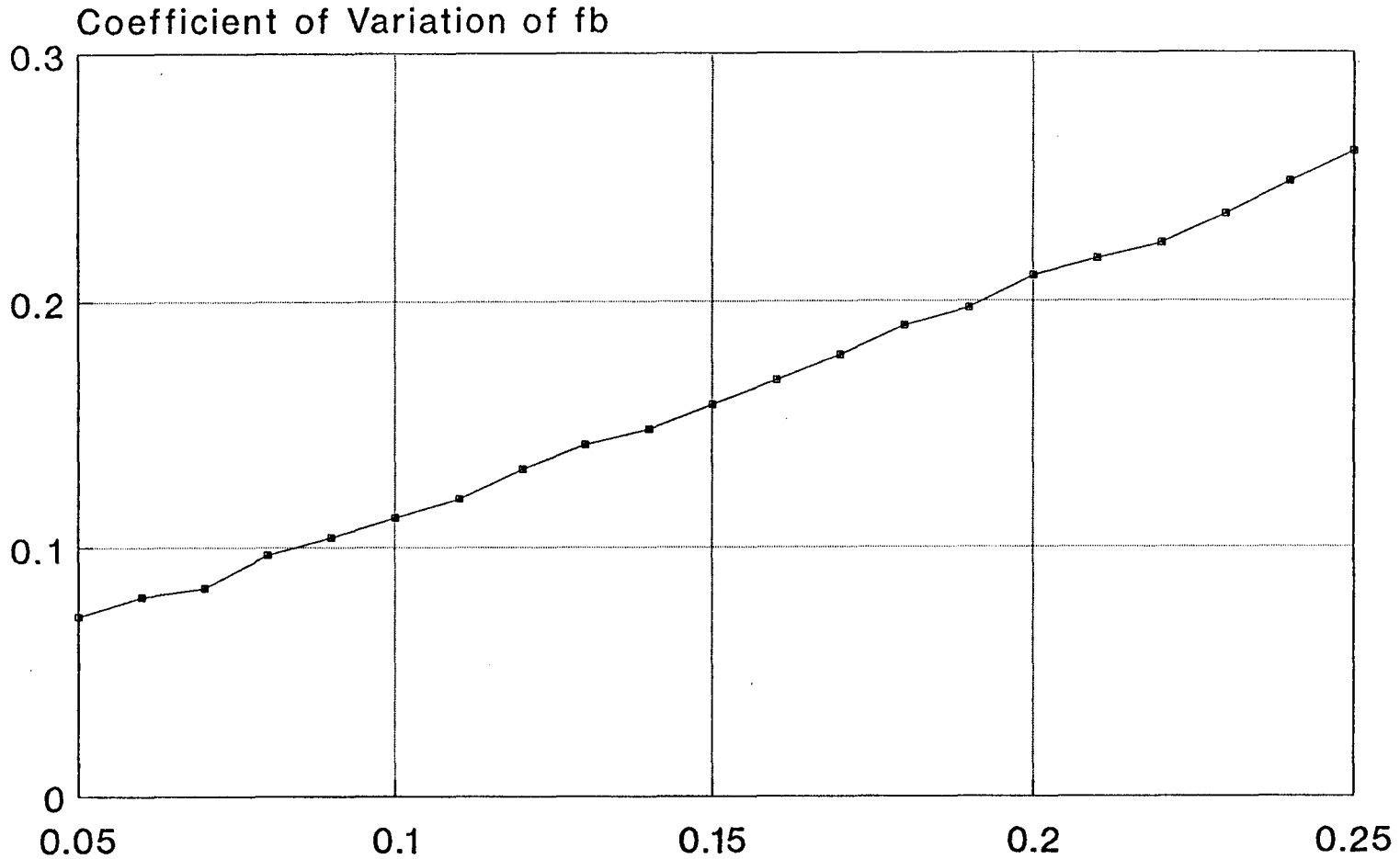

FIGURE C.4.1 C.O.V. OF fb AS A FUNCTION OF C.O.V. OF f'm

$$V_{\epsilon_{mu}} = 0.25e^{-\frac{0.001}{\overline{\epsilon_{mu}}-0.002}} \qquad \text{(C.4.2)}$$

where $\overline{\epsilon_{mu}}$ and $V_{\epsilon_{mu}}$ are, respectively, the mean value and the coefficient of variation of the maximum usable strain. Consequently, if the dependency between the mean and coefficient of variation of the maximum usable strain is considered, the sensitivity of the coefficient of variation of f_b to their joint change will almost vanish.

According to the results of Monte-Carlo simulations, a change in mean value of the steel yielding stress from 65 Ksi to 69 Ksi does not produce meaningful change in the coefficient of variation of f_b. The same result is obtained when changing the coefficient of variation of the steel yield stress from 4% to 15%.

C.5 CAPACITY REDUCTION FACTOR ϕ

According to Hong (1989)

$$\phi < e^{-0.75\beta V} \qquad \text{(C.5.1)}$$

where ϕ is the capacity reduction factor, β is the target safety index and V is the coefficient of variation of P_b, and hence the coefficient of variation of f_b. Therefore, to calculate the capacity reduction factor ϕ for a target reliability index value β, the coefficient of variation of f_b must be found. In this appendix, this coefficient of variation is determined using a Monte Carlo analysis.

As concluded in Section C.4, the coefficient of variation of f_b does not significantly depend on ϵ_{mu} or f_y. Using Equations (C.5.1) and (C.4.1), the capacity reduction factor ϕ may be expressed as a function of two variables only: the coefficient of variation of the maximum masonry compression strength $V_{f'_m}$ and the target safety index β. This dependence is graphically shown as a three-dimensional plot in Figure C.5.1. Contours of equal $V_{f'_m}$ are presented in Figure C.5.2. As expected, the capacity reduction factor will decrease with increasing safety index as well as increasing coefficient of variation of the masonry compression strength.

Hart and Sajjad (1989) have recommended, based on reliability analysis, to adopt an upper limit for the design axial load of 65% of the balanced axial load where minimum specified values were used for f'_m. Thus, in the context of this section, where typically the expected value would be equal to 1.3 times the specified value, the Hart and Sajjad value of 65% corresponds to (65%)/(1.3) = 50%. This appears to be conservative based on Figure C.5.2, because for values of ϕ = 0.5 and β = 3 the corresponding value of a coefficient of variation $V_{f'_m}$ must be equal to 33%.

For example, according to Figure C.5.2, ϕ = 0.5 and $V_{f'_m}$ = 10% corresponds to $\beta >> 3$. Using the approach in Chapter 4, the normalized mean axial load

$$\frac{\overline{P}}{P_{max}} = \Phi f_b = (0.5)(0.51) = 0.25 \qquad \text{(C.5.2)}$$

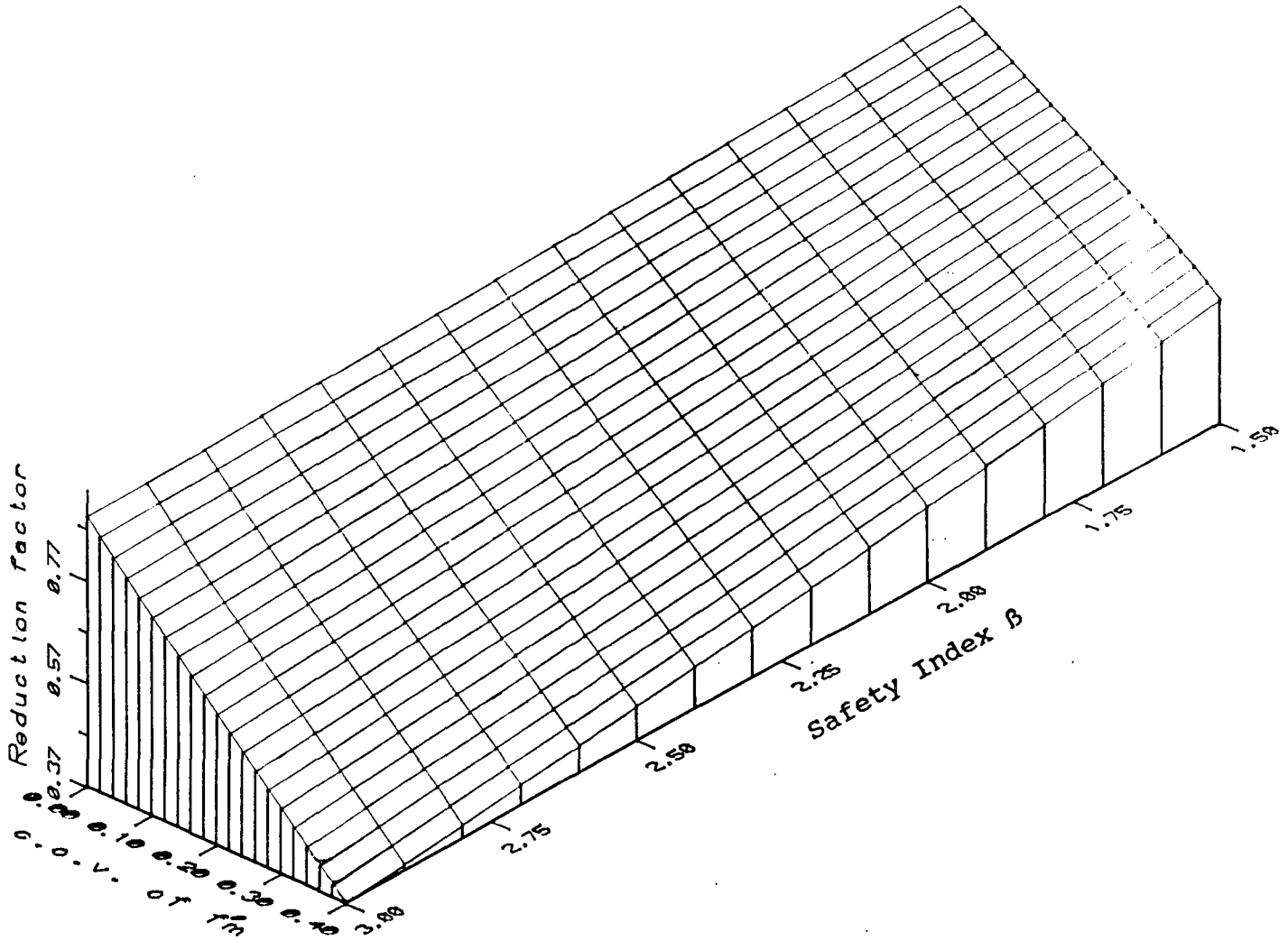

FIGURE C.5.1 CAPACITY REDUCTION FACTOR OF THE AXIAL BALANCED LOAD

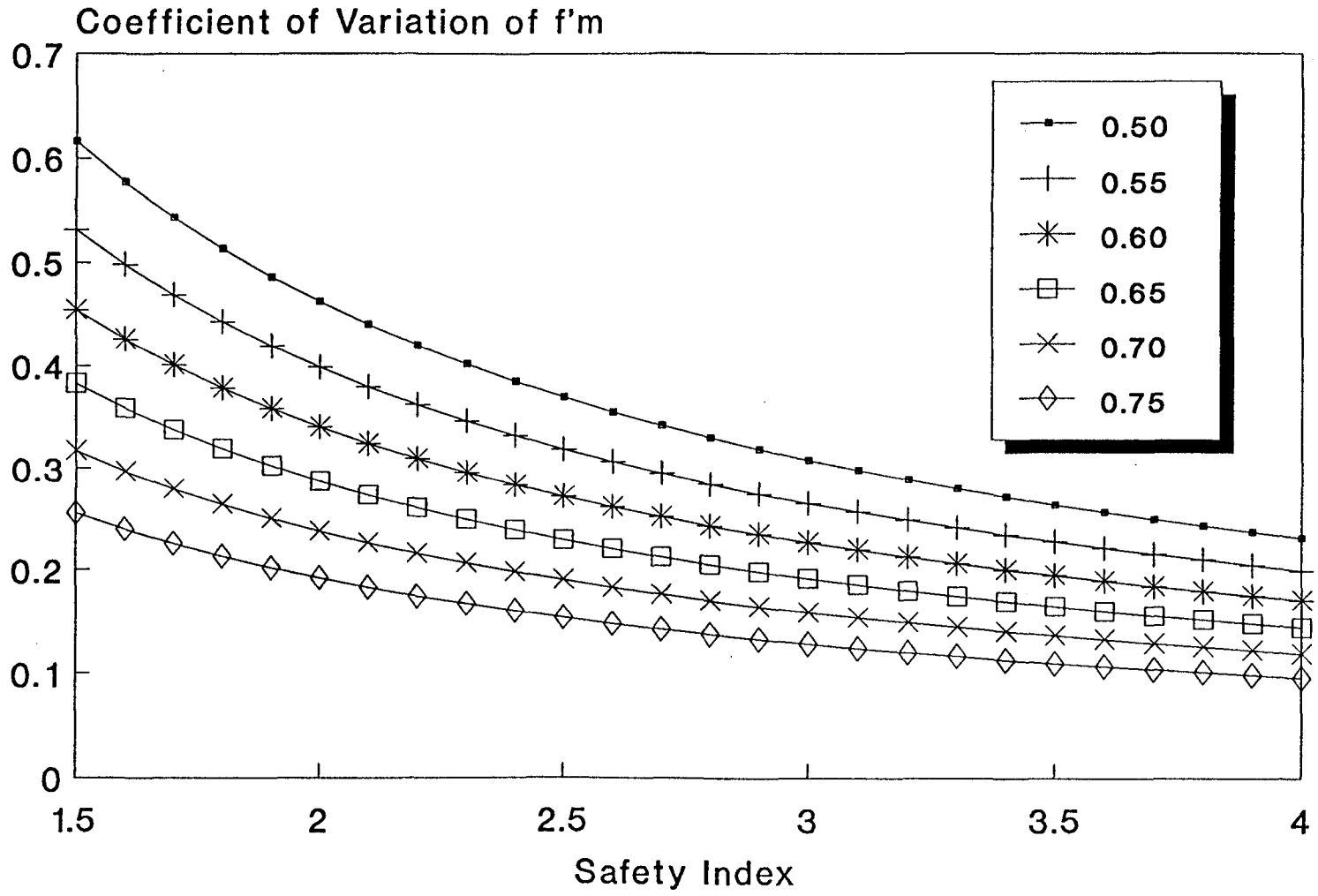

FIGURE C.5.2 CONTOURS OF EQUAL CAPACITY REDUCTION FACTOR

and a coefficient of variation of the axial load equal to 20% (according to the estimation in Section 5.3.1) correspond to a Ductility Index of 1.6 (see Figure 4.7.3 and Table 4.7.3). However, considering the *robustness* of the structural system composed of reinforced masonry walls, the System Ductility Index is equal to 2.3 for two-wall systems and 5.0 for eight-wall systems (see Figure 5.6.1 and Table 5.6.1). The safety index recommended for seismic loads by Ellingwood et al. (1980) is 1.75. Consequently, the value of Capacity Reduction Factor recommended by Hart and Sajjad is conservative.

C.6 THE HASOFER-LIND SAFETY INDEX

As suggested in Chapter 3 and Appendix E, a simplified (but inaccurate) approach to estimating the safety index with respect to ductile behavior is to apply the Rackwitz-Fiessler algoritm to Equation (3.3.1) or Equation (C.1.4). We calculated the Hasofer-Lind Index corresponding to a mean axial load equal to 40% of the maximum axial load and a coefficient of variation of the axial load ranging between zero and 25%. The results are compared in Table C.6.1 with the corresponding results obtained from Table 4.7.3.

The results in Table C.6.1 exhibit a difference between the two safety indices of 0.5 to 0.8. If the approach using Equation (C.1.4) was correct, the corresponding safety index would have been smaller than Ductility Index because of the former index is invariant with respect to different mappings of the limit state

surface. Hence, the error introduced by ignoring the multistate character of the problem is even greater than 0.5 units of safety index.

Table C.6.1
Comparison Between the Hasofer-Lind Safety Index Calculated with Equation (C.1.4) and the Ductility Index

C.O.V. of Axial Load (%)	Safety Index	
	Equation C.1.4	Ductility Index
0	2.0	1.4
5	1.9	1.3
15	1.6	1.1
15	1.4	0.6
20	1.2	0.5
25	1.0	0.5

APPENDIX D

CORRELATION OF CONCRETE COMPRESSIVE STRENGTH AMONG WALLS OF AN ACTUAL STRUCTURE

Standard tests on concrete cubes obtained during construction of an eight story building in Los Angeles were used to estimate the correlation coefficient of the compressive strength among different walls. The plan shape of the building is presented in Figure D.1. The lateral force resisting systems in both directions consist of reinforced concrete structural walls.

The casting of concrete was performed, for each story, in three stages. Figure D.1 shows the areas of the floor plan that are associated to each stage of concrete pouring. For each stage of pouring, two cubes were set aside for testing: one after 28 days and the other for a later date. The results obtained on the 27 cubes tested after 28 days are used in this research.

We consider that the three values of the compressive strength associated with each area of a given story are the components of a random vector X. Thus, each story of the building generates a realization of X. The correlation matrix of the vector X can provide information on the correlation coefficients of the concrete compressive strength among the walls of this structure.

Table D.1 presents the values obtained for the concrete compressive strength for each story and area.

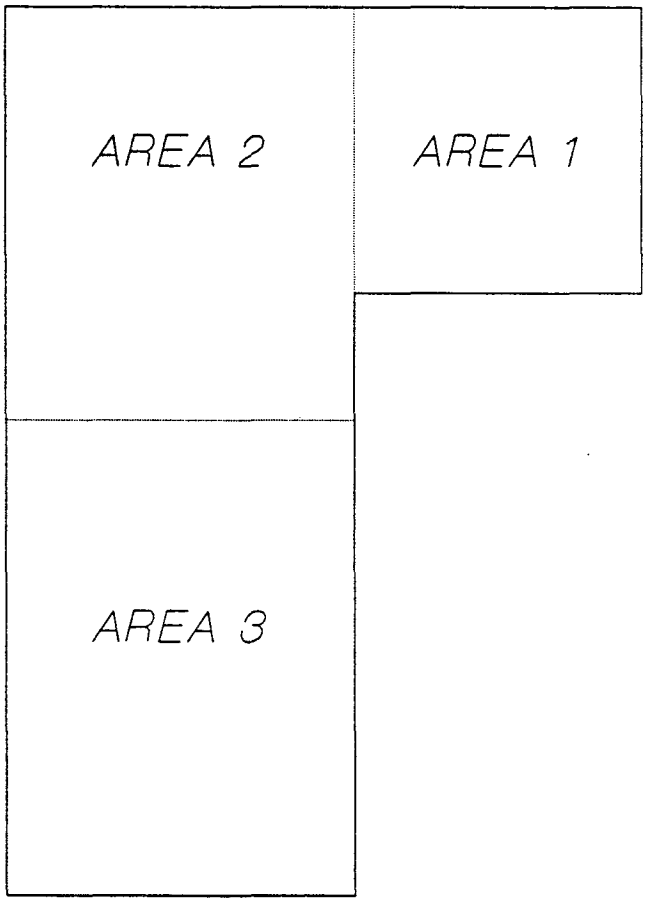

FIGURE D.1 BUILDING PLAN

Table D.1 Test Results for the Compressive Strength of Concrete

Story	Compressive Strength (psi)		
	Area 1	Area 2	Area 3
Basement	4560	4420	4830
1	4420	3780	4470
2	4420	4920	4920
3	4600	5060	4320
4	4600	4760	3800
5	4700	5390	4420
6	5270	4990	4810
7	5090	5870	5870
8	5310	4760	6120

The correlation matrix of the random vector is

$$\begin{bmatrix} 1.00 & 0.44 & 0.67 \\ 0.44 & 1.00 & 0.32 \\ 0.67 & 0.32 & 1.00 \end{bmatrix}$$

The correlation matrix indicates that a possible range of correlation coefficient for this structure is 0.3 to 0.7. The average value of the three upper nondiagonal terms is 0.48. We consider that 0.5 is a reasonable value for the correlation coefficient of compression strength. Since similar data for concrete masonry walls are not available, this value is used extensively in this research.

APPENDIX E

SAFETY INDEX IN A MULTISTATE SPACE

E.1 PROBLEM SETTING

When the design point must be searched on a curve rather than a surface, the use of Lagrange Multipliers appears to be most suitable solution procedure. For simplicity we consider only two conditional limit states.

Consider the following optimization problem;

minimize:

$$\gamma = \sqrt{X^T X} \tag{E.1.1}$$

subject to the constraints $g_1(X)=0$ and $g_2(X)=0$. Here X is a vector of uncorrelated, standard random variables $X=(x_1,x_2,...,x_n)^T$, $g_1(X)$ and $g_2(X)$ are the equations of the conditional surfaces in the n dimensional space of standard random variables, and γ is the distance from the origin to the point corresponding to the random vector X. The constraints $g_1(X)=0$ and $g_2(X)=0$ represent the condition that the point be on the n-dimensional curve at the intersection of

surfaces $g_1(X)=0$ and $g_2(X)=0$. To solve the problem, a vector of Lagrange Multipliers

$$\Lambda = (\lambda_1, \lambda_2)^T$$

is introduced to construct

$$L = \sqrt{X^T X} + \lambda_1 g_1(X) + \lambda_2 g_2(X)$$

The solution X_* and the Lagrange Multipliers Vector can be obtained by setting

$$\frac{\partial L}{\partial \Lambda} = \frac{\partial L}{\partial X} = 0 \qquad \text{(E.1.2)}$$

Defining the matrix G as the generalized Jacobian of functions $g_1(X)$ and $g_2(X)$ the solution for X_* is

$$X_* = -\gamma G \Lambda_* \qquad \text{(E.1.3)}$$

where the star subscript denotes a solution of Equation (E.1.2) and

$$G = \begin{bmatrix} \dfrac{\partial g_1(X)}{\partial x_1} & \dfrac{\partial g_2(X)}{\partial x_1} \\ \vdots & \vdots \\ \dfrac{\partial g_1(X)}{\partial x_n} & \dfrac{\partial g_2(X)}{\partial x_n} \end{bmatrix} \qquad \text{(E.1.4)}$$

Since γ is a scalar, the Equation (E.1.3) can be also written as

$$G\Lambda_* = -\frac{1}{\gamma} X_* \qquad \text{(E.1.5)}$$

Premultiplying Equation (E.1.5) by G^T we obtain

$$G^T G \Lambda_* = -\frac{1}{\gamma} G^T X_* \qquad \text{(E.1.6)}$$

Since G^TG is a square matrix, it can be inverted. Consequently, the Lagrange Multipliers Vector is:

$$\Lambda_* = -\frac{1}{\gamma}(G^T G)^{-1} G^T X_* \qquad \text{(E.1.7)}$$

It is possible to obtain a matrix equation where X_* is eliminated. This can be achieved by substituting Equation (E.1.3) into Equation (E.1.1) and thus

$$\gamma_* = \sqrt{(\gamma_* G_* \Lambda_*)^T (\gamma_* G_* \Lambda_*)} \qquad \text{(E.1.8)}$$

or

$$\Lambda_*^T G_*^T G_* \Lambda_* = 1 \qquad \text{(E.1.9)}$$

An exact solution can not be obtained from the above equations. However, these equations can be used to construct an iterative method to obtain a solution for the Design Point X_* and the distance γ from the origin to the curve.

E.2 ITERATIVE METHOD FOR THE SAFETY INDEX

The proposed iterative method has five steps:

Step 1: Chose arbitrarily n-2 values for the coordinates of the X_*; the remaining two coordinates result from the system of equations $g_1(X_*)=0$ and $g_2(X_*)=0$.

Step 2: Compute the scalar γ using Equation (3.2.1) and the Jacobian G using Equation (3.2.4).

Step 3: Obtain the Lagrange Multipliers Vector from Equation (3.2.7).

Step 4: Obtain a better estimate of X_* using Equation (3.2.3).

Step 5: Repeat steps 2 through 4 until convergence is achieved for the value γ. This value is the safety index. The last estimate for X_* is the solution for the Design Point.